An investigation into recent outlet glacier dynamics within Vincennes Bay, Wilkes Land, East Antarctica.

HANNAH JANE PICTON

Abstract

The Antarctic Ice Sheet has been in a state of negative mass balance over recent decades, with mass loss largely occurring from the West Antarctic Ice Sheet. However, recent studies indicate that Wilkes Land, East Antarctica, has lost mass at accelerating rates over the past two decades, exhibiting a dynamic response to oceanic forcing. Overlying the marine-based Aurora Subglacial Basin (ASB), Wilkes Land has been referred to as the potential 'weak underbelly' of the East Antarctic Ice Sheet and is drained by several major outlet glaciers. Despite their potential importance, few of these glaciers have been studied in detail. This includes the six outlet glaciers draining into Vincennes Bay, a region recently reported to have the warmest intrusions of modified Circumpolar Deep Water (mCDW) ever recorded in East Antarctica. This thesis seeks to improve our understanding of the understudied Vincennes Bay outlet glaciers, providing a first overview of recent ice dynamics observed between 1963 and 2022. Optical satellite imagery, differential satellite synthetic aperture radar interferometry (DInSAR) techniques and a range of secondary datasets were employed in order to assess change across four fundamental glacier parameters: terminus position, ice surface velocity, ice surface elevation, and grounding line position. Decadal fluctuations between terminus advance and terminus retreat recorded across the Vincennes Bay outlet glaciers correspond closely with wider patterns reported across Wilkes Land, potentially correlated to variations in sea ice production. Ice surface velocities were generally stable between 2000 and 2021, with some fluctuations measured across the grounding line of Bond East Glacier. Observed changes in ice surface elevation were spatially variable, with a consistent, albeit relatively modest, thinning trend seen across Vanderford Glacier between 2003 and 2017. Enhanced rates of ice thinning were measured across each of the Vanderford, Adams, Anzac, and Underwood Glaciers between 2017 and 2020, potentially linked to the widespread decline in Antarctic sea ice extent reported during the austral spring of 2016. Most importantly, extensive grounding line retreat was observed at Vanderford Glacier, measured at 18.6 km between 1996 and 2020. Such rapid grounding line retreat (0.8 km yr^{-1}) is consistent with the notion that warm mCDW is able to access deep cavities formed below the Vanderford Ice Shelf, driving high rates of basal melting. With an inland retrograde bed slope observed along the Vanderford Trench, such oceanic forcing may have significant implications for the future stability of Vanderford Glacier. This study shows that the dynamic response of Vanderford Glacier has been more muted than expected given the high magnitude of grounding line retreat observed. Enhanced thinning and the onset of ice flow acceleration may therefore be predicted over the coming decades.

An investigation into recent outlet glacier dynamics within Vincennes Bay, Wilkes Land, East Antarctica

Hannah Picton

Thesis submitted for M.Sc. by Research degree

Department of Geography
Durham University

February 2023

Table of Contents

List of Tables

List of Figures

Statement of Copyright

Acknowledgements

I would like to thank my supervisors Professor Chris Stokes and Professor Stewart Jamieson for their support and guidance throughout the year. I would also like to thank Dana Floricioiu and Lukas Krieger for producing the DInSAR derived grounding line positions across Vincennes Bay.

1. Introduction

1.1. Ice sheet dynamics

The Antarctic Ice Sheet (AIS) and Greenland Ice Sheet (GrIS) represent the Earth's largest ice masses, containing a sea level equivalent (SLE) of 57.9 m (Morlighem et al., 2020) and 7.2 m (Aschwanden et al., 2019) respectively. Accelerated mass loss from these ice sheets is therefore predicted to enhance rates of sea level rise over the twenty-first century, posing a potentially severe threat to the 680 million people currently estimated to populate low-lying coastal regions (Navarro, 2021). During the last interglacial ~ 125,000 years ago (Marine Isotope Stage [MIS] 5e), global sea levels are evidenced to have been elevated at least 6.6 m above present, indicative of substantial mass loss from both the AIS and GrIS (Kopp et al., 2009). The mass balance of an ice sheet represents the net difference between mass gain, primarily in the form of snowfall, and mass loss. Across the GrIS, recent mass loss has been roughly equally partitioned between ice dynamics and surface meltwater runoff (Choi et al., 2021), with a significant increase in surface melt observed since the end of the 1990s, largely driven by atmospheric warming (Fettweis et al., 2017; Trusel et al., 2018; Hanna et al., 2020). In contrast, the comparatively colder climatic regime of the AIS limits the occurrence of surface melting (Hanna et al., 2020). Mass is instead predominantly lost through outlet glaciers and fast-flowing ice streams which act as arteries, draining ice from the Antarctic interior to the ocean (Rignot & Thomas, 2002).

With 75% of Antarctica's coastline fringed by floating ice shelves (Rignot et al., 2013), mass loss from the AIS is partitioned roughly equally between two key processes, ice shelf basal melting and calving (Holland et al., 2020; Pattyn & Morlighem, 2020), the latter described as the mechanical loss of icebergs from the ice front (Benn et al., 2007). Whilst the Archimedes principle dictates that mass loss from floating ice shelves will have a negligible direct impact on sea level rise (Schoof, 2010), such ice shelves exert a critical buttressing force upstream, restraining the outflow of grounded ice (Fürst et al., 2016). Basal melting and iceberg calving is understood to reduce this buttressing potential, thereby allowing enhanced ice discharge across the grounding line, representing the critical transition between grounded and floating ice (Fürst et al., 2016). Satellite observations suggest that this dynamic response has been occurring across many glacier systems within Antarctica, with discharge acceleration of 5.3 ± 2.2 Gt yr^{-2} measured across the AIS between 2002 and 2020 (Diener et al., 2021). Such increased ice discharge directly contributes to global sea level rise; analysis of changing ice dynamics across marine-terminating outlet glaciers is thus fundamental in order to facilitate the accurate prediction of future ice sheet mass balance (Aschwanden et al., 2019).

Recent estimates of AIS mass balance suggest that the majority of mass loss has occurred from the West Antarctic Ice Sheet (WAIS) (Martín-Español et al., 2016; Gardner et al., 2018; The IMBIE Team, 2018; Schröder et al., 2019; Shepherd et al., 2019), predominantly driven by increased discharge from the Pine Island and Thwaites Glaciers located in the Amundsen Sea embayment (Mouginot et al., 2014; Medley et al., 2014; Christianson et al., 2016; Yu et al., 2018). The Amundsen Sea embayment has been referred to as the 'weak underbelly' of the WAIS (Hughes, 1981); recent increased discharge has widely been attributed to oceanic forcing, with the enhanced intrusion of warm Circumpolar Deep Water (CDW) driving basal melting of the ice shelves known to buttress these glaciers (Feldmann & Levermann, 2015; Scambos et al., 2017; Rignot et al., 2019; Pattyn & Morlighem, 2020). Whilst the East Antarctic Ice Sheet (EAIS) has generally been considered relatively stable (Schröder et al., 2019), recent studies have provided evidence of dynamic mass loss from the Wilkes Land sector (McMillan et al., 2015; Martín-Español et al., 2016; Smith et al., 2020; Wang et al., 2021; Stokes et al., 2022). With Wilkes Land characterised by a 'warm shelf' regime (Thompson et al., 2018), such increased mass loss has been attributed to the enhanced incursion of modified CDW (mCDW) towards sub-ice shelf cavities, driving basal ice shelf melting analogous to that seen within the Amundsen Sea embayment (Miles et al., 2016; Rignot et al., 2019). Indeed, Miles et al. (2016) therefore highlight Wilkes Land as the potential 'weak underbelly' of the EAIS. The warmest intrusion of mCDW ever recorded within East Antarctica was seen within Vincennes Bay (Feb – Nov 2012), a shelf region located on the Wilkes Land coast (Ribeiro et al., 2021) (Figure 1). This oceanographic data, collected using instrumented elephant seals tagged at Casey Station, recorded such mCDW spreading laterally over the continental shelf, with a core distribution between 300 and 600 m depth (Ribeiro et al., 2021). However, despite Rignot et al. (2019) briefly noting a dramatic 17 km retreat of Vanderford Glacier's grounding line between 1996 and 2017, limited attention has been afforded to the potentially vulnerable Vincennes Bay outlet glaciers.

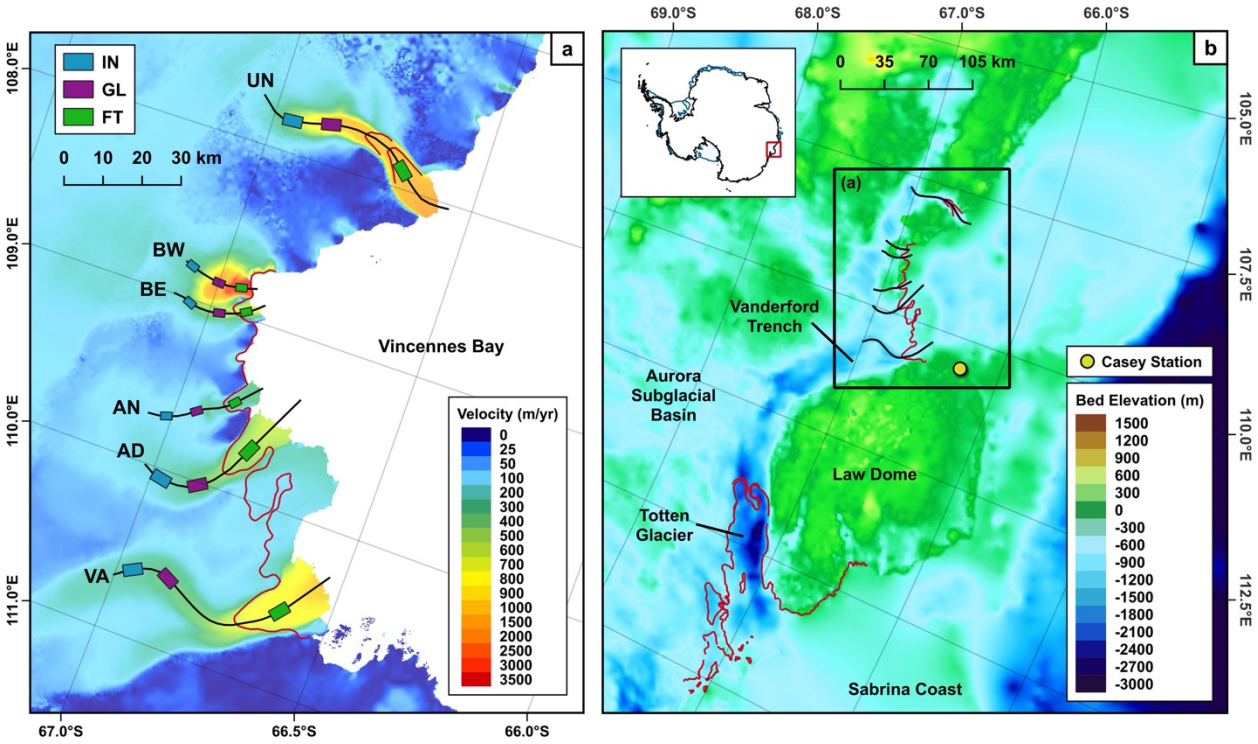

Figure 1. (a) Ice velocity map of Vincennes Bay extracted from the 2018 ITS_LIVE ice velocity mosaic (Gardner et al., 2022). Central flowlines are digitised down each of the studied glaciers: Vanderford (VA), Adams (AD), Anzac (AN), Bond East (BE), Bond West (BW), and Underwood (UN). Red lines display the 1996 MEaSUREs grounding line product (Rignot et al., 2016). Sampling boxes digitised across the inland (IN), grounding line (GL) and floating tongue (FT) areas are shown. **(b)** Location map of Vincennes Bay and the Aurora Subglacial Basin. Background represents the bed elevation extracted from BedMachine (Morlighem, 2020) and inset map shows the location of the Aurora Subglacial Basin within Antarctica.

1.2. Thesis aims and objectives

The overall aim of this project is to assess recent changes in the ice dynamics of the largely unstudied outlet glaciers located in Vincennes Bay, Wilkes Land. In order to achieve this aim, the following objectives were established:

1. To use remotely sensed satellite imagery to manually digitise the termini positions of the Vincennes Bay outlet glaciers between 1963 and 2022.
2. To use secondary datasets in order to assess changes in ice surface velocity across each of the Vincennes Bay outlet glaciers between 2000 and 2021.
3. To use secondary datasets in order to assess changes in ice surface elevation across each of the Vincennes Bay outlet glaciers between 1992 and 2020.
4. To use both differential satellite synthetic aperture radar interferometry (DInSAR) and secondary datasets in order to assess changes in the grounding line position of each of the Vincennes Bay outlet glaciers since 1996.
5. To explore potential forcing mechanisms of any observed dynamic changes.

1.3. Study area – Vincennes Bay

Vincennes Bay is defined as the shelf region located on the Wilkes Land coast between 104 and 111°E (Ribeiro et al., 2021). The bay overlies the northern Aurora subglacial basin and is drained by several marine-terminating outlet glaciers named Vanderford, Adams, Anzac, Bond, and Underwood (Figure 1a). Bond Glacier has two distinct outlets separated by an ice rise; these two outlets are referred to as Bond East and Bond West hereafter. Vanderford Glacier occupies the Vanderford Trench, a deep subglacial channel bounded to the north by the Law Dome ice cap (Davis et al., 1986; Morgan et al., 1997; Chen et al., 2011; Sun et al., 2016). The primary outlet of the Aurora subglacial basin, Totten Glacier, is also joined to this deep subglacial trough (Sun et al., 2016; Greenbaum et al., 2015), with ice flow diverted into the two respective tributaries along the flanks of Law Dome (Li et al., 2016) (Figure 1b). Two distinct polynya regions exist within Vincennes Bay, formed adjacent to the Vanderford and Underwood Glaciers, respectively (Ribeiro et al., 2021). This polynya system is thought to be an important, albeit relatively weak, source of Antarctic Bottom Water (AABW) for the Australian-Antarctic Basin (Kitade et al., 2014; Ribeiro et al., 2021).

1.4. Thesis structure

This thesis comprises six chapters following the introduction (**Chapter 1**). **Chapter 2** provides an overview of AIS mass balance using previously published literature, with a particular emphasis placed on both the past and predicted future mass balance of the EAIS. **Chapter 3** describes the methods employed in order to address objectives 1 – 4 outlined in Section 1.2. **Chapter 4** presents the findings of this project, with results separated according to the four fundamental glacier parameters assessed: terminus position, ice surface velocity, ice surface elevation, and grounding line position. **Chapter 5** then discusses these findings, exploring the potential forcing mechanisms driving any observed dynamic change, thereby addressing objective 5. This chapter also acknowledges the limitations of the study, before providing recommendations for future work within Vincennes Bay. **Chapter 6** summarises the findings of this project. It should be noted that **Chapters 3, 4, 5 and 6** are based on a research paper submitted for publication in *The Cryosphere,* drafted and lead-authored by HP (Picton et al., 2022). Within this thesis, these sections are largely identical to the paper, with the addition of minor grammatical changes and clearer acknowledgement of the direct contribution of Dana Floricioiu and Lukas Krieger.

Chapter 2. A review of Antarctic ice sheet mass balance

2.1. Introduction

Estimations of AIS mass balance are typically produced using one of three main techniques: (i) the input-output method (IOM), sometimes referred to as the mass budget or component method (Gardner et al., 2018), (ii) radar and laser altimetry (Shepherd et al., 2019), and (iii) satellite gravimetry (Sasgen et al., 2013; Harig & Simons, 2015). The IOM method compares the net difference between mass input, estimated using surface mass balance (SMB) model outputs (Hanna et al., 2020), and mass loss through ice discharge, calculated using observations of ice velocity across the grounding line (Gardner et al., 2018). The altimetry method employs measurements of surface elevation change obtained over repeat surveys (McMillan et al., 2015; Schröder et al., 2019; Shepherd et al., 2019; Smith et al., 2020); such measurements are then interpolated over a given region before being converted into a mass change (Hanna et al., 2020). The gravimetry method provides the most direct measurement of mass change (Hanna et al., 2020), using gravitational anomaly data collected from the Gravity Recovery and Climate Experiment (GRACE) twin satellites (Chen et al., 2009; Velicogna et al., 2014; Haring & Simons, 2015). However, each technique of mass balance estimation requires the use of uncertain forward models in order to make corrections for influential parameters such as rates of firn compaction or glacio-isostatic adjustment (GIA) (Chen et al., 2009; McMillan et al., 2015; Martín-Español et al., 2016; Gao et al., 2019). A wide range of AIS mass balance estimates have therefore been produced, often with large uncertainties (Martín-Español et al., 2016).

Whilst the estimated magnitude of AIS mass balance change has been highly variable, there is a widespread consensus that the overall direction of change has been negative, with the AIS losing mass at accelerating rates over recent decades (Gardner et al., 2018; Rignot et al., 2019). A reconciled estimate collated using 24 independent studies indicates that during the period 1992-2017, mass loss across the AIS occurred at a rate of 109 ± 56 Gt yr^{-1} (The IMBIE Team, 2018). However, such mass loss was highly spatially variable. The majority of studies suggest that recent mass loss primarily occurred from the WAIS (Martín-Español et al., 2016; Gardner et al., 2018; Schröder et al., 2019; Shepherd et al., 2019), with additional losses observed from the Antarctic Peninsula (AP) (Figure 2) (The IMBIE Team, 2018). In contrast, the recent mass balance of the EAIS has typically been estimated as either stable (Schröder et al., 2019), or slightly positive (Martín-Español et al., 2016; Gardner et al., 2018; The IMBIE Team, 2018; Shepherd et al., 2019), with rates of proposed mass change ranging from +3 ± 36 Gt yr^{-1} (2010 – 2013) (McMillan et al., 2015) to +90 ± 21 Gt yr^{-1} (2003 – 2019)

(Smith et al., 2020). However, Rignot et al (2019) have instead suggested that the EAIS has been a significant contributor to recent sea level rise, with mass loss estimated at a rate of 57.0 ± 2 Gt yr^{-1} between 1992 and 2017. With such contrasting estimates regarding both the magnitude and sign of change (Stokes et al., 2022), the mass balance of the EAIS therefore remains a considerable source of uncertainty regarding the accurate prediction of future sea level contributions from the AIS.

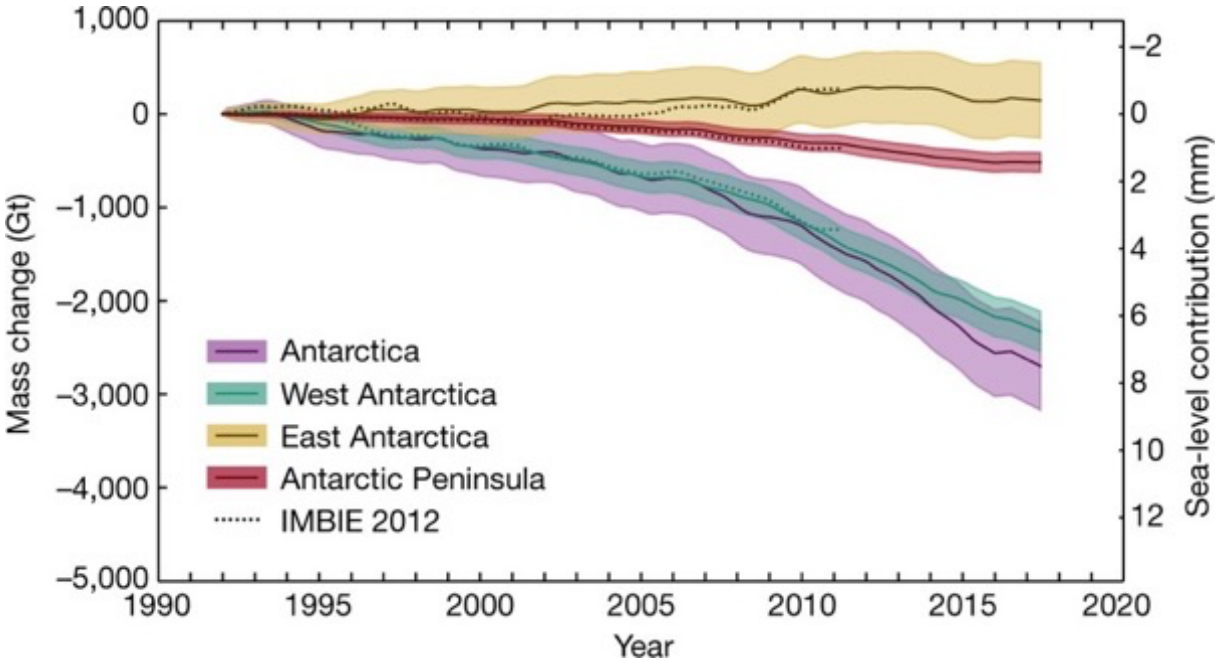

Figure 2. Estimated cumulative mass change across the AIS between 1992 and 2017, with shaded areas representing the estimated 1σ uncertainty (The IMBIE Team, 2018).

2.2. The Antarctic Peninsula

2.2.1. Oceanic forcing driving spatial variations in glacier retreat

The AP comprises a relatively small component of the overall ice mass of the AIS, containing an estimated SLE of 0.27 m (Morlighem et al., 2020). However, the AP represented one of the most rapidly warming regions on Earth between 1950 and 2020 (Sato et al., 2021), with surface air temperatures increasing by ~ 2.8 °C at Vernadsky Station over this 50 year period (Turner et al., 2016). Despite recent regional cooling (Oliva et al., 2017; Jones et al., 2019), the AP remains the only region of the AIS warm enough for widespread surface melt to occur (van Wessem et al., 2016). Analysis of 860 marine-terminating glaciers across the AP thus revealed extensive change over recent decades, with 91% measured to have retreated from their earliest recorded position (Cook et al., 2014a). Whilst this widespread pattern of retreat has been broadly attributed to atmospheric warming (Cook et al., 2005; Zhao et al., 2017), a clear north to south gradient of increasing mass loss is observed along the western coast

(Figure 3) (Cook et al., 2016). Cook et al. (2016) suggest that this spatial variation is related to ocean-induced melting, with the most extensive retreat seen across the southern glaciers exposed to warm CDW in the Bellingshausen Sea (Figure 3).

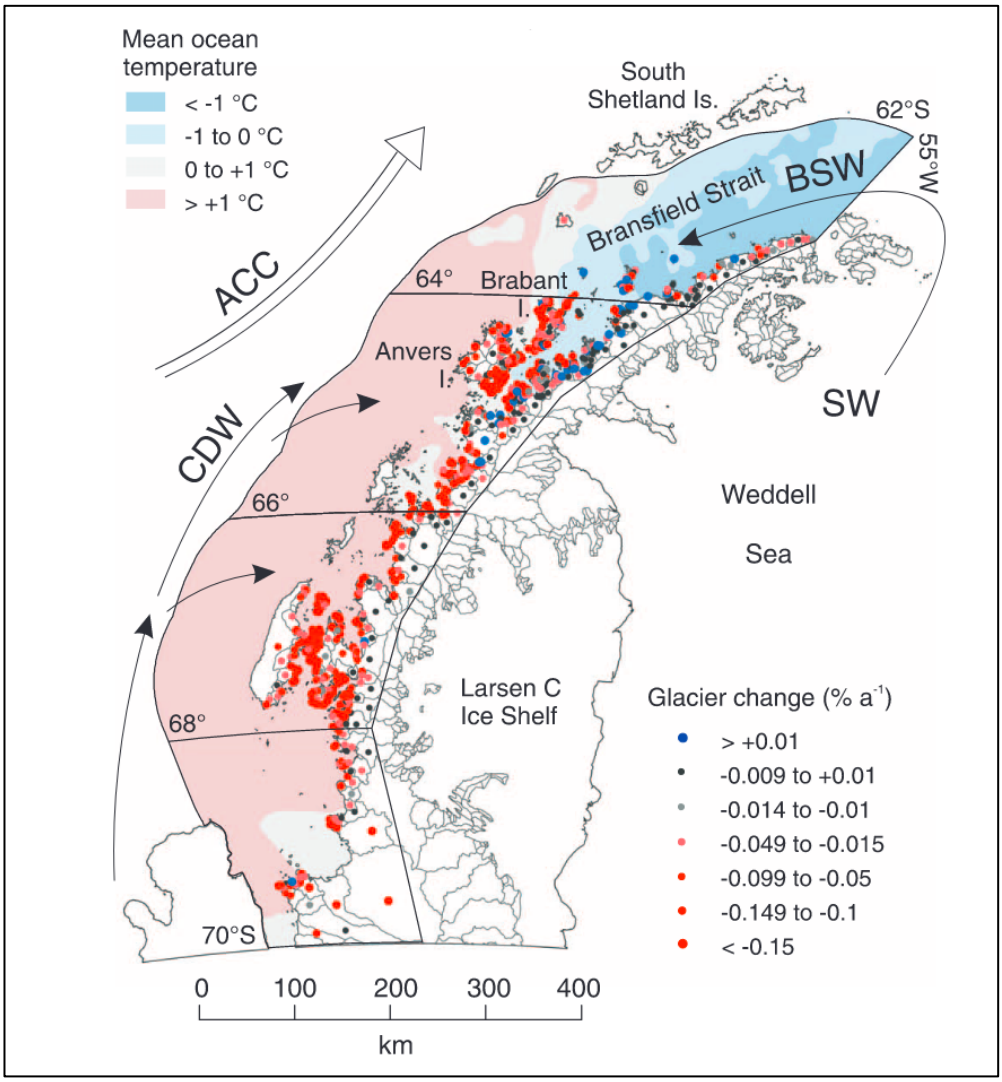

Figure 3. Mean ocean temperatures and overall glacier area changes measured between 1945 and 2009 across the western Antarctic Peninsula (Cook et al., 2016). Shaded areas reflect mean in situ ocean temperatures at a depth of 150 m, whilst points reflect the overall change in glacier frontal position, relative to the basin size. Schematic ocean circulation is shown, with Circumpolar Deep Water (CDW), Bransfield Strait Water (BSW), Shelf Water (SW), and the Antarctic Circumpolar Current (ACC) labelled.

2.2.2. Dynamic changes associated with ice shelf collapse

Enhanced discharge from the outlet glaciers of the AP has also been observed in response to dramatic ice shelf collapse events (Cook et al., 2014a; Rignot et al., 2004; Berthier et al., 2012), often driven by enhanced surface melting (van den Broeke, 2005). Surface meltwater may initiate ice shelf collapse through two primary mechanisms: (1) hydrofracture, described as the downward propagation of water-filled fractures (van der Veen, 2007), and (2) flexure, induced as supraglacial lakes fill and drain (Bell et al., 201 8). The spectacular disintegration

of the Larsen B Ice Shelf in 2002 is often attributed to this latter mechanism (Leeson et al., 2020), with more than 2750 supraglacial meltwater lakes observed to drain in the days prior to break up (Banwell et al., 2013). This collapse initiated significant dynamic change across the former tributary glaciers, with the Hektoria, Green and Evans Glaciers seen to accelerate eightfold in response to the loss of buttressing (Rignot et al., 2004). However, Shepherd et al. (2003) also emphasise the potential importance of oceanic forcing, arguing that ice shelf thinning inevitably enhances fracture propagation and thus likely preconditioned the Larsen Ice Shelf to collapse. Nonetheless, with the AP predicted to experience significant increases in surface melt under a high emissions scenario (Bell et al., 2018), further ice shelf collapse and associated increased ice discharge may be expected over the coming century.

2.3. The West Antarctic Ice Sheet

2.3.1. The marine ice sheet instability hypothesis

The WAIS is estimated to hold a SLE of 5.3 m (Morlighem et al., 2020) and is predominantly grounded below sea level (Figure 4). This marine ice sheet has hence long been considered inherently unstable (Weertman, 1974; Mercer, 1978), being vulnerable to complete collapse via a self-sustaining feedback termed the Marine Ice Sheet Instability (MISI) (Schoof, 2007), conceptualised in Figure 5 (Pattyn & Morlighem, 2020).

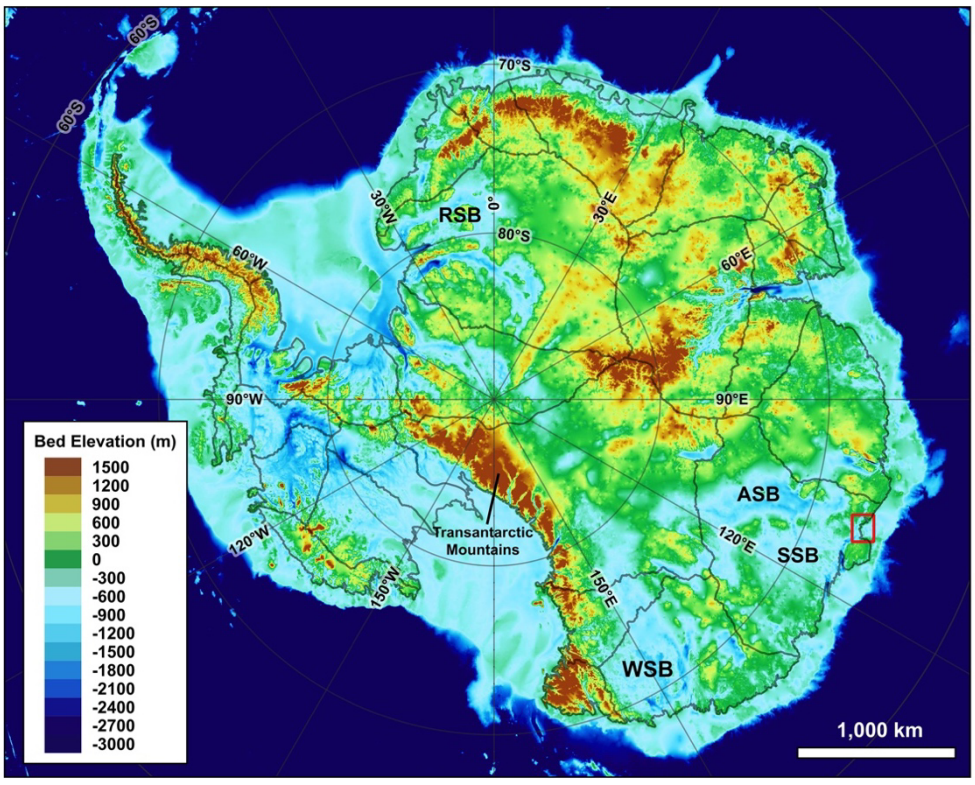

Figure 4. Bed elevation of the Antarctic Ice Sheet derived from BedMachine (Morlighem, 2020). Red box shows the location of Vincennes Bay, whilst the black lines display the grounded drainage system divides according to Zwally et al. (2012). The marine-based Wilkes Subglacial Basin (WSB), Sabrina Subglacial Basin (SSB), Aurora Subglacial Basin (ASB) and Recovery Subglacial Basin (RSB) are labelled.

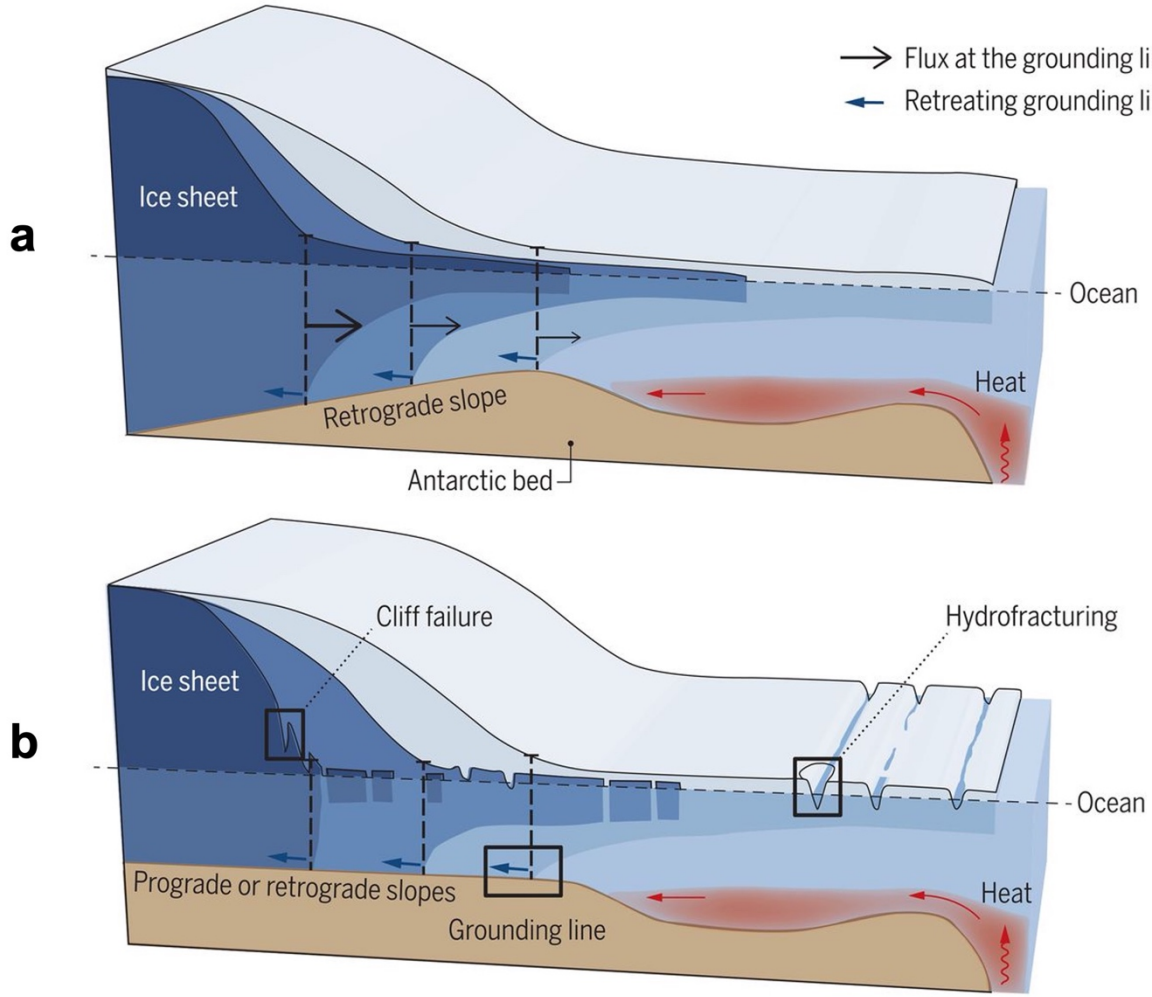

Figure 5. Schematic diagrams of **(a)** marine ice sheet instability (MISI), and (**b)** marine ice cliff instability (MICI) provided by Pattyn & Morlighem (2020).

The MISI hypothesis dictates that the rate of ice discharge across the grounding line of an unconfined ice shelf increases nonlinearly with ice thickness (Joughin & Alley, 2011). When an ice sheet is grounded on a retrograde bedrock slope, i.e. bed elevation decreases inland, minimal retreat of the grounding line position results in increased ice thickness across the grounding line and hence increased ice discharge (Joughin & Alley, 2011). This promotes thinning of the ice sheet and thus further grounding line retreat, initiating a positive feedback only halted once a prograde bedrock slope or pronounced bump is encountered (Durand et al., 2009; Pattyn & Morlighem, 2020). It is therefore argued that an ice sheet grounded on a retrograde bedrock slope cannot be stable (Schoof, 2007). With the WAIS characterised by such retrograde slopes, a small perturbation to the grounding line position therefore has the potential to initiate complete collapse of the marine ice sheet (Pattyn & Morlighem, 2020).

There is significant evidence that the WAIS has collapsed previously during the Pleistocene, but constraining the precise timing of such events remains challenging. Glacial sediment collected from boreholes below the Whillans Ice Stream revealed marine diatoms indicative of open-ocean conditions in the West Antarctic interior during at least one late Pleistocene interglacial (Scherer et al., 1998). As discussed previously, global sea levels are understood to have been at least 6.6 m higher than present during the last interglacial, MIS 5e (Kopp et al., 2009). Whilst a number of estimates have been made regarding the potential contribution from the GrIS (Colville et al., 2011; Robinson et al., 2011; Quiquet et al., 2013), Stone et al. (2013) suggest a very likely contribution between 0.3 and 3.6 m. Further contributions from thermal expansion and the melting of land-based glaciers are estimated at 0.4 m (McKay et al., 2011; Turney et al., 2020) and 0.3 m (Fox-Kemper et al., 2021) respectively. It is thus proposed that a partial or complete collapse of the WAIS must have occurred, providing the residual sea level contribution needed to produce the estimated MIS 5e highstand (Kopp et al., 2009; Sutter et al., 2016). With the last interglacial often described as a partial analogue for future climatic warming (Candy et al., 2016; Thomas et al., 2020; Turney et al., 2020), such evidence indicates that the WAIS could potentially be vulnerable to future collapse. It has recently been estimated that such collapse may be initiated at a temperature threshold of +1.5°C above pre-industrial levels (McKay et al., 2022).

2.3.2. Negative mass balance driven by oceanic forcing

The recent mass balance of the WAIS has been strongly negative, with mass loss occurring at an average rate of 94 ± 27 Gt yr^{-1} during the period 1992-2017 (The IMBIE Team, 2018). Mass loss has primarily been concentrated in the Amundsen Sea embayment (Feldmann & Levermann, 2015; Harig & Simons, 2015; McMillan et al., 2015; Gardner et al., 2018; Shepherd et al., 2019) (Figure 6), driven by increased discharge from the fast-flowing Pine Island and Thwaites Glaciers (Mouginot et al., 2014; Medley et al., 2014; Christianson et al., 2016; Yu et al., 2018). Ice flow acceleration (Mouginot et al., 2014; Sutterley et al., 2014) and dynamic thinning (Pritchard et al., 2009; Flament & Rémy, 2012) of these outlet glaciers has been attributed to enhanced ice shelf thinning and reduced buttressing, a process forced by the wind-driven intrusion of warm CDW across the continental shelf towards sub-ice shelf cavities (Feldmann & Levermann, 2015; Scambos et al., 2017; Rignot et al., 2019; Pattyn & Morlighem, 2020). Significant grounding line retreat has therefore been observed, averaged at a rate of 1.6 km yr^{-1} (1992-2011) (Rignot et al., 2014) and 0.8 km yr^{-1} (1992-2017) (Milillo et al., 2019) for the Pine Island and Thwaites Glaciers, respectively. Grounded on retrograde bedrock slopes well below sea level, there has been widespread concern that these glaciers

could be vulnerable to MISI (Joughin & Alley, 2011; Parizek et al., 2013; Nias et al., 2016; Lhermitte et al., 2020). Indeed, Favier et al. (2014), Rignot et al. (2014) and Joughin et al. (2014) suggest that such irreversible retreat may already be underway, potentially triggering another collapse of the WAIS. However, the significant uncertainty associated with ice sheet modelling makes it challenging to conclusively determine whether such a critical tipping point has been crossed (Sutter et al., 2016).

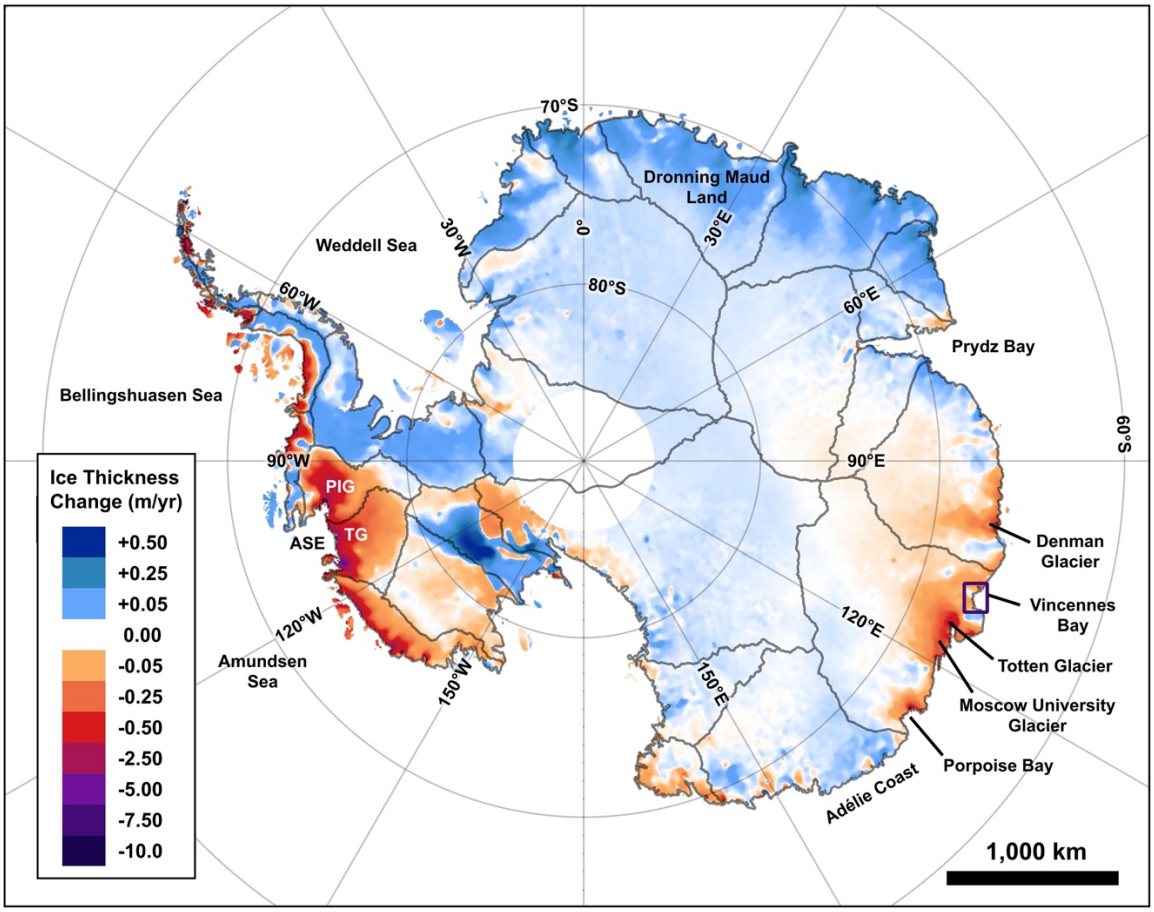

Figure 6. The rate of ice thickness change observed over the grounded areas of the Antarctic Ice Sheet between 2003 and 2019 (Smith et al., 2020). Purple box shows the location of Vincennes Bay, whilst the black lines display the grounded drainage system divides according to Zwally et al. (2012). TG = Thwaites Glacier, PIG = Pine Island Glacier, (ASE) = Amundsen Sea Embayment.

2.4. The East Antarctic Ice Sheet

2.4.1. The Oligocene and Miocene

The EAIS is an order of magnitude larger than the WAIS, holding an estimated SLE of 52.2 m (Morlighem et al., 2020). Whilst the EAIS is generally considered less sensitive to oceanic and climatic forcing, significant fluctuations in EAIS extent have occurred since the onset of widespread glaciation ~ 34 million years ago (Ma), influenced by orbital cycles (Naish et al., 2001; Young et al., 2011; Stokes et al., 2022). For example, the bedrock topography of the marine-based Aurora subglacial basin is characterised by a series of well-defined channels

(Figure 7a) (Young et al., 2011). This fjord landscape is interpreted to have been formed by an ice sheet configuration significantly different from that observed today, with the deepest edge of the EAIS located up to 700 km inland from the present ice sheet margin (Figure 7b) (Young et al., 2011). Whilst it remains challenging to constrain the precise timing of channel incision (Young et al., 2011), ice-sheet modelling simulates substantial mass loss from each of the marine Aurora, Wilkes, and Recovery subglacial basins (Figure 4) during the early to mid-Miocene (23–14 Ma) (Gasson et al., 2016). However, the climatic optimum of the mid-Miocene (17 – 14.5 Ma) was significantly warmer than today, with mean global temperatures estimated to be 7 – 8°C higher than observed at present (Steinthorsdottir et al., 2021).

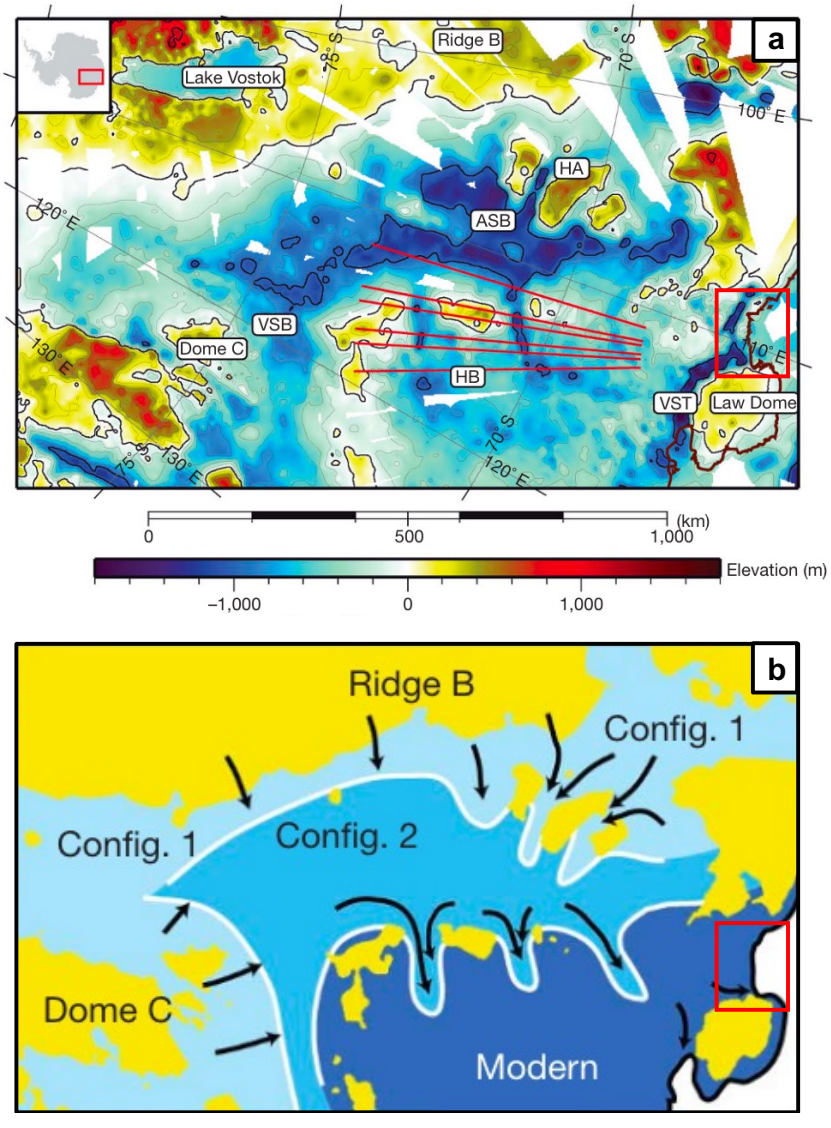

Figure 7. (a) Bed elevation of the Aurora Subglacial Basin derived by Young et al. (2011). Red box shows the location of Vincennes Bay, whilst the red lines show the position of radar profiles analysed by Young et al. (2011). VSB = Vincennes Subglacial Basin, ASB = Aurora Subglacial Basin, HA = Highland A, HB = Highland B, VST = Vanderford Subglacial Trench. **(b)** Potential ice sheet configurations during the early Miocene or Oligocene epoch inferred from the subglacial topography (Young et al., 2011).

2.4.2. The Pliocene

The mid-Pliocene warm period (3.3 – 3.0 Ma) is often used as a potential analogue for future climatic conditions, with mean global temperatures estimated to be just 2 – 3°C warmer than present (Dowsett, 2007; Haywood et al. 2011), and atmospheric CO_2 concentrations similar to current levels, ranging from 330 to 400 ppm (Seki et al., 2010). Whilst significant modelling uncertainty precludes the accurate prediction of eustatic sea level rise during this interglacial (Dutton et al., 2015), Miller et al. (2012) estimated that global sea level was likely 22 ± 5 m higher than the current highstand, therefore requiring a significant contribution from the EAIS (Cook et al., 2013; Grant et al., 2019). Nonetheless, the stability of the EAIS has been the focus of significant contention over recent decades, with discussions between 'stabilists' and 'dynamicists' often being referred to as the Sirius debate (Barrett, 2013).

The Sirius debate began in the 1980s following the discovery of Pliocene-age marine diatoms within tillites extracted from the Transantarctic Mountains (Figure 4), collectively referred to as the Sirius Group (Webb et al., 1984; Scherer et al., 2016). Webb et al. (1984) argued that such diatoms had accumulated in the deep marine subglacial basins of the EAIS during a Pliocene warm period, before being transported and redeposited within the Transantarctic Mountains during subsequent ice sheet readvance. However, with these marine diatoms largely concentrated in the upper surface diamicton and seen to decrease in abundance with depth, Bleakley (1996), Kellogg & Kellogg (1996) and Stroeven et al. (1996) all refuted this suggestion, instead proposing that the diatoms had been deposited through aeolian transport. With the diatoms found across various outcrops in South Victoria Land (Bleakley, 1996; Stroeven et al., 1996) and within an ice core drilled at the South Pole (Kellogg & Kellogg, 1996), a critical question therefore remained as to how such apparently windblown diatoms represented the same Pliocene assemblage.

Recent modelling conducted by Scherer et al. (2016) suggests that aspects of both opposing theories could be reconciled. Scherer et al. (2016) simulate that extensive retreat within both the Wilkes and Aurora subglacial basins (Figure 4) allowed for deposition of marine diatoms during the Pliocene epoch. Subsequent isostatic uplift is thought to have then exposed these unconsolidated marine deposits, thus facilitating their transport and emplacement within the Transantarctic Mountains via aeolian processes (Scherer et al., 2016). Evidence for such retreat within the Wilkes subglacial basin is provided by Cook et al. (2013); the geochemical provenance of detrital material recovered off the Adélie Coast (Figure 6) is indicative of the

active erosion of continental bedrock, hence requiring substantial retreat of the EAIS margin. Analysis of ice-rafted detritus (IRD) observed within marine sediments extracted from Prydz Bay (Figure 6) also provides evidence of significant retreat within the Aurora subglacial basin (Williams et al., 2010; Cook et al., 2014b). Pulsed increases in IRD are interpreted to reflect the enhanced delivery of icebergs associated with large-scale destabilisations of the Aurora subglacial basin during Pliocene interglacials (Williams et al., 2010; Cook et al., 2014b). It is therefore thought that the marine-based basins of the EAIS may be vulnerable to predicted future warming (Cook et al., 2013; Scherer et al., 2016). However, it is important to recognise that the majority of models capable of simulating extensive mid-Pliocene retreat of the EAIS require further parameterisations in order to accelerate mass loss (Gasson & Keisling, 2020; Stokes et al., 2022), often including the debated feedback of marine-ice-cliff instability (MICI) (Pollard et al., 2015; Scherer et al., 2016) (Figure 5). This feedback is premised on the notion that tall ice cliffs are inherently unstable and thus may rapidly collapse following an ice shelf disintegration event, however the process remains controversial (Edwards et al., 2019).

2.4.3. The Pleistocene

Geological evidence also suggests that the marine-based margin of the EAIS was oscillatory during the Pleistocene (2.58 – 0.0117 Ma), with significant retreat inferred across the Wilkes subglacial basin (Figure 4) (Wilson et al., 2018; Blackburn et al., 2020; Stokes et al., 2022). Analysis of Uranium-234 accumulation, recorded within the subglacial chemical precipitates of opal and calcite, indicates that the Wilkes basin experienced significant mass loss during MIS 11, an interglacial period approximately 400,000 years before present (Blackburn et al., 2020). Blackburn et al. (2020) estimate that such mass loss resulted in the ice sheet margin retreating around 700 km inland from the present grounding line, contributing an estimated 3 – 4 m to global sea level rise (Mengel & Levermann, 2014). Whilst the extent of EAIS mass loss during the last interglacial period (MIS 5e) is more uncertain (Noble et al., 2020; Stokes et al., 2022), Wilson et al. (2018) suggest that variations in sediment provenance observed off the coast of the Wilkes subglacial basin are indicative of ice marginal retreat during each of the late Pleistocene interglacials. However, Sutter et al. (2020) simulate that the sea level contribution from the Wilkes basin was relatively limited during the last interglacial compared to MIS 11, estimated between 0.4 and 0.8 m. Sutter et al. (2020) therefore suggest that the majority of sea level rise observed during MIS 5e was instead derived from the WAIS.

2.4.4. Recent mass balance

The recent mass balance of the EAIS is typically estimated as either stable (Schröder et al., 2019), or slightly positive (Martín-Español et al., 2016; Gardner et al., 2018; The IMBIE Team, 2018; Shepherd et al., 2019), however significant spatial variation has been observed (Figure 6). Substantial mass gain has been concentrated in the Dronning Maud Land region (Velicogna et al., 2014; Harig & Simons, 2015; Martín-Español et al., 2016; Gardner et al., 2018), thought to be driven by increased precipitation events related to atmospheric blocking over the Atlantic sector of Antarctica (Boening et al., 2012). This region is thus estimated to have increased in mass by nearly +500 Gt between 2008 and 2014 (Velicogna et al., 2014). Whilst the majority of outlet glaciers draining the EAIS have been stable over recent decades (Gardner et al., 2018), recent studies have shown evidence of dynamic mass loss from some of the major outlet glaciers draining the Aurora subglacial basin along the Wilkes Land coast (Figure 6) (McMillan et al., 2015; Martín-Español et al., 2016; Smith et al., 2020; Miles et al., 2021; Wang et al., 2021; Stokes et al., 2022). For example, the main outlet of Wilkes Land, Totten Glacier (Figure 6), contains a SLE of 3.9 m (Li et al., 2015) and is estimated to have lost -236 Gt of ice between 1979 and 2017 (Rignot et al., 2019). In addition, Denman Glacier (1.5 m SLE) (Miles et al., 2021), and Moscow University Glacier (1.3 m SLE) (Mohajerani et al., 2018) (Figure 6), are also estimated to have lost -191 and -93 Gt of ice respectively over the same time period (Rignot et al., 2019).

2.4.5. Dynamic mass loss from Wilkes Land

Wilkes Land is characterised by a 'warm shelf' regime, whereby weaker easterly winds and an absence of dense shelf water formation facilitates the intrusion of warm mCDW onto the continental shelf (Thompson et al., 2018; Stokes et al., 2022). Ribeiro et al. (2021) describes such mCDW as a warm and relatively saline water mass, with a neutral density between 28 and 28.27 kg m^{-3} and an average temperature ranging from -1.7 to 1.5 °C. The recent increase in mass loss across Wilkes Land has thus primarily been linked to the enhanced intrusion of such mCDW towards sub-ice shelf cavities, accessed through deep subglacial troughs (Miles et al., 2016; Shen et al., 2018). For example, increased ice discharge (Rignot et al., 2019) and dynamic thinning (Pritchard et al., 2009; Flament & Rémy, 2012; Li et al., 2016; Shepherd et al., 2019; Schröder et al., 2019) across Totten Glacier has been correlated to enhanced rates of basal melt below the Totten Ice Shelf (Roberts et al., 2018; Pelle et al., 2021), estimated to range from 10.5 ± 0.7 m yr^{-1} (2003-2008) (Rignot et al., 2013) to 17.9 ± 1.2 m yr^{-1} (2005-2011) (Liu et al., 2015). Such enhanced basal melt rates have been attributed to a number of different forcings, including reduced polynya formation

(Khazender et al., 2013; Gwyther et al., 2014; Miles et al., 2016; Li et al., 2016), enhanced polar westerlies (Spence et al., 2014; Li et al., 2015; Greene et al., 2017; Rignot et al., 2019) and increased rates of basal melting beneath the nearby Dalton Ice Shelf (Gwyther et al., 2014). Whilst the mechanism of each of these processes varies, they share a common fundamental outcome of increasing the volume of warm mCDW intruding into the Totten Ice Shelf cavity, thereby facilitating enhanced basal melt. It is therefore increasingly recognised that oceanic forcing has the potential to drive dynamic glaciological change along the Wilkes Land coastline (Stokes et al., 2022).

2.4.6. Potential oceanic forcing in Vincennes Bay

The warmest and most widespread intrusion of mCDW recorded within East Antarctica was observed within Vincennes Bay (Figure 1) (Ribeiro et al., 2021). However, despite Rignot et al. (2019) briefly noting a spectacular 17 km retreat of Vanderford Glacier's grounding line between 1996 and 2017, the Vincennes Bay outlet glaciers remain largely unstudied (Stokes et al., 2022). Nonetheless, recent analysis of data obtained using 22 instrumented elephant seals revealed ocean temperatures higher than -0.5ºC are able to reach the Vanderford Ice Shelf, potentially capable of driving basal melting (Ribeiro et al., 2021). Ribeiro et al. (2021) therefore suggest that a positive feedback may be initiated, whereby continued freshwater input from basal melt could limit the formation of Dense Shelf Water (DSW) in the Vanderford polynya, thus strengthening water column stratification and enabling the enhanced intrusion of warm mCDW at depth. Recent analysis by Herraiz-Borreguero & Garabato (2022) shows that this potential feedback may already be underway, with an observed decline in DSW concurrent with consistent sea ice production indicative of increased penetration of mCDW within Vincennes Bay. Whilst Vanderford is currently grounded on a prograde bedrock slope (Rignot et al., 2019), it overlies the Vanderford Trench (Figure 1b), a deep subglacial trough characterised by an inland retrograde bedrock slope (Davis et al., 1986; Chen et al., 2011; Sun et al., 2016). Ice sheet modelling simulates that retreat of the grounding line beyond the present stabilising bedrock ridge may thus initiate future MISI (Sun et al., 2016).

2.4.7. Future projections of EAIS mass balance

The future response of the EAIS remains the most significant source of uncertainty regarding the prediction of potential sea level contributions from the AIS (Figure 2) (The IMBIE Team, 2018). The recent Ice Sheet Model Intercomparison Project (ISMIP6) (Seroussi et al., 2020) provides the most comprehensive prediction of AIS evolution (Stokes et al., 2022), applying ice flow simulations developed by 13 different international modelling groups. The simulated

evolution of the AIS varies significantly between each respective model, with the estimated sea level contribution from the EAIS (2015-2100) ranging from -6.1 cm to +8.3 cm (Seroussi et al., 2020). Statistical emulation of the ISMIP6 projection reduces this uncertainty, however the overall signal of future mass balance remains unclear (Edwards et al., 2021); forced by a medium-emissions scenario, SSP2-4.5 (Shared Socioeconomic Pathway), the EAIS sea level contribution (2015-2100) is estimated to range between -4.3 and +7.0 cm (Edwards et al., 2021). The main source of such uncertainty is the challenge associated with attempting to predict the complex balance between mass input to the system, and dynamic loss (Stokes et al., 2022). Future trends of mass input are difficult to predict, with recent trends subject to extreme inter-annual variability, whilst dynamic loss will likely be highly dependent on future oceanic conditions and the associated sensitivity of basal melting (Stokes et al., 2022).

Despite the uncertainty associated with the potential future evolution of the EAIS, a number of models simulate extensive retreat across the marine-based subglacial basins, particularly under high-emissions scenarios (Golledge et al., 2015; DeConto & Pollard, 2016; Sun et al., 2020; DeConto et al., 2021). Golledge et al. (2015) used a coupled ice sheet/ice shelf model in order to simulate the response of the AIS to the oceanic and climatic forcing represented in the IPCC's Representative Concentration Pathways (RCP) scenarios. A high-emissions scenario (RCP8.5) was observed to simulate substantial mass loss in East Antarctica, with extensive grounding line retreat seen within the Wilkes and Aurora subglacial basins (Figure 8). Golledge et al. (2015) also emphasised that the inclusion of polar amplification, i.e. near surface air temperatures warming more rapidly at polar latitudes compared to lower latitudes (Graversen & Wang, 2009), resulted in grounding line retreat into the Wilkes subglacial basin under both low (RCP2.6) and high (RCP8.5) emissions scenarios.

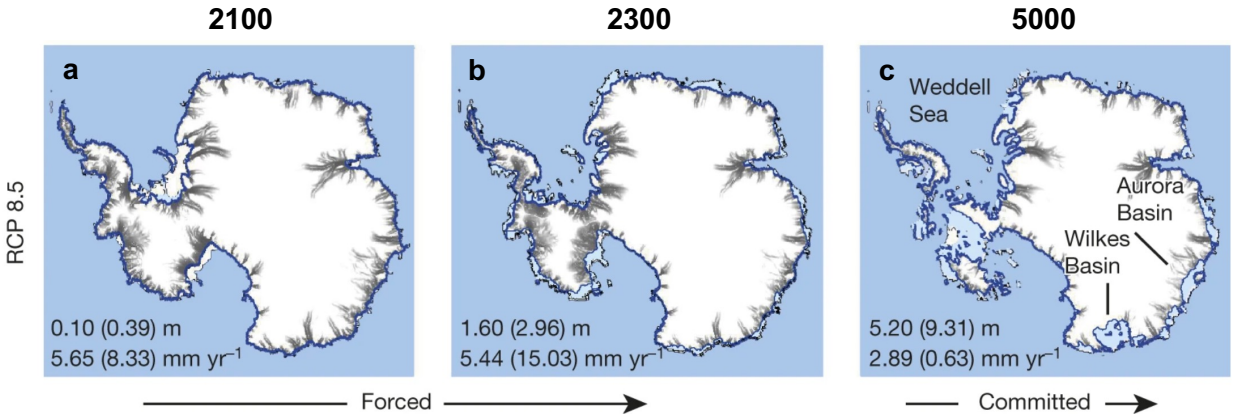

Figure 8. Simulated evolution of the AIS under a high-emissions scenario (RCP8.5) by the year **a)** 2100, **b)** 2300, and **c)** 5000 (Golledge et al., 2015). Magnitude and rates of sea-level contribution are shown for each panel; leading values and those in parentheses represent 'low' and 'high' scenarios, respectively.

DeConto & Pollard (2016) applied an ice sheet model constrained using sea level estimates from the Pleistocene and last interglacial in order to simulate future AIS evolution under the same RCP scenarios used by Golledge et al (2015). However, the model used by DeConto & Pollard (2016) included dynamic processes such as meltwater-induced hydrofracture and MICI. The model results simulated that retreat of the Wilkes subglacial basin and Law Dome sector occurred under a medium-emissions scenario (RCP4.5) (Figure 9), with an estimated global sea level contribution of 5 m by 2500. This retreat accelerated under a high-emissions scenario (RCP8.5), with a sea level contribution of 12.3 m projected by 2500.

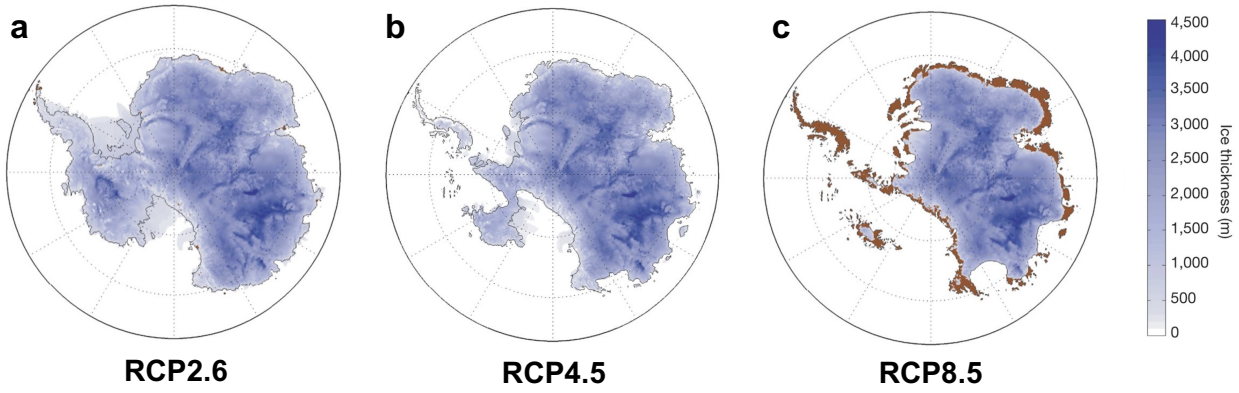

Figure 9. Simulated evolution of the AIS by 2500 under **a)** RCP2.6, **b)** RCP4.5, and **c)** RCP8.5 (DeConto & Pollard, 2016). Ice free land surfaces are shown in brown. Note the extensive retreat of the Wilkes and Aurora subglacial basins under a high-emissions scenario.

DeConto et al. (2021) recently built on the work of DeConto & Pollard (2016), improving the ice sheet model with new formulations of ice shelf buttressing and hydrofracturing, including additional viscous and brittle processes related to MISI and MICI, respectively (Figure 5). The outputs of the model supported the previous findings of DeConto & Pollard (2016), with thinning and hydrofracturing triggering MISI within the marine subglacial basins of the EAIS under a high emissions (RCP8.5) scenario (DeConto et al., 2021). Sun et al. (2020) also simulated the potential impact of the removal of Antarctica's floating ice shelves, resulting from either high sub-shelf melt rates or sustained and complete collapse. Whilst deliberately unrealistic, the Antarctic Buttressing Model Inercomparison Project (ABUMIP) thus allowed specific assessment of the full potential of MISI (Sun et al., 2020). The 15 different ice sheet models used showed a range of responses, however a number simulated extensive mass loss within the Wilkes, Recovery and Aurora subglacial basins. However, Sun et al. (2020) highlight that the measured standard deviation was highest within the Wilkes and Aurora subglacial basins, indicative of a high level of disagreement between each model.

Whilst the future evolution of the AIS remains uncertain, geological evidence indicates that the marine-based sectors of the EAIS have been unstable during previous warm interglacial periods. Although the tipping point of such instability remains unknown, Stokes et al. (2022) suggest that a temperature increase of +2.0°C above pre-industrial levels could represent a potentially critical threshold. Indeed, McKay et al. (2022) estimate that the subglacial basins of the EAIS may collapse completely in response to +3.0°C of warming. A range of numerical models also support the notion that climatic warming has the potential to initiate extensive mass loss across the Wilkes, Recovery and Aurora subglacial basins (Golledge et al., 2015; DeConto & Pollard, 2016; Sun et al., 2020; DeConto et al., 2021). It is therefore paramount that ice dynamics within these marine basins are fully understood, with early-warning signs of dynamic change, such as ice flow acceleration or grounding line retreat, closely monitored (Stokes et al., 2022). This is particularly pertinent for the Vincennes Bay outlet glaciers which are understood to abut the warmest intrusions of mCDW ever recorded in East Antarctica (Ribeiro et al., 2021).

Chapter 3. Methods

Evidence for recent dynamic change in Vincennes Bay was assessed through the analysis of four fundamental glacier parameters:

1. **Terminus Position** – Manually digitised from satellite imagery.
2. **Ice surface velocity** – Extracted from ITS_LIVE (Inter-Mission Time Series of Land Ice Velocity and Elevation) (Gardner et al., 2022) and ENVEO (Environmental Earth Observation) (ENVEO, 2021) velocity mosaics.
3. **Ice surface elevation** – Assessed using surface elevation change datasets provided by Schröder et al. (2019), Smith et al. (2020) and Nilsson et al. (2022).
4. **Grounding line position** – Mapped using DInSAR techniques and downloaded from datasets provided by Haran et al. (2005; 2014; 2018), Bindschadler et al. (2011) and Rignot et al. (2016).

3.1. Terminus position image acquisition

A combination of Landsat 1, 4, 5, 7 and 8, Sentinel-2A and Sentinel-2B images (1973 – 2022) were downloaded from the USGS EarthExplorer (https://earthexplorer.usgs.gov), with the majority of images selected from the austral summer months of December - February (Appendix 1). With each of the Vincennes Bay glaciers occupying a proportionally small area of each scene, cloud cover thresholds were not applied; instead, images were manually inspected to ensure cloud cover did not obscure the terminus. Application of a crude cloud cover threshold may have resulted in images with some visible termini being unnecessarily omitted. The Landsat 1, 4 and 5 scenes were each co-registered to a Sentinel-2B scene collected in 2021. Ground control points (GCPs) digitised across coastal rock outcrops, nunataks, and visibly stable ice features (Glasser et al., 2011) were then used in order to apply a first-order polynomial transformation with nearest neighbour resampling (Miles, 2013). An orthorectified mosaic of Antarctica assembled using declassified ARGON satellite photographs collected in 1963 was also downloaded (Kim et al., 2007). The spatial resolution of imagery used in this study therefore ranged from 10 to 140 m (Appendix 1).

3.2. Terminus position mapping

Annual terminus positions were manually digitised within QGIS. In May 2003, failure of the Scan Line Corrector onboard the Landsat 7 satellite resulted in striped data loss (Paul et al., 2017), however the majority of these gaps were observed to be perpendicular to the studied glacier termini. In these cases, terminus positions were thus digitised across the data gaps, with temporally close images with alternative striping patterns used in order to inform each

digitisation (Black & Joughin, 2022). Once digitised, changes in terminus position were quantified by applying the well-established box method outlined by Moon & Joughin (2008). This method accounts for asymmetrical changes across glacier termini, using an open-ended box digitised across the main region of ice flow. Errors associated with this method of analysis arise from the co-registration of satellite imagery, generally estimated at 1 pixel, and manual digitisation of the terminus position, typically calculated as 0.5 pixels (Miles et al., 2018; Miles et al., 2021; Black & Joughin, 2022). The total estimated error was therefore calculated as 1.5 pixels; when applied to the spatial resolution of imagery previously stated, estimated errors thus ranged between 15 and 210 m (Appendix 1).

3.3. Ice surface velocity

With a lack of suitable data prior to 2000, the ITS_LIVE (Gardner et al., 2022) and ENVEO (ENVEO, 2021) datasets were used to extract ice surface velocity between 2000 and 2021. ITS_LIVE velocity mosaics are available at an annual resolution between 2000 and 2018 and were derived from Landsat 4, 5, 7 and 8 imagery using auto-RIFT algorithms (Gardner et al., 2018). The autonomous Repeat Image Feature Tracking (auto-RIFT) algorithm is an open-source Python module capable of calculating ice velocity through the analysis of pixel displacement between two images (Gardner et al., 2018). Each annual velocity mosaic has a spatial resolution of 240 m and reflects the error weighted average of all image-pairs with a centre date that falls within that calendar year (Gardner et al., 2022). In contrast, ENVEO velocity mosaics are provided at a monthly resolution between 2019 and 2021 and were derived from repeat-pass Sentinel-1 synthetic aperture radar (SAR) data using feature tracking techniques (Nagler et al., 2015). Each of the monthly velocity mosaics has a spatial resolution of 200 m and was processed using the ENVEO software package (ENVEO, 2021). In order to allow for comparison to the ITS_LIVE annual velocity mosaics, mean velocity across each 12-month period was calculated.

Ice surface velocity profiles were extracted along central flowlines manually digitised along each main glacier trunk (Figure 1a). Each longitudinal profile was sampled at an interval spacing of 240 m, reflecting the coarsest spatial resolution of the two velocity datasets used. To analyse changes in ice surface velocity over time, mean annual velocity was extracted from within defined boxes for each given year. In order to assess the spatial variability in ice velocity, three sampling boxes were defined across each glacier; the first box was positioned on the floating tongue (FT), the second located immediately up-glacier of the most landward observed grounding line position (GL), and the third placed inland a further 5 km upstream

(IN) (Figure 1a). Each box remained static over time. It must therefore be noted that the GL box was intended to capture ice dynamics across a grounded section of the primary glacier flow, rather than analysing dynamics across the transient grounding zone. The GL box was hence placed immediately up-glacier of the most landward observed grounding line position in order to ensure that the ice was grounded at each time step. A potential limitation of this static placement is that an observed change in ice surface velocity could be misinterpreted as a change in ice dynamics, rather than being recognised as a product of the box position changing relative to the transient grounding line. This limitation was thus considered when analysing and interpreting any observed changes within the GL box.

The sampling boxes placed over the larger Vanderford, Adams and Underwood Glaciers each covered an area of 15 km^2, whilst the sampling boxes placed across the smaller Anzac, Bond East, and Bond West Glaciers each had a proportionally smaller area of 6 km^2. Gardner et al. (2022) emphasise that data scarcity is a significant limiting factor in the early ITS_LIVE product, with the auto-RIFT processing chain being limited by the number of image-pairs available across any given year. Such incomplete coverage was seen across the Vincennes Bay outlet glaciers, particularly prior to the launch of Landsat 8 in February 2013. Average annual velocity values were therefore only extracted from each respective FT, GL and IN box if greater than 25% data coverage was observed (Appendix 2).

The errors associated with each velocity measurement were also provided at the pixel scale. The mean velocity error was thus extracted from within each FT, GL and IN box across each given year. The velocity errors provided for each ITS_LIVE velocity mosaic were calculated according to the technical details outlined by Gardner et al. (2022). The errors are updated following co-registration and represent the standard deviation of the difference between the image-pair component velocities and the annual mean component velocities (Gardner et al., 2022). The uncertainty associated with each ENVEO velocity mosaic reflects the standard deviation of the calculated ice velocity magnitude, provided for both the northing and easting components (ENVEO, 2021). Velocity measurements were not included within the analysis if the mean error extracted across each box was calculated to be more than 50% of the mean velocity magnitude. However, this threshold resulted in the omission of just 5% of velocity measurements, largely concentrated across Bond West Glacier (Appendix 2).

3.4. Ice surface elevation

Variations in ice surface elevation were analysed using ice surface elevation datasets provided by Schröder et al. (2019), Smith et al. (2020) and Nilsson et al. (2022). Schröder et al. (2019) calculated the monthly surface elevation change (SEC) observed between 1978 and 2017, relative to the reference epoch 09/2010. SEC measurements were provided at a horizontal resolution of 10 km and were obtained using combined altimetry data from each of the Seasat, Geosat, ERS-1, ERS-2, Envisat, ICESat and CryoSat-2 satellite missions (Schröder et al., 2019). Similarly, Nilsson et al. (2022) calculated the monthly SEC seen between 1985 and 2020, relative to the reference epoch 12/2013. Produced as part of NASA's ITS_LIVE project, SEC measurements were provided at a horizontal resolution of 1,920 m and included additional altimetry data from the ICESat-2 mission, launched in October 2018, thus facilitating further coverage between 2018 and 2020 (Nilsson et al., 2022). Mean monthly SEC values provided by both Schröder et al. (2019) and Nilsson et al. (2022) were extracted from each respective grounded GL and IN box. In order to allow comparison between the two datasets, all monthly SEC measurements were calculated relative to 09/1992, representing the earliest shared epoch for which data coverage was seen across all of the Vincennes Bay glaciers. Elevation anomalies were then calculated relative to the long-term mean derived from each respective dataset between 1992 and 2017.

The ice surface elevation dataset provided by Smith et al. (2020) represents the rate of SEC observed between 2003 and 2019, provided at a horizontal resolution of 5 km using altimetry data from the ICESat and ICESat-2 satellite missions. The mean rate of SEC observed over this period was extracted from each GL and IN box. In order to allow for comparison across all three elevation datasets, mean rates of SEC were also calculated from the monthly SEC data provided by Schröder et al. (2019) and Nilsson et al. (2022), extracted between 2003 and 2017 and 2003 and 2019, respectively.

3.5. Grounding line position

Grounding line positions were derived by Dana Floricioiu and Lukas Krieger at the Remote Sensing Technology Institute (IMF) of the German Aerospace Center (DLR). DInSAR techniques were applied in order to delineate grounding line positions from ERS-1, ERS-2, and Sentinel-1 imagery collected between 1996 and 2020, carried out as part of the European Space Agency's Antarctic Ice Sheet Climate Change Initiative (AIS CCI). Satellite imagery used within this study is outlined below (Table 1).

Satellite	Relative orbit/ Pass Direction	T1	T2	T3
ERS	231/D	1996-04-10	1996-04-11	-
Sentinel-1	133/D	2016-06-29	2016-07-11	2016-07-23
Sentinel-1	99/A	2017-07-22	2017-07-28	2017-08-03
Sentinel-1	99/A	2017-12-01	2017-12-07	2017-12-13
Sentinel-1	99/A	2017-12-07	2017-12-13	2017-12-19
Sentinel-1	70A	2020-11-13	2020-11-19	2020-11-25
Sentinel-1	70A	2020-11-19	2020-11-25	2020-12-01

Table 1. ERS and Sentinel-1 acquisitions used for interferogram generation in the Vincennes Bay region. Relative orbits and pass direction are stated, with A and D representing ascending and descending pass directions, respectively. T1, T2 and T3 refer to the dates of scenes used for interferogram pairs; T2 was chosen as the primary scene, with two interferograms T2-T1 and T2-T3 then formed. In the case of the ERS satellite, the grounding line was delineated directly on a 1-day repeat pass interferogram.

DInSAR processing is based on the notion that the vertical motion of an ice shelf and hence the hinge line, representing the landward limit of ice flexure, can be observed from a single interferogram (Goldstein et al., 1993). However, the exact location of the hinge line is often obscured by phase contributions due to horizontal ice displacement and topography. Three consecutive repeat pass acquisitions are therefore typically used in order to form two interferograms. The difference of such interferograms eliminates the phased contributions from horizontal ice displacement, when assuming a constant ice velocity throughout the observed time period (Rignot, 1996), thereby revealing a dense fringe belt at the grounding zone. The landward limit of this fringe belt is then delineated as the interferometrically derived grounding line position. Within the AIS CCI programme, a processing workflow has been developed in order to systematically map the grounding line of the AIS using the Sentinel-1 SAR constellation. In order to reduce the temporal decorrelation due to changing surface conditions, acquisitions from Sentinel-1 A and B (6-day repeats) were favoured wherever available.

A number of secondary grounding line datasets were also employed (Table 2). The Making Earth Science Data Records for Use in Research Environments (MEaSUREs) grounding line product was provided using similar DInSAR techniques as previously described for the AIS CCI product, also applied to ERS-1 and ERS-2 imagery collected in 1996 (Rignot et al., 2016). Whilst localised variations in positional accuracy are observed (Rignot et al., 2011), the MEaSUREs grounding line product had an associated standard error of ± 100 m (Rignot et al., 2016) (Table 2).

Dataset	Date	Method	Error (m)
AIS CCI	1996 2016 2017 2020	Grounding line derived using differential satellite synthetic aperture radar interferometry from ERS-1, ERS-2, and Sentinel-1 imagery.	± 200
MEaSUREs (Rignot et al., 2016).	1996	Grounding line derived using differential satellite synthetic aperture radar interferometry from ERS-1 and ERS-2 imagery.	± 100
ASAID (Bindschadler et al., 2011)	2001 (1999 – 2003)	Manually digitisation of break-in-slope using observable change in image brightness from Landsat 7 imagery, aided by ICESat surface elevation profiles.	± 502
MOA (Haran et al., 2005; 2014; 2018)	2004 2009 2014	Manually digitised break-in-slope from contrast-enhanced imagery derived from the 2004, 2009 and 2014 Mosaics of Antarctica.	± 250

Table 2. Details of the different mapping methods employed to derive each of the grounding line datasets used in this study. Note that the MEaSUREs, ASAID and MOA products represent secondary datasets.

The Antarctic Surface Accumulation and Ice Discharge (ASAID) grounding line dataset was provided through manual delineation of the most seaward break-in-slope, observed using a combination of Landsat-7 images collected between 1999 and 2003, and surface elevation data obtained from the ICESat satellite mission (Bindschadler et al., 2011). At outlet glacier boundaries such as those studied within Vincennes Bay, the ASAID grounding line dataset had an estimated positional error of ± 502 m (Bindschadler et al., 2011). The Mosaic of Antarctica (MOA) grounding lines were also provided through the manual digitisation of the most seaward break-in-slope, observed from the 2004 (Haran et al., 2005), 2009 (Haran et al., 2014), and 2014 (Haran et al., 2018) mosaics, respectively, each composed using MODIS imagery (Scambos et al., 2007). Each MOA grounding line delineation therefore had an estimated associated error of ± 250 m (Haran et al., 2005; 2014; 2018). Whilst the AIS CCI and MEaSUREs products represent the inner limit of tidal flexure and thus approximate the actual grounding line position (Fricker et al., 2009; Rignot et al., 2016), the ASAID and MOA datasets instead reflect the break-in-slope. This narrow region is observed seaward of the grounding line and is typically inferred to be the surface expression of the abrupt change in basal ice interface produced at the transition between grounded and floating ice (Scambos et al., 2007; Fricker et al., 2009; Bindschadler et al., 2011).

To quantify changes in grounding line position, change was measured from the earliest 1996 delineation along each main flowline (Figure 1a). It should be highlighted that grounding line positions at Vanderford Glacier in 1996 were provided by both AIS CCI and the MEaSUREs datasets, but were digitised in slightly different locations. Similarly, the MEaSUREs dataset also delineated two different 1996 grounding line positions at Underwood Glacier, separated by ~ 7 km (Figure 1a). This significantly exceeds the associated uncertainty listed in Table 2 and therefore suggests that any observed grounding line change must be interpreted with caution. Conservative grounding line retreat values were thus calculated for these glaciers, with retreat measured relative to the minimum observed 1996 position.

3.6. Bed and ice surface topography

In order to assess the potential vulnerability to MISI, bedrock elevation profiles were derived from BedMachine (Morlighem, 2020) along each digitised flowline (Figure 1a). Bed elevation values and their associated errors were sampled at an interval spacing of 500 m, reflecting the horizontal resolution of the dataset. Whilst BedMachine was mostly mapped using mass conservation methods across regions of fast-moving ice, a range of different methods were employed across Vincennes Bay (Figure 10). Sampled errors therefore ranged between 10 and 202 m. Surface topography profiles obtained using the Reference Elevation Model of Antarctica (REMA) (Howat et al., 2019) were also extracted along each central flowline, sampled at the same 500 m interval spacing as the bed elevation.

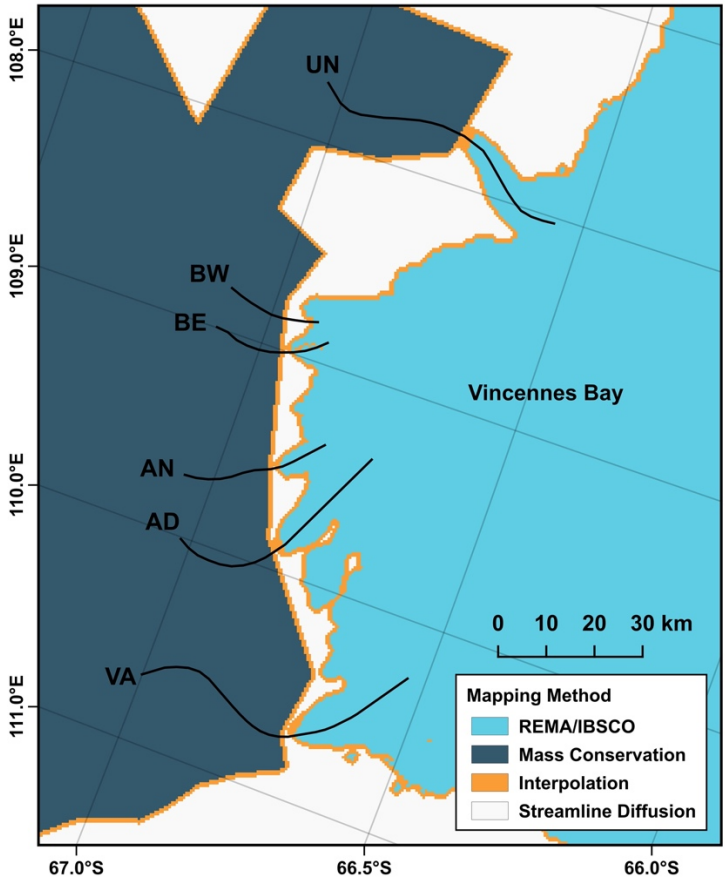

Figure 10. Map displaying the different mapping methods employed within BedMachine to map bed elevation across Vincennes Bay (Morlighem, 2020).

Chapter 4. Results

4.1. Terminus position

The terminus positions of the Vanderford, Adams, and Underwood Glaciers displayed the greatest variability across the Vincennes Bay outlet glaciers, each of them fluctuating by ~7 km over the study period (Figure 11). Vanderford Glacier retreated ~4 km between 2007 and 2010 (Figure 11a), with a large extension of ice seen to protrude from the central terminus region (Figure 12a) before being removed via calving. Following initial terminus advance, Adams Glacier showed a significant overall retreat, measured at ~6.3 km between 1973 and 2022 (Figure 11b). A spectacular disintegration of Underwood's floating tongue resulted in ~4.6 km of retreat between 2020 and 2022 (Figure 11f), with calved ice blocks clearly visible within the frontal sea ice mélange (Figure 12f). The Bond East and Bond West termini were comparatively stable, fluctuating by a maximum of ~ 1.5 km over the study period (Figure 11). In clear contrast, Anzac Glacier exhibited an overall advance, measured at ~ 2 km between 1963 and 2022 (Figure 11c).

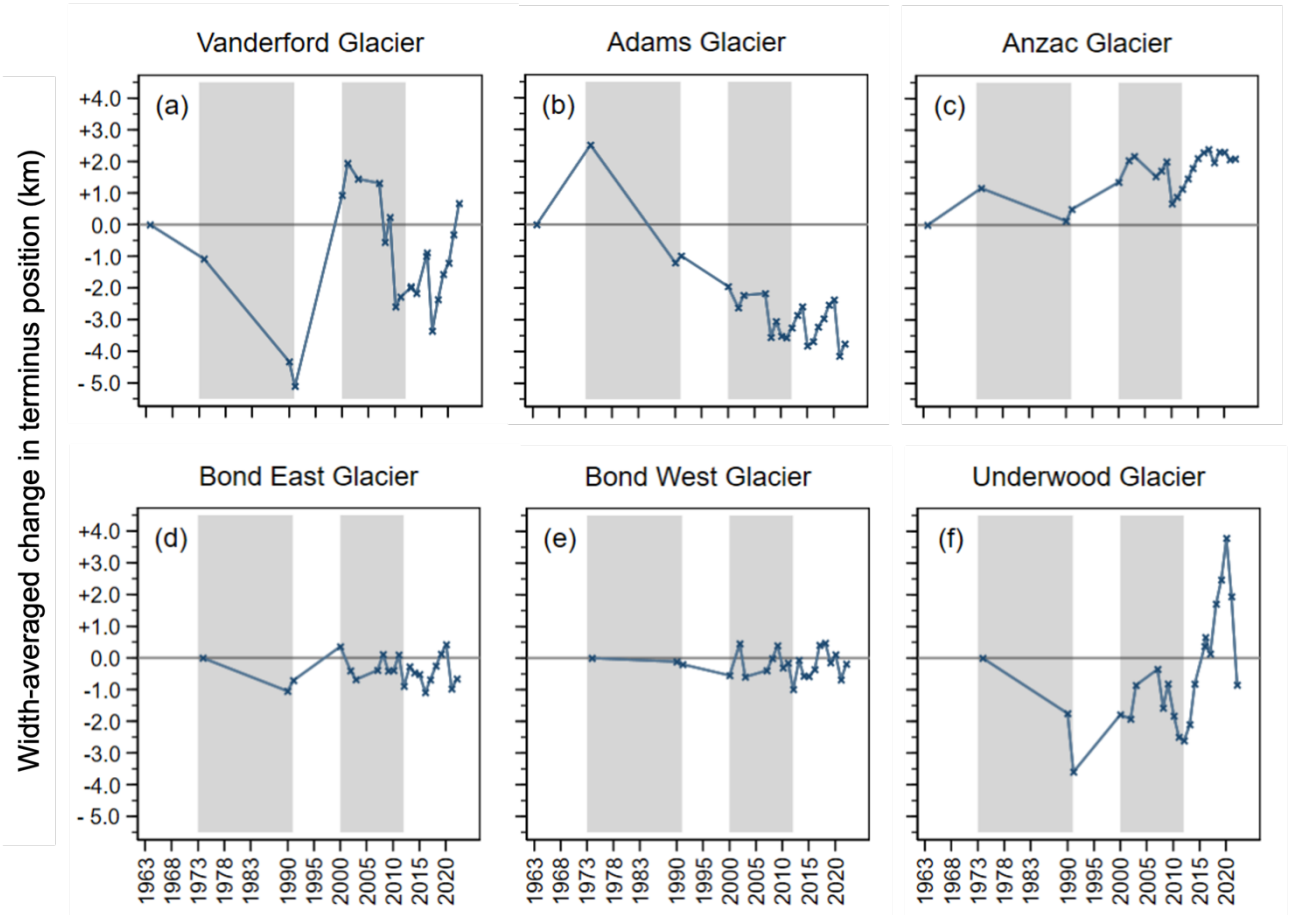

Figure 11. Width-averaged terminus position change observed relative to the first measurement point at **a)** Vanderford Glacier, **b)** Adams Glacier, **c)** Anzac Glacier, **d)** Bond East Glacier, **e)** Bond West Glacier, and **f)** Underwood Glacier. The time periods 1973-1991 and 2000-2012 are shaded in grey.

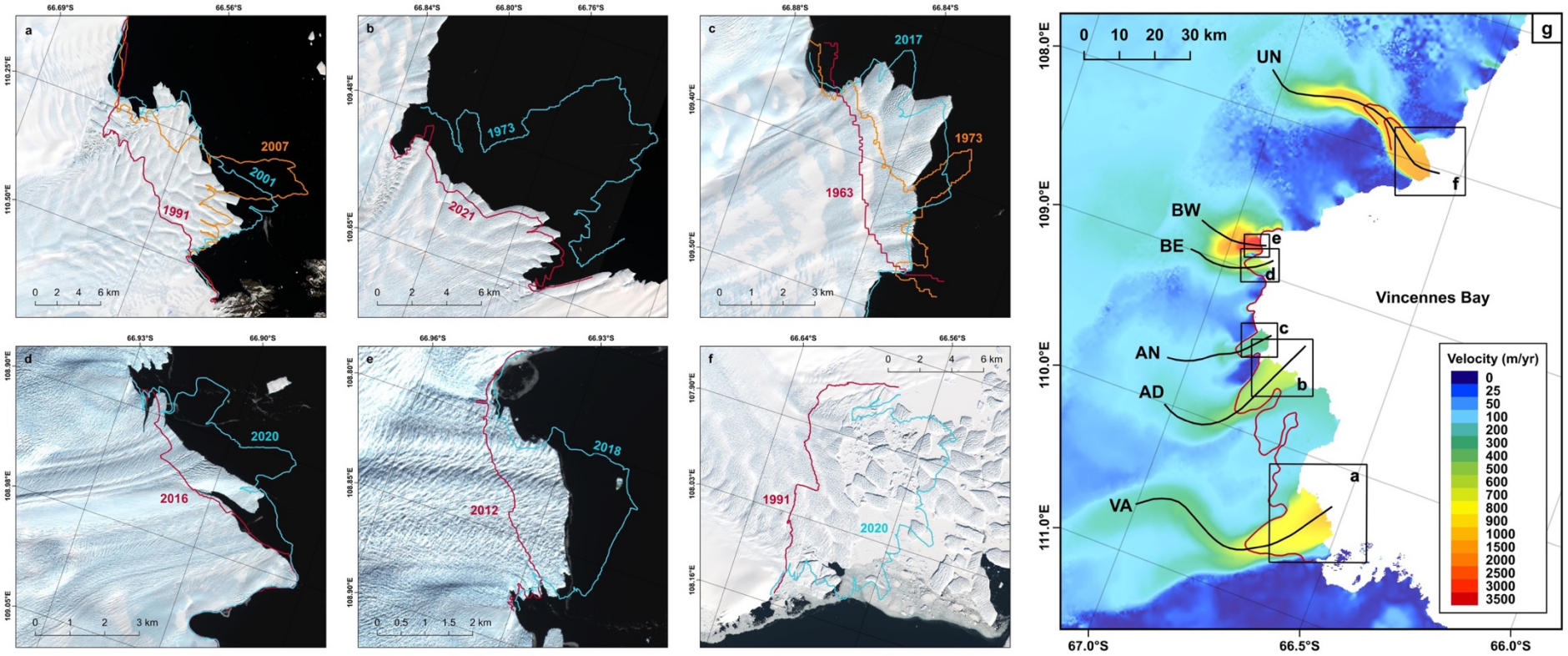

Figure 12. Minimum (red), maximum (blue), and notably asymmetrical (orange) terminus positions manually digitised across **(a)** Vanderford Glacier, **(b)** Adams Glacier, **(c)** Anzac Glacier, **(d)** Bond East Glacier, **(e)** Bond West Glacier, and **(f)** Underwood Glacier. All background satellite imagery displayed was collected in February 2022. Panel **(g)** shows the extent of boxes **(a-f)** within Vincennes Bay, overlain on the 2018 ITS_LIVE ice velocity mosaic (Gardner et al., 2022).

At the decadal scale, the Vincennes Bay outlet glaciers fluctuated between periods of largely synchronous terminus retreat and terminus advance. Between 1973 and 1991, each of the six glaciers displayed an overall retreat (Figure 11), calculated at a median rate of -116.8 m yr^{-1} (Table 3). In contrast, between 1991 and 2000, four glaciers were observed to advance (Figure 11); a median rate of terminus position change of +106.8 m yr^{-1} was thus calculated across the six glaciers (Table 3). Between 2000 and 2012, all six glaciers showed an overall retreat (Figure 11), calculated at a median rate of -86.3 m yr^{-1} (Table 3). Between 2012 and 2022, five glaciers were seen to advance (Figure 11), resulting in a median terminus position change rate of +88.1 m yr^{-1} across Vincennes Bay (Table 3).

	Rate of Terminus Position Change (m yr^{-1})			
	1973 - 1991	**1991 - 2000**	**2000 - 2012**	**2012 - 2022**
Mean	-117.4	+156.5	-96.6	+98.6
Median	-116.8	+106.8	-86.3	+88.1
STD	97.8	275.3	80.5	111.7

Table 3. Rate of terminus position change observed across the Vincennes Bay outlet glaciers. STD represents the calculated standard deviation.

4.2. Ice surface velocity

Significant variability in ice surface velocity was observed between the Vincennes Bay outlet glaciers (Figure 1a), with spatial variations also seen along-flow at each glacier (Figure 13). In 2018, Anzac Glacier was measured to be the slowest flowing outlet glacier, with velocity increasing from 128 ± 1 m yr^{-1} inland at AN (Figure 1a) to a maximum of 331 ± 1 m yr^{-1} at the terminus (Figure 13c). In contrast, Bond West was measured to be the fastest flowing outlet glacier, accelerating rapidly from 241 ± 4 m yr^{-1} inland at BW (Figure 1a) to a maximum velocity of 3,339 ± 2 m yr^{-1} (Figure 13e), representing one of the highest recorded velocities within Antarctica. The maximum velocity measured across each of the Vanderford, Adams, Bond East and Underwood Glaciers ranged from 598 ± 1 to 1,625 ± 4 m yr^{-1} (Figure 13).

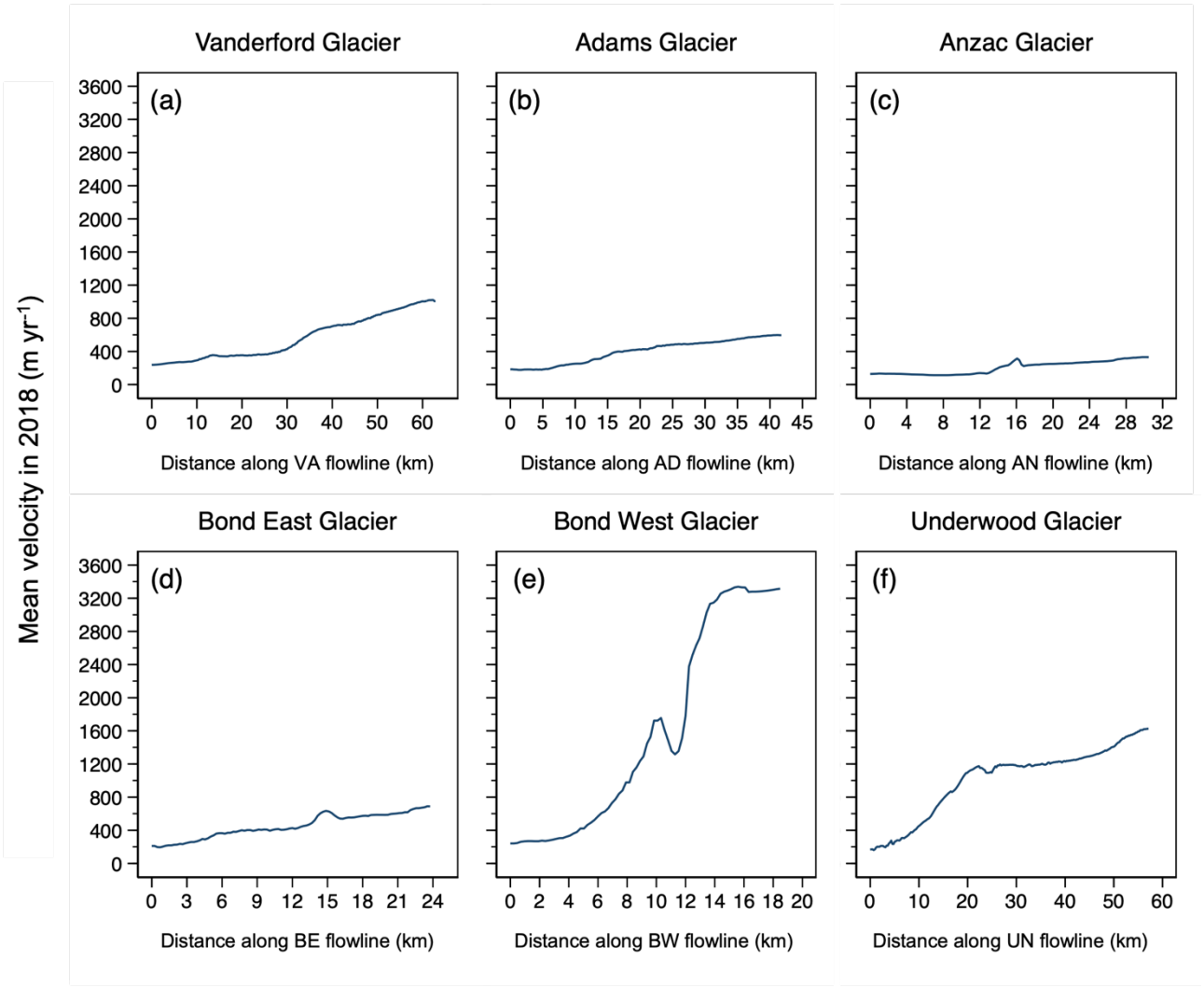

Figure 13. Ice surface velocity profiles extracted using the ITS_LIVE 2018 velocity mosaic (Gardner et al., 2022) along the central flowlines of **(a)** Vanderford Glacier, **(b)** Adams Glacier, **(c)** Anzac Glacier, **(d)** Bond East Glacier, **(e)** Bond West Glacier, and **(f)** Underwood Glacier.

Temporal variations in ice surface velocity were limited over the observational period (Figure 14) with ice surface velocity measured to be stable across each of the Adams, Bond West, and Underwood Glaciers. Whilst ice surface velocity was seen to increase by 12% across the FT of Anzac Glacier between 2009 and 2021 (Figure 14c), this velocity increase was not deemed notable, with the absolute value of acceleration (30 m yr^{-1}) being smaller than the associated error (± 82 m yr^{-1}). However, a 31% increase in velocity was seen at Vanderford Glacier, with ice surface velocity at box IN recorded to accelerate from 201 ± 39 to 264 ± 6 m yr^{-1} between 2000 and 2013 (Figure 14a). Significant variations were also seen at Bond East Glacier, with a period of deceleration measured between 2006 and 2009, followed by a subsequent acceleration between 2009 and 2021 (Figure 14d). Such variation in ice surface velocity was consistent across each of the IN, GL, and FT boxes. At the GL box, ice surface velocity slowed by 15%, decreasing from 508 ± 42 m yr^{-1} in 2006 to 430 ± 66 m yr^{-1}

in 2009 (Figure 14d). Subsequent acceleration was also calculated at 15%, with the ice surface velocity observed to increase to 496 m yr^{-1} in 2021 (Figure 14d).

Figure 14. Mean annual velocity extracted within the inland (IN), grounding line (GL) and floating tongue (FT) boxes across **(a)** Vanderford Glacier, **(b)** Adams Glacier, **(c)** Anzac Glacier, **(d)** Bond East Glacier, **(e)** Bond West Glacier, and **(f)** Underwood Glacier. Velocity data extracted from the ITS_LIVE velocity mosaics between 2000 and 2018 (Gardner et al., 2022) and ENVEO datasets between 2019 and 2021 (ENVEO, 2021). Note the different scales on the y-axes.

4.3. Ice surface elevation

The ice surface elevation data provided by both Schröder et al. (2019) and Nilsson et al. (2022) were associated with high levels of uncertainty prior to 2003, particularly during the early 1990s (Figure 15). However, with the exception of Anzac Glacier (Figure 15c), there was a general agreement between each respective dataset regarding the overall pattern of ice surface elevation change measured across each GL box. A clear and consistent thinning trend was measured at Vanderford Glacier throughout the observational period (Figure 15a). Between 2003 and 2017, Schröder et al. (2019) and Nilsson et al. (2022) observed thinning at an average rate of 0.12 and 0.07 m yr^{-1}, respectively. However, Nilsson et al. (2022) observed an enhanced rate of thinning between 2017 and 2020, measured at 0.22 m yr^{-1}. Despite their observed stability between 2003 and 2017, Nilsson et al. (2022) also measured enhanced thinning rates across the Adams, Anzac, and Underwood Glaciers between 2017

and 2020, calculated at an average rate of 0.32, 0.44, and 0.38 m yr^{-1}, respectively (Figure 15). In contrast, ice surface elevation was observed to be stable across both Bond East and Bond West between 2003 and 2020, with Nilsson et al. (2022) measuring minor thickening at an average rate of just 0.01 m yr^{-1}. The patterns of surface elevation change observed were consistent across both the GL (Figure 15) and IN (Figure 16) boxes for each respective glacier.

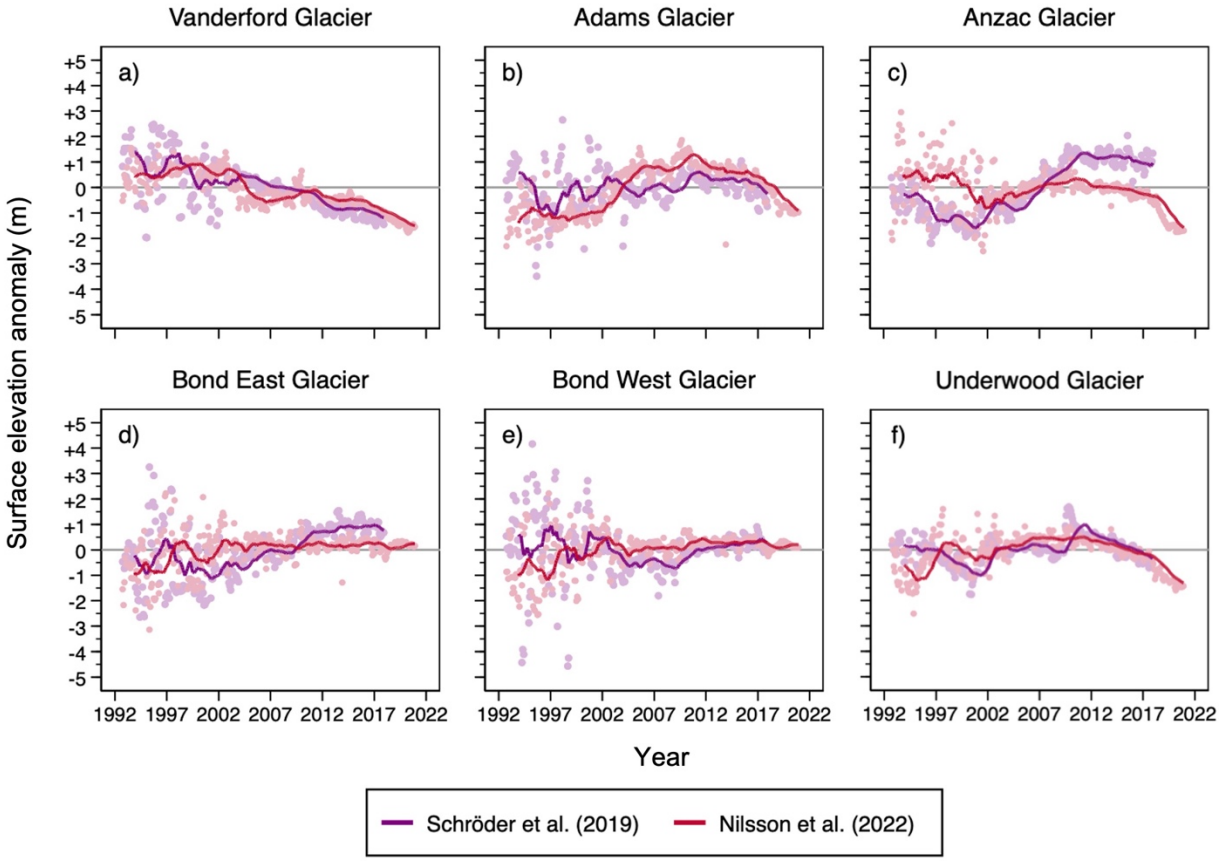

Figure 15. Monthly surface elevation anomalies observed in each GL box at **(a)** Vanderford Glacier, **(b)** Adams Glacier, **(c)** Anzac Glacier, **(d)** Bond East Glacier, **(e)** Bond West Glacier, and **(f)** Underwood Glacier between 1992 and 2020. Elevation anomalies are calculated relative to the long-term 1992-2017 mean. Bold lines represent 24-month rolling means.

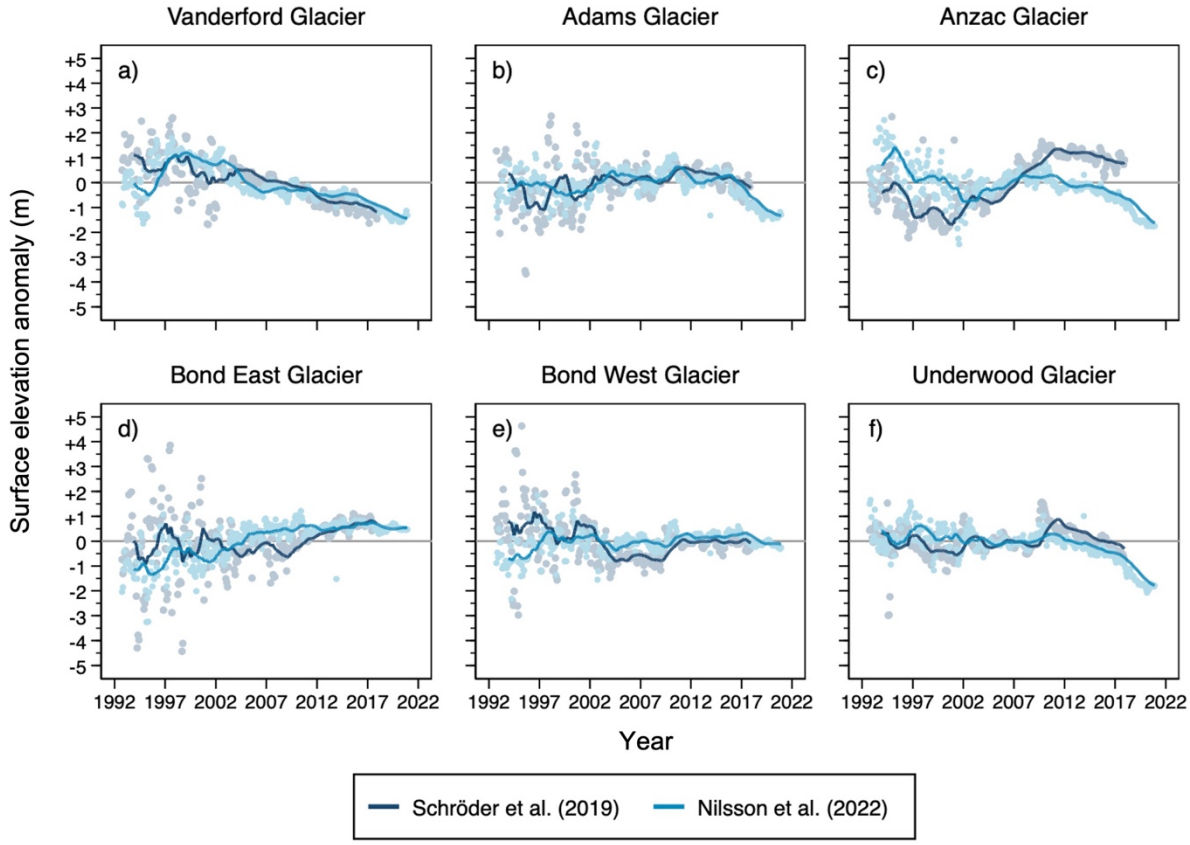

Figure 16. Monthly surface elevation anomalies observed in each IN box at **(a)** Vanderford Glacier, **(b)** Adams Glacier, **(c)** Anzac Glacier, **(d)** Bond East Glacier, **(e)** Bond West Glacier, and **(f)** Underwood Glacier between 1992 and 2020. Elevation anomalies are calculated relative to the long-term 1992-2017 mean. Bold lines represent 24-month rolling means.

Such trends of ice surface elevation change were also reflected in the dataset produced by Smith et al. (2020) (Figure 17). Whilst Vanderford, Adams, Anzac and Underwood Glaciers showed an overall decrease in ice surface elevation between 2003 and 2019, both the Bond East and Bond West Glaciers exhibited minor thickening across the same time period. Such minor thickening was concentrated within ~ 35 km of the coastline, with ice surface elevation comparatively stable inland of the Bond East and Bond West flowlines (Figure 17).

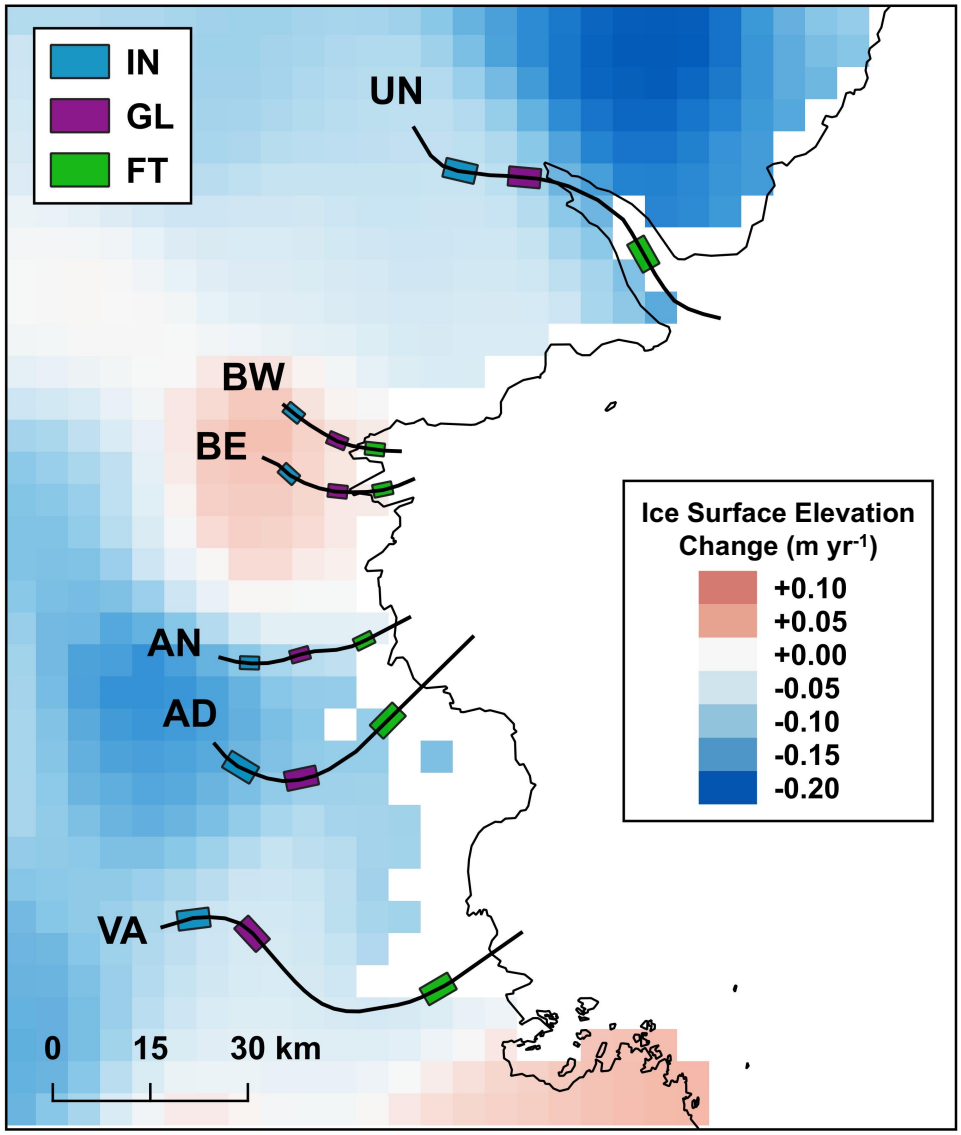

Figure 17. Rate of ice surface elevation change observed inland of Vincennes Bay between 2003 and 2019, as calculated by Smith et al. (2020). Coastline, shown in black, downloaded from the SCAR Antarctic Digital Database, accessed using Quantarctica 3 (Matsuoka et al., 2021).

4.4. Grounding line position

Vanderford Glacier showed the greatest and most consistent grounding line retreat across the observational period, retreating ~ 18.6 km between 1996 and 2020, at an average rate of -0.8 km yr^{-1} (Figure 18a). Such grounding line retreat primarily occurred down a retrograde bedrock slope, but the most recent observed grounding line position appears to be situated on a stabilising ridge (Figure 19a). Between 2016 and 2020, the average rate of grounding line retreat increased to 1.0 km yr^{-1}, with ~4.1 km of grounding line retreat measured over this 4-year period (Figure 18a).

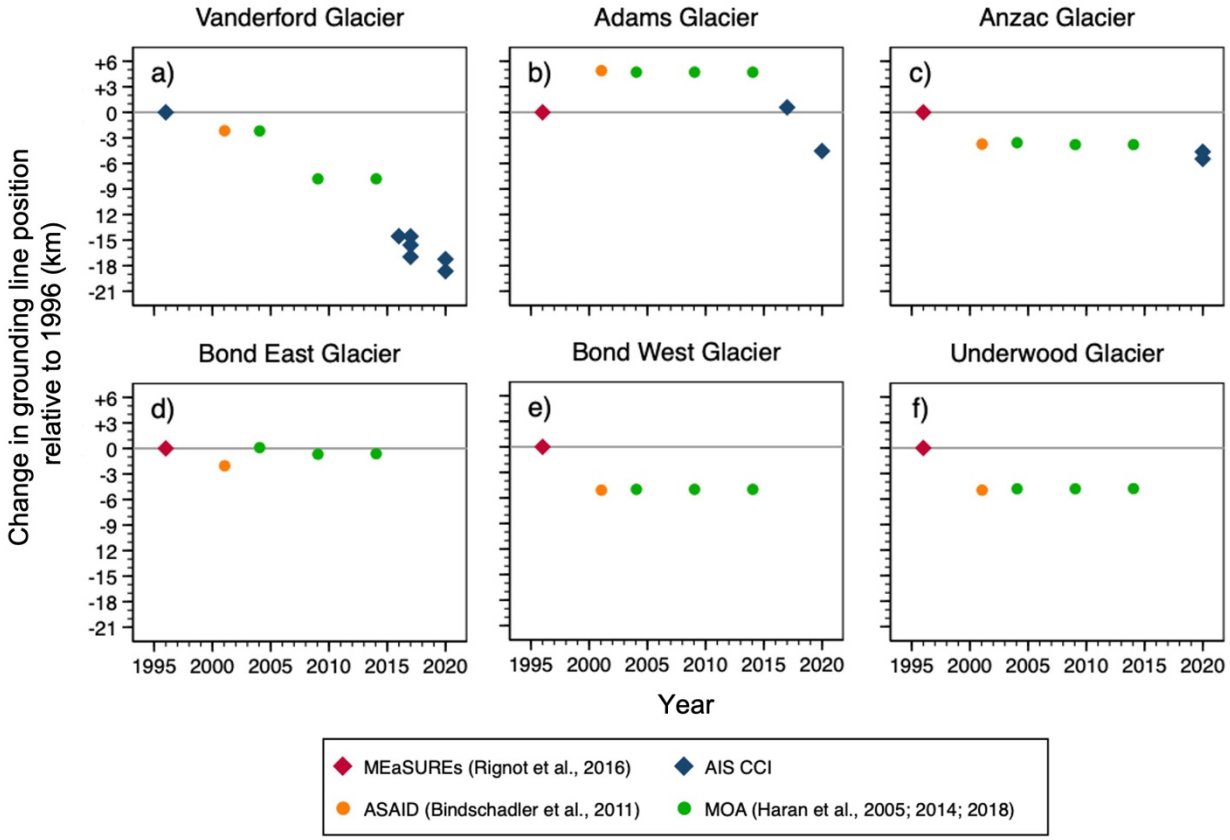

Figure 18. Change in grounding line position measured relative to the minimum observed 1996 position at **(a)** Vanderford Glacier, **(b)** Adams Glacier, **(c)** Anzac Glacier, **(d)** Bond East Glacier, **(e)** Bond West Glacier, and **(f)** Underwood Glacier. Note that circles represent grounding line positions manually derived from optical imagery, whilst diamonds represent grounding line products derived using DInSAR.

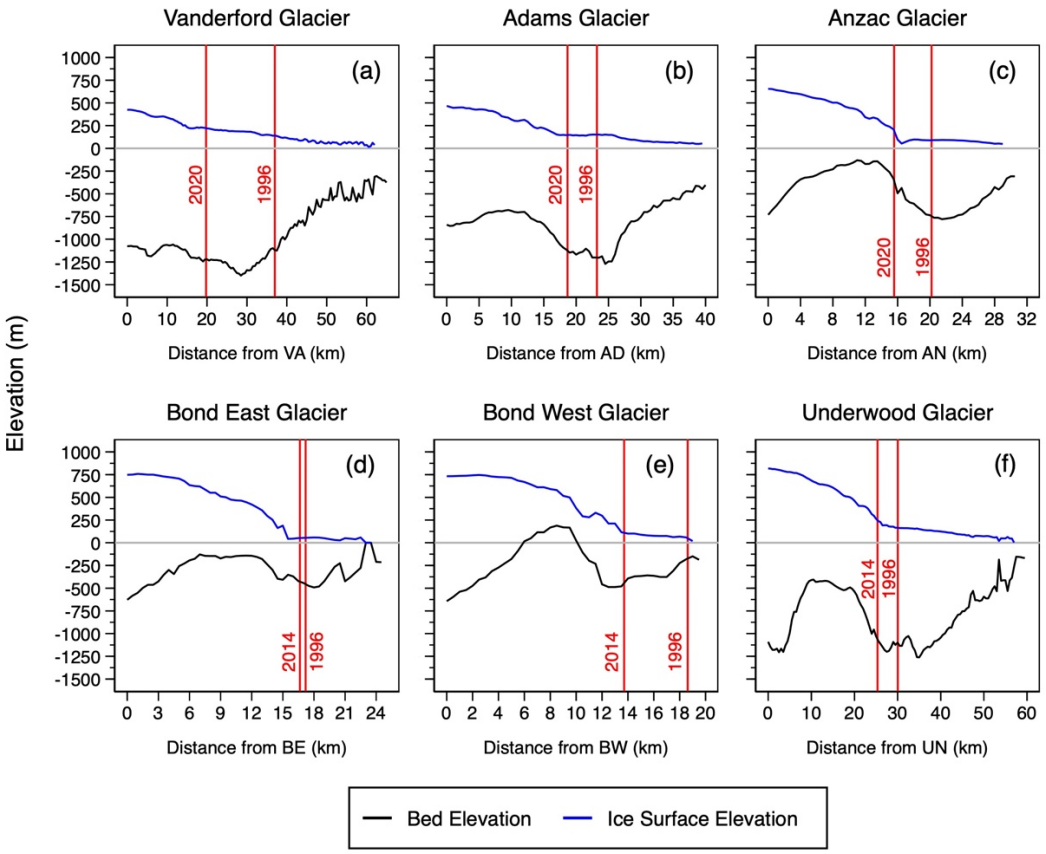

Figure 19. Ice surface (Howat et al., 2019) and bedrock elevation (Morlighem, 2020) profiles extracted along the central flowlines of **(a)** Vanderford Glacier, **(b)** Adams Glacier, **(c)** Anzac Glacier, **(d)** Bond East Glacier, **(e)** Bond West Glacier, and **(f)** Underwood Glacier. Dated vertical red lines represent the oldest and most recent grounding line positions observed respectively.

In contrast, the grounding line positions of the Adams, Anzac, Bond East, Bond West, and Underwood Glaciers were observed to be stable between 2001 and 2014, with the ASAID and MOA grounding line products digitised in nearly identical locations (Figure 18). Despite an initial grounding line advance of ~ 5 km between 1996 and 2001, an overall retreat of ~ 4.5 km was observed at Adams Glacier between 1996 and 2020 (Figure 18b). A similar overall pattern of grounding line retreat was observed at Anzac Glacier, measured at ~ 5.4 km over the same time period (Figure 18c).

Between 1996 and 2014, Bond West and Underwood Glacier exhibited very similar patterns of grounding line retreat, retreating ~4.9 and ~4.7 km, respectively (Figure 18). The majority of this retreat was observed between 1996 and 2001. Unlike the other outlet glaciers within Vincennes Bay, Bond East's grounding line was seen to be stable across the observational period (Figure 18d). Between 1996 and 2001, the grounding line was estimated to have retreated ~2 km. However, between 2004 and 2014, Bond East's grounding line remained within ~600 m of the observed 1996 position. It should be noted that more recent grounding line positions were not available at the Bond East, Bond West, and Underwood Glaciers.

Chapter 5. Discussion

The following section provides a discussion and interpretation of the results presented within Chapter 4. **Section 5.1** discusses the primary finding of this thesis, exploring the potential forcing mechanisms driving the extensive and anomalous grounding line retreat observed at Vanderford Glacier. Focus is then placed on wider dynamics seen across Vincennes Bay; **Section 5.2** discusses the potential correlation between sea ice production and the decadal patterns of terminus position change observed. **Section 5.3** further expands on the potential impact of sea ice, outlining a possible link between reduced sea ice extent and the onset of enhanced thinning across each of the Vanderford, Adams, Anzac, and Underwood Glaciers between 2017 and 2020. A short interpretation of the notably high velocity observed at Bond West Glacier is then provided in **Section 5.4**. **Section 5.5** summarises a key methodological finding of the thesis, emphasising the critical importance of DInSAR processing for accurate mapping of grounding line positions in potentially dynamic regions. **Section 5.6** then further extends such reflections, acknowledging the limitations of the study and highlighting areas that may improve future understanding.

5.1. Recent dynamic change and future evolution of Vanderford Glacier

The results reveal extensive grounding line retreat at Vanderford Glacier, measured at 18.6 km between 1996 and 2020 (Figure 18a). This corresponds to an average rate of retreat of 0.78 km yr^{-1}, representing the fastest decadal-scale grounding line retreat reported in East Antarctica (Stokes et al., 2022). Such retreat is comparable with that observed at Thwaites Glacier, measured at 0.8 km yr^{-1} between 1992 and 2017 (Milillo et al., 2019) and widely considered to result from the enhanced intrusion of warm mCDW across the continental shelf towards sub ice-shelf cavities (Thoma et al., 2008; Steig et al., 2012; Paolo et al., 2015; Turner et al., 2017a; Scambos et al., 2017; Rignot et al., 2019). The near-identical rate of grounding line retreat observed at Vanderford Glacier is therefore consistent with the notion that warm mCDW is able to access local ice-shelf cavities below the Vanderford Ice Shelf, driving high rates of basal melting (Depoorter et al., 2013; Ribeiro et al., 2021).

The rapid rate of grounding line retreat measured at Vanderford Glacier is anomalous within Vincennes Bay, calculated to be nearly four times greater than the average rate of retreat (0.20 km yr^{-1}) recorded across the Adams, Anzac, Bond East, Bond West, and Underwood Glaciers. With mCDW typically observed to access sub ice-shelf cavities via deep subglacial troughs (Jenkins et al., 2010; Scambos et al., 2017; Rignot et al., 2019), this significant difference may be indicative of a bathymetric pathway that favours preferential intrusion of

mCDW towards the Vanderford Ice Shelf, rather than the other studied glaciers. Bathymetric data remains limited across Vincennes Bay, but recent echosounding carried out onboard RSV *Nuyina* revealed an undiscovered canyon at the front of Vanderford Glacier, estimated to be more than 55 kilometres in length, reaching a maximum depth of 2200 m (Figure 20) (Australian Antarctic Division, 2022). This canyon might provide a potential pathway for the incursion of mCDW at depth towards the Vanderford Ice Shelf, thereby facilitating enhanced rates of grounding line retreat relative to the other Vincennes Bay outlet glaciers. In addition, the anomalously high rate of grounding line retreat observed at Vanderford Glacier may be attributed to the underlying bedrock geometry. Figure 19a indicates that between 1996 and 2020, the majority of Vanderford's grounding line retreat occurred down a retrograde slope. In contrast, with the exception of Bond West Glacier (Figure 19e), the grounding line retreat observed at other glaciers within Vincennes Bay generally occurred along prograde slopes. As retrograde bedrock slopes favour more extensive grounding line retreat for a given basal melt rate (Milillo et al., 2019; Millan et al., 2022), the high rate of grounding line retreat seen at Vanderford Glacier may hence also be the product of the underlying bedrock geometry.

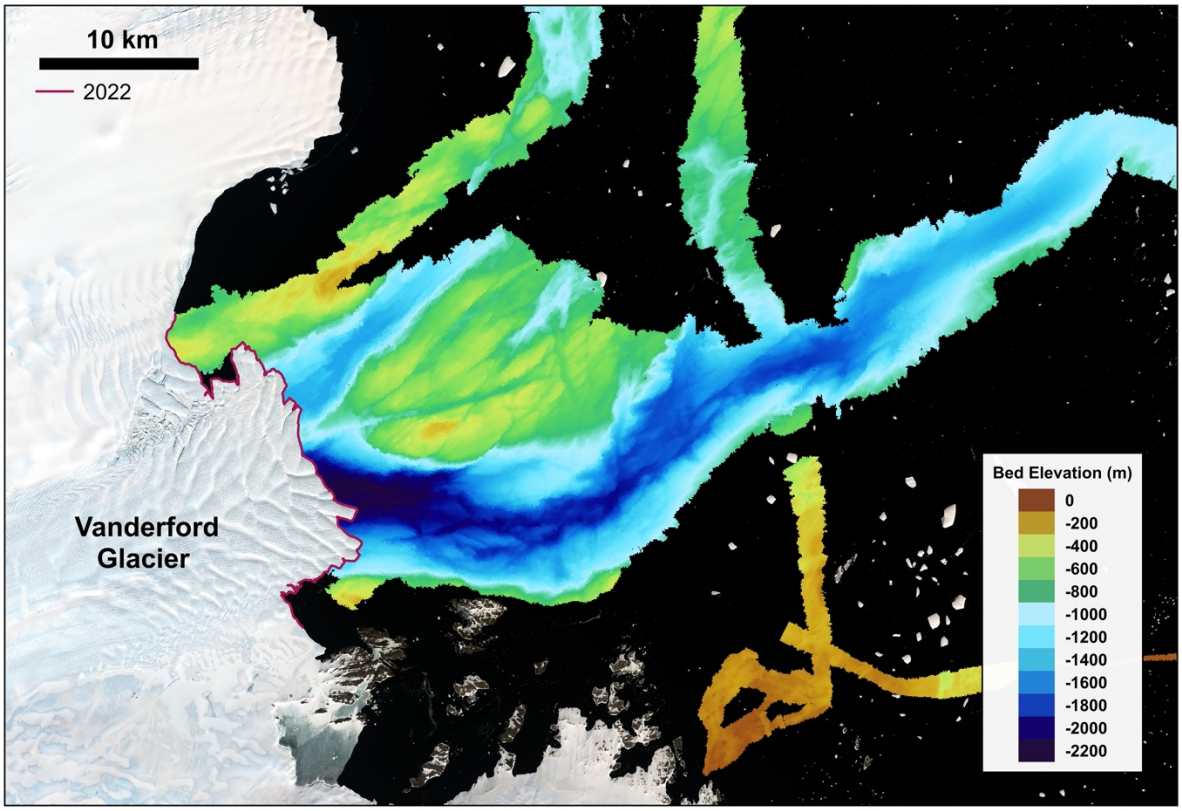

Figure 20. Bathymetry mapped at the front of Vanderford Glacier, collected during RSV *Nuyina's* maidan voyage to Antarctica (Commonwealth of Australia, 2022). Background satellite imagery was collected in February 2022, with red line showing the associated digitised terminus position.

The intrusion of warm mCDW to sub ice-shelf cavities facilitates enhanced oceanic thinning of floating ice shelves (Paolo et al., 2015), reducing their buttressing potential and thus often triggering dynamic thinning and ice flow acceleration across upstream glaciers (Fürst et al., 2016; Reese et al., 2018). For example, Thwaites Glacier accelerated by 33% between 2006 and 2013 (Mouginot et al., 2014), with dynamic thinning occurring at a rate of at least 1.5 m yr^{-1} between 2012 and 2020 (Bevan et al., 2021). Whilst the results presented in this study reveal a 31% increase in inland velocity at Vanderford Glacier between 2000 and 2013, ice surface velocity was seen to be stable across the grounding line throughout the study period (2000 – 2021), with no significant acceleration observed (Figure 14a). In addition, although a consistent decrease in surface elevation was measured across Vanderford Glacier (Figure 15a) the average rate of ice thinning, calculated to range between 0.07 and 0.12 m yr^{-1} (2003 – 2017), was an order of magnitude lower than recorded at other glaciers undergoing similar rapid grounding line retreat within the Amundsen Sea Embayment, such as Thwaites Glacier (Pritchard et al., 2009; Flament & Rémy, 2012; Konrad et al., 2017). This could be attributed to variations in surface mass balance, with a comparatively higher rate of snowfall within the Aurora subglacial basin potentially obscuring a dynamic thinning signal. However, the rate of surface lowering measured across the neighbouring Totten Glacier (Figure 1b) was also significantly higher than at Vanderford Glacier, estimated up to 1.7 m yr^{-1} between 2003 and 2008 (Khazendar et al., 2013). This therefore suggests that the comparatively moderate rate of thinning seen across Vanderford Glacier is not the product of high regional snowfall. Thus, rather than a dynamic thinning signal being obscured, the rate of thinning observed across Vanderford Glacier appears to have been significantly lower. This indicates that the ocean-driven reduction in buttressing force exerted by the Vanderford Ice Shelf has presently been limited. Nonetheless, Fürst et al. (2016) calculated that just 20.2% of the Vanderford Ice Shelf is categorised as passive, i.e. can be removed without initiating a dynamic glaciological response. It may thus be predicted that continued intrusion of warm mCDW will likely reduce the buttressing force exerted by the Vanderford Ice Shelf, potentially initiating acceleration and enhanced dynamic thinning across Vanderford Glacier in the coming decades.

Whilst Vanderford Glacier is currently grounded on a stabilising bedrock ridge (Figure 19a), extension of the central flowline shows that retrograde slopes are observed inland along the Vanderford Trench, with a significant decrease in bedrock elevation seen approximately 70 km inland of the present grounding line position (Figure 21c). If the current rate of grounding line retreat (0.78 km yr^{-1}) was to continue, this steep bedrock slope would be reached within 100 years, potentially triggering MISI. Indeed, using the BISICLES adaptive mesh ice-sheet

model, Sun et al. (2016) simulated Vanderford's grounding line to retreat rapidly along the Vanderford Trench, separating Law Dome (Figure 1b) from the continental ice sheet within 1000 years. However, Sun et al. (2016) also emphasised that such extensive grounding line retreat is dependent on the future oceanic forcing, requiring basal melt rates elevated above those observed at present.

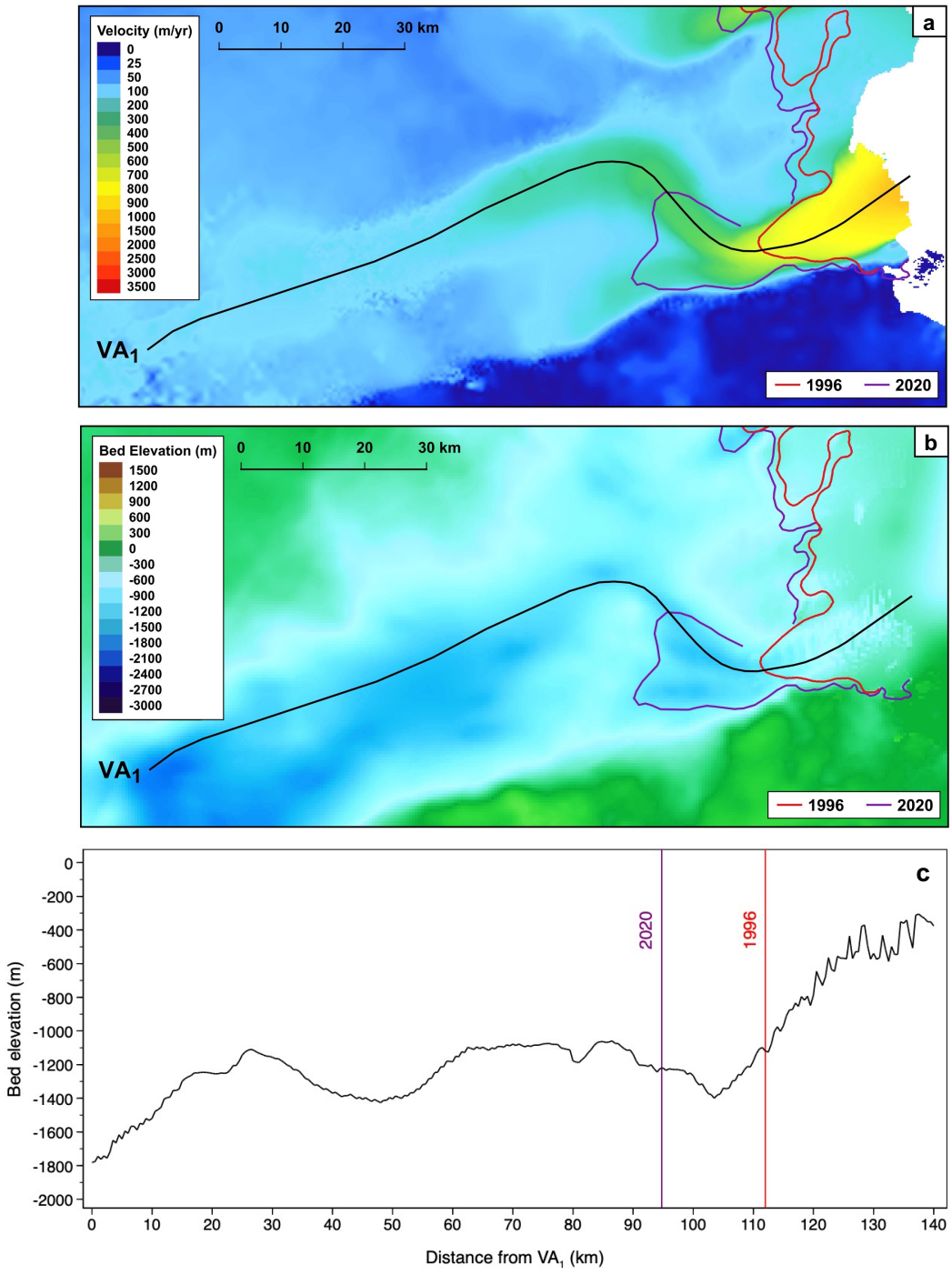

Figure 21. Extended flowline digitised along the main flow of Vanderford Glacier overlain on maps of **a)** ice velocity extracted from the 2018 ITS_LIVE ice velocity mosaic (Gardner et al., 2022), and **b)** bedrock topography extracted from BedMachine (Morlighem, 2020). **c)** Bed elevation sampled from BedMachine (Morlighem, 2020) along the extended flowline. 1996 MEaSUREs (Rignot et al., 2016) and 2020 AIS CCI grounding line positions are displayed in red and purple respectively.

Recent oceanographic observations suggest that the oceanic heat supply to East Antarctica is increasing (Herraiz-Borreguero & Garabato, 2022), potentially facilitating such increased basal melt rates. The mid-depth CDW found along the continental slope off East Antarctica has warmed significantly since the 1990s, with an increase of 0.29°C per decade estimated near Vincennes Bay (105 °E – 111°E). This warming has been attributed to the southward shift of the Antarctic Circumpolar Current (ACC) (Yamazaki et al., 2021), understood to have been driven by a poleward shift of the westerlies over the Southern Ocean associated with summertime positive trends in the southern annular mode (Herraiz-Borreguero & Garabato, 2022). With climatic models predicting that the southern annular mode will continue trending towards its positive phase under high-emission scenarios (Zheng et al., 2013; Lim et al., 2016; Lee et al., 2021), further CDW warming may be expected off East Antarctica, enabling enhanced basal melt rates (Herraiz-Borreguero & Garabato, 2022). Subsequent increased outflow of glacial meltwater will likely further hinder the formation of DSW in the Vanderford polynya, thereby facilitating the enhanced incursion of warm mCDW at depth (Ribeiro et al., 2021). This positive feedback could drive rapid grounding line retreat at Vanderford Glacier, potentially providing the oceanic forcing required to initiate MISI (Sun et al., 2016).

5.2. Decadal patterns of terminus position change observed across the Vincennes Bay outlet glaciers potentially correlated to sea ice production

Decadal variations in terminus position observed across Vincennes Bay (Table 3) are seen to correspond closely with the wider decadal-scale patterns reported along the Wilkes Land coast (Miles et al., 2016) (Figure 22). The majority of Wilkes Land outlet glaciers were seen to retreat between 1974-1990, switch to a period of sustained advance between 1990-2000, before retreating between 2000-2012 (Miles et al., 2016). Miles et al. (2016) suggested that such decadal fluctuations between terminus retreat and advance are strongly correlated to rates of sea-ice production around East Antarctica. They noted that enhanced brine rejection from increased sea-ice production can result in destratification of the water column (Petty et al., 2014), facilitating the formation of DSW and hence production of Antarctic Bottom Water (AABW) (Kusahara et al., 2011). Representing the densest water mass in the ocean (Ribeiro et al., 2021), AABW is understood to inhibit intrusion of mCDW, thereby suppressing basal melting and facilitating terminus advance (Miles et al., 2016). In contrast, decreased sea-ice production leads to a reduction in DSW formation and thus decreased production of AABW. This allows enhanced intrusion of mCDW, driving basal melting and hence terminus retreat (Miles et al., 2016). Whilst detailed analysis of decadal trends in sea ice production is yet to be carried out within Vincennes Bay, Miles et al. (2016) noted a negative correlation between

sea-ice production and average air temperatures over the sea-ice production season (April to October) along the Wilkes Land coast.

To consider this potential correlation within Vincennes Bay, monthly surface air temperature data collected at Casey Station (Figure 1b) were downloaded and analysed (Met-READER, 2022). The results indicated such a negative correlation was also observed within Vincennes Bay, with higher temperatures observed to be coincident with the periods of terminus retreat (Figure 22). The decrease in mean surface air temperature and overall pattern of terminus advance observed between 2012-2022 (Figure 22) may therefore be indicative of increased sea ice production within Vincennes Bay over this most recent decade.

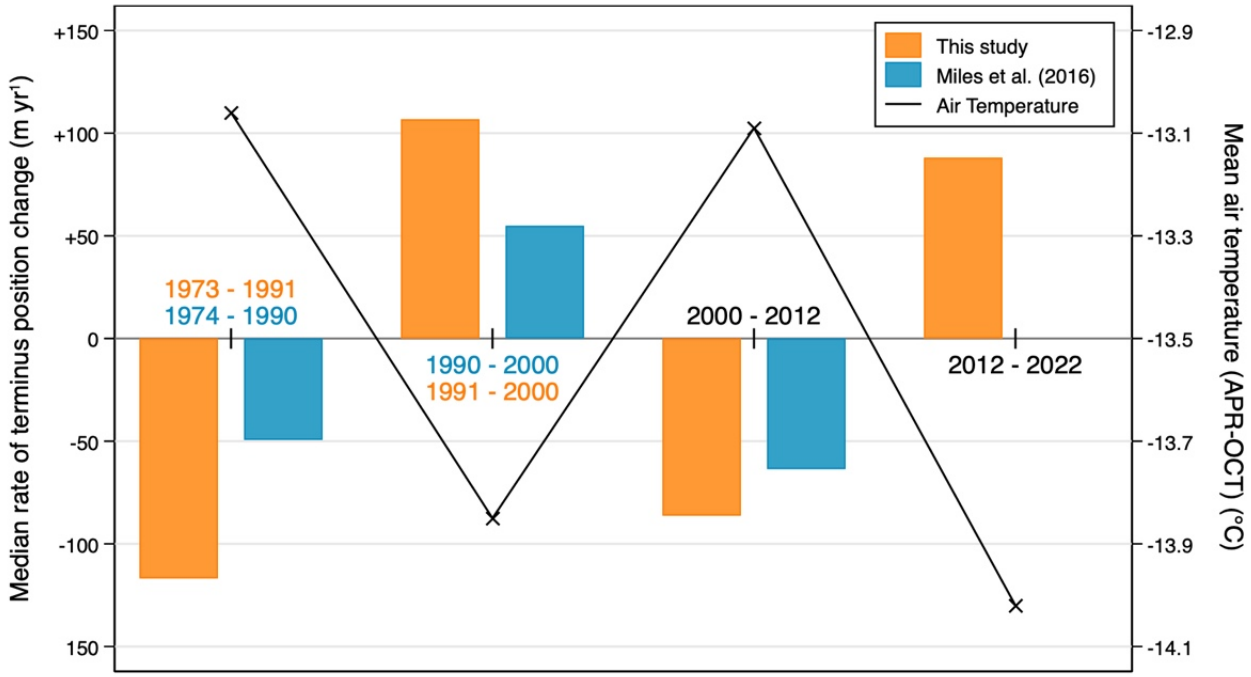

Figure 22. Median decadal terminus position change reported in this study within Vincennes Bay, shown in orange, in comparison to that observed along the Wilkes Land coastline by Miles et al. (2016), shown in blue. This study (n = 6), Miles et al. (2016) (n= 15 (1974-1990), 37 (1990-2000), 39 (2000-2012)). Mean surface air temperatures measured at Casey Station (66.3°S 110.5°E) over the sea ice production season (April to October), extracted from Met-READER (2022), displayed in black.

5.3. Enhanced thinning of the Vanderford, Adams, Anzac, and Underwood Glaciers observed between 2017 and 2020

Analysis of ice surface elevation shows a pattern of accelerated thinning across each of the Vanderford, Adams, Anzac, and Underwood Glaciers between 2017 and 2020 (Figure 15). The most significant acceleration was measured at Anzac Glacier, with the average rate of thinning increasing from -0.01 m yr^{-1} between 2003 and 2017 to -0.44 m yr^{-1} between 2017 and 2020 (Table 4) (Nilsson et al., 2022).

	Average rate of thinning (m yr^{-1})			
	Vanderford	**Adams**	**Anzac**	**Underwood**
2003 - 2017	-0.07	-0.02	-0.01	-0.03
2017 – 2020	-0.22	-0.32	-0.44	-0.38

Table 4. The average rate of thinning observed within the GL box of the Vanderford, Adams, Anzac, and Underwood Glaciers between 2003-2017 and 2017-2020, respectively. Note that these rates of thinning were extracted from the ice surface elevation dataset provided by Nilsson et al. (2022).

Whilst the observational period is relatively short, this synchronous dynamic response may potentially be indicative of a common external forcing. With the negative correlation between sea ice production and the intrusion of mCDW previously outlined (Miles et al., 2016), such enhanced thinning could be related to the significant decline in Antarctic sea ice extent seen during the austral spring of 2016 (Turner et al., 2017b). Whilst negative sea ice anomalies were observed to be transient across the Western Pacific Ocean (90°E – 160°E) (Turner et al., 2017b), decreased production of sea ice may have facilitated the increased incursion of warm mCDW within Vincennes Bay, thereby driving enhanced basal melting and dynamic thinning across the studied outlet glaciers. With a satellite-era record minimum Antarctic sea ice extent observed in February 2022 (Turner et al., 2022), such accelerated thinning may be expected to continue in the immediate future.

In addition, the significant decline in Antarctic sea ice extent observed in 2016 (Turner et al., 2017b) may have had potentially important implications for the stability of the glacier termini. Analysis of outlet glacier dynamics within Porpoise Bay (Figure 6) revealed that large calving events observed in January 2007 and March 2016 were linked to the break-up of multi-year landfast sea ice within the bay (Miles et al., 2017). Miles et al. (2017) therefore emphasise that sea ice concentrations can exert a significant control on terminus stability, supporting correlations between terminus change and sea ice mélange conditions previously observed in Greenland (Reeh et al., 2001; Moon et al., 2015). The negative sea ice anomalies seen in 2016 (Turner et al., 2017b) may thus have reduced the stability of the outlet glacier termini, facilitating terminus advance and associated longitudinal thinning across the grounding line. Indeed, analysis of terminus position change indicates that each of the Vanderford, Adams, and Underwood glaciers underwent a period of sustained advance between 2017 and 2020 (Figure 11). However, Anzac Glacier was recorded to be comparatively stable between 2017 and 2020, retreating by just -86 m (Figure 11). This suggests the enhanced rate of thinning measured across Anzac Glacier was not the product of longitudinal thinning. It may therefore

be inferred that the thinning instead occurred in situ, perhaps further supporting the notion of increased basal melt rates driven by enhanced mCDW intrusion.

5.4. High velocity at Bond West Glacier

Ice discharge across the grounding line is dependent on ice velocity (Moon et al., 2015); the accurate assessment of ice velocity is hence crucial for determining sea level contributions. In comparison to the other outlet glaciers within Vincennes Bay, Bond West Glacier flows at a significantly higher velocity (Figure 13). The fastest flowing outlet glacier in East Antarctica, Shirase Glacier, is measured to reach speeds in excess of 2,200 m yr^{-1} across the grounding line (Miles et al. 2022), with a maximum speed of 2,700 m yr^{-1} measured at the calving front (Pattyn & Derauw, 2002). Whilst Bond West flows more slowly across its grounding line, at an average velocity of 1,463 m yr^{-1} (2002 – 2021), a more extreme acceleration is observed across Bond West's floating tongue, with a maximum flow speed of 3,344 m yr^{-1} measured in 2002 (Figure 13E). The floating tongue is thus heavily fractured (Figure 12A), showing a crevasse pattern more typically observed across fast-moving Greenlandic glaciers, such as Jakobshavn Isbræ (Mayer & Herzfeld, 2000). The high ice surface velocity measured across Bond West's floating tongue may be a product of the underlying bedrock topography, with a steep slope of 9.6° measured immediately upstream of the grounding line (Figure 19E). In addition, fast-flowing upstream ice is observed to converge through a comparatively narrow ice shelf, constrained to the east by a stable ice rise and to the west by elevated bedrock topography (Figure 1b). Enhanced ice velocity must thus occur in order to maintain constant ice discharge through a smaller cross-sectional area (Winsborrow et al., 2010).

5.5. Importance of accurate DInSAR grounding line mapping

The grounding line represents the critical boundary between grounded and floating ice; the accurate mapping of grounding line positions is therefore fundamental for understanding ice sheet mass balance and assessing potential future contributions to sea level rise (Rignot et al., 2014; Mohajerani et al., 2021). However, Antarctic grounding line positions have been mapped using a variety of different methods, with the term 'grounding line' often being used to refer to different distinct features across the grounding zone (Bindschadler et al., 2011). The most accurate mapping technique is typically considered to be DInSAR, with grounding line positions derived precisely through the analysis of tidally induced vertical motion (Rignot et al., 2014; Li et al., 2021; Mohajerani et al., 2021). In contrast, the manual digitisation of grounding line positions from optical imagery, delineated using the most seaward observed break-in-slope, can be associated with high levels of uncertainty (Fricker et al., 2009; Rignot

et al., 2011), particularly at fast-flowing outlet glaciers such as those found within Vincennes Bay (Bindschadler et al., 2011; Christie et al., 2016). This has been attributed to the notion that fast-flowing ice streams are typically moving via basal sliding, meaning the transition to zero basal resistance across the ice shelf therefore produces a less marked break-in-slope (Rignot et al., 2011). With the exception of Vanderford Glacier, the results presented in this study show that the grounding line positions mapped from optical imagery (ASAID and MOA datasets) are located in near-identical locations at each of the Vincennes Bay outlet glaciers between 2001 and 2014 (Figure 18). Whilst this may be indicative of grounding line stability, the distinct lack of precise DInSAR grounding line mapping over this time period precludes such inferences being made with certainty.

5.6. Limitations and future work

5.6.1. Limited availability of DInSAR derived grounding line positions

As previously emphasised in Section 5.5, DInSAR is generally considered to reflect the most precise technique for the accurate mapping of grounding line positions (Rignot et al., 2014; Li et al., 2021; Mohajerani et al., 2021). However, such processing requires both knowledge of interferometric techniques and availability of suitable short repeat pass data (Friedl et al., 2020). Analysis of grounding line position variability was hence limited to the data provided, with DInSAR derived positions only available across each of the Vanderford, Adams, and Anzac Glaciers. With the grounding line position representing such a critical parameter for the accurate assessment of glacier stability, future work should thus prioritise such DInSAR techniques, particularly across potentially dynamic regions such as Vincennes Bay. Friedl et al. (2020) state that such focus necessitates further mid or lower frequency SAR missions, with several scheduled for the near future. Indeed, improved understanding of the grounding zone has been highlighted as a fundamental priority of the Antarctic RINGS Action Group, an international collaboration aiming to address major knowledge gaps across the margins of Antarctica (RINGS Action Group, 2022).

5.6.2. Lack of detailed analysis of sea ice variability

An important finding of this study was the potential influence of variable sea ice production in modulating the intrusion of mCDW within Vincennes Bay. This feedback was attributed to observed decadal patterns of terminus position change, as well as the onset of enhanced thinning across the Vanderford, Adams, Anzac, and Underwood Glaciers in 2017. However, due to the time constraints associated with this project, sea ice production within Vincennes

Bay was assumed to be consistent with wider trends reported across Wilkes Land (Miles et al., 2016), rather than being measured directly. Whilst this study used a previously observed negative correlation between mean air surface temperatures (April to October) and sea ice production (Miles et al., 2016) in order to extrapolate regional sea ice trends, such inferences remain an assumption based on theory. Direct observations could provide further certainty that changes in sea ice production may modulate the intrusion of mCDW within Vincennes Bay and hence drive dynamic change across the Vincennes Bay outlet glaciers. Potential data which could be utilised includes the Bootstrap sea ice concentrations used by Miles et al. (2016), or the daily gridded sea ice concentrations provided by Meier et al. (2021).

5.6.3. Further bathymetric analysis and future modelling

The rate of grounding line retreat observed is strongly dependent on the underlying bedrock topography (Milillo et al., 2019; Millan et al., 2022). Rignot et al. (2014) therefore emphasise that developing accurate bed topographies across the grounding lines of potentially unstable glaciers is fundamental, facilitating more reliable predictions of ice flow evolution. Stokes et al. (2022) reiterate this suggestion, also highlighting the importance of detailed observations of continental-shelf bathymetry. This could be particularly pertinent for Vanderford Glacier, with the results presented in this study indicating it may be vulnerable to future MISI. Further ice flow modelling, constrained using improved bed topographies and the results presented in Chapter 4, could also provide further important insights into the potential ice flow evolution of Vanderford Glacier. With the Aurora subglacial basin estimated to hold a SLE of between 3 and 5 m (Gulick et al., 2017), such modelling could be useful for reducing the high levels of uncertainty associated with the prediction of future sea level contributions from the EAIS.

Chapter 6. Conclusions

This thesis provides the first detailed analysis of ice dynamics across the largely unstudied outlet glaciers draining into Vincennes Bay, a region recently recorded to have the warmest intrusions of mCDW ever observed around East Antarctica (Ribeiro et al., 2021). The results reveal extensive grounding line retreat at Vanderford Glacier, measured at 18.6 km between 1996 and 2020, representing an average retreat rate of 0.8 km yr^{-1}. This reflects the highest rate of grounding line retreat reported for any glacier within East Antarctica and is consistent with the notion that warm mCDW is able to intrude at depth, accessing cavities formed below the Vanderford Ice Shelf and driving high rates of basal melt (Depoorter et al., 2013; Ribeiro et al., 2021). Although currently grounded on a stabilising bedrock ridge, retrograde slopes are observed inland along the Vanderford Trench. If grounding line retreat continues at the present rate, this retrograde slope will be reached within 100 years, raising the potential for MISI. With basal melt predicted to further inhibit the formation of DSW within the Vanderford polynya (Ribeiro et al., 2021; Herraiz-Borreguero & Garabato, 2022), mCDW intrusion may be enhanced, thereby providing the oceanic forcing required to drive further grounding line retreat. Although the dynamic response of Vanderford Glacier has been limited thus far, a consistent thinning trend was measured over the observational period, measured between -0.07 and -0.12 m yr^{-1} (2003-2017). Ocean forcing may be expected to enhance this dynamic response, with both accelerated thinning and increased ice surface velocities predicted over the coming decades. This thesis therefore highlights the potential vulnerability of Vanderford Glacier, emphasising the importance of accurate ice flow modelling.

The study also revealed broader trends, with decadal changes in frontal position measured across the Vincennes Bay outlet glaciers corresponding closely with wider patterns reported along the Wilkes Land coastline (Miles et al., 2016). Analysis of air surface temperature data collected at Casey Station supports the notion that such trends may be correlated to variable sea ice production. It is suggested that decreased sea-ice production limits the formation of DSW, thereby facilitating the enhanced intrusion of mCDW at depth (Miles et al., 2016). An accelerated thinning signal measured across each of the Vanderford, Adams, Anzac, and Underwood Glaciers between 2017 and 2020 could be attributed to this feedback, with the preceding widespread decline in sea ice extent seen across Antarctica (Turner et al., 2017b) potentially facilitating enhanced mCDW intrusion and increased basal melting. This decline in sea ice extent may have also decreased the stability of the outlet glacier termini, with the Vanderford, Adams, and Underwood Glaciers each observed to advance between 2017 and 2020. Such terminus advance is suggested to have driven longitudinal thinning, thus further

contributing to the enhanced thinning signal observed. With sea ice inferred to exert such a potentially significant control on glacier dynamics within Vincennes Bay, future work may be strengthened through the direct measurement of this variable. In comparison to Vanderford Glacier, the extent of grounding line retreat observed across the Adams, Anzac, Bond East, Bond West, and Underwood Glaciers was significantly lower, averaged at a rate of 0.2 km yr^{-1}. With a recently discovered canyon providing a potential bathymetric pathway for mCDW intrusion towards Vanderford Glacier, the comparatively lower rates of grounding line retreat observed across the remaining Vincennes Bay outlet glaciers may be indicative of a relative lack of bathymetric pathways towards these termini. Indeed, the grounding line positions of the Adams, Anzac, Bond East, Bond West, and Underwood Glaciers were seen to be stable between 2001 and 2014. However, such stability was inferred from datasets derived through manual digitisation of the most seaward observed break-in-slope and are hence associated with higher levels of uncertainty. The results of this study therefore emphasise the need to prioritise precise mapping of grounding line positions using DInSAR techniques, particularly across dynamic regions, such as Wilkes Land. The accurate assessment of grounding line positions will be fundamental in order to simulate future ice flow evolution across the EAIS and thus constrain estimations of potential sea level rise.

7. References

Aschwanden, A., Fahnestock, M., Truffer, M., Brinkerhoff, D., Hock, R., Khroulev, C., Mottram, R., Khan, S. (2019) Contribution of the Greenland Ice Sheet to sea level over the next millennium. *Science Advances.* 5(eaav9396): 1-11.

Australian Antarctic Division (2022) *RSV Nuyina discovers deep glacial canyon.* Available at: https://www.antarctica.gov.au/nuyina/stories/2022/rsv-nuyina-discovers-deep-glacial-canyon/ [Accessed: 21st January 2022].

Banwell, A., MacAyeal, D., Sergienko, O. (2013) Breakup of the Larsen B Ice Shelf triggered by chain reaction drainage of supraglacial lakes. *Geophysical Research Letters.* 40(22): 5872-5876.

Barrett, P. (2013) Resolving views on Antarctic Neogene glacial history - The Sirius debate. *Earth and Environmental Science Transactions of the Royal Society of Edinburgh.* 104: 31-53.

Bell, R., Banwell, A., Trusel, L., Kingslake, J. (2018) Antarctic surface hydrology and impacts on ice-sheet mass balance. *Nature Climate Change.* 8(12): 1044-1052.

Benn, D., Warren, C., Mottram, R. (2007) Calving processes and the dynamics of calving glaciers. *Earth-Science Reviews.* 82(3-4): 143-179.

Berthier, E., Scambos, T., Shuman, C. (2012) Mass loss of Larsen B tributary glaciers (Antarctic Peninsula) unabated since 2002. *Geophysical Research Letters.* 39(L13501): 1-6.

Bevan, S., Luckman, A., Benn, D., Adusumilli, S., Crawford, A. (2021) Brief communication: Thwaites Glacier cavity evolution. *The Cryosphere.* 15: 3317-3328.

Bindschadler, R., Choi, H., Wichlacz, A., Bingham, R., Bohlander, J., Brunt, K., Corr, H., Drews, R., Fricker, H., Hall, M., Hindmarsh, R., Kohler, J., Padman, L., Rack, W., Rotschky, G., Urbini, S., Vornberger, P., Young, N. (2011) Getting around Antarctica: new high-resolution mappings of the grounded and freely-floating boundaries of the Antarctica ice sheet created for the International Polar Year. *The Cryosphere*. 5: 569-588.

Blackburn, T., Edwards, G., Tulaczyk, S., Scudder, M., Piccione, G., Hallet, B., McLean, N., Zachos, J., Cheney, B., Babbe, J. (2020) Ice retreat in Wilkes Basin of East Antarctica during a warm interglacial. *Nature.* 583(7817): 554-559.

Black, T. & Joughin, I. (2022) Multi-decadal retreat of marine-terminating outlet glaciers in northwest and central-west Greenland. *The Cryosphere.* 16: 807-824.

Bleakley, N. (1996) *Geology of the Sirius Group at Mount Feather and Table Mountain, South Victoria Land, Antarctica*. Masters theses: Victoria University of Wellington. Available at: http://hdl.handle.net/10063/2751

Boening, C., Lebsock, M., Landerer, F., Stephens, G. (2012) Snowfall-driven mass change on the East Antarctic ice sheet. *Geophysical Research Letters.* 39(L21501): 1-5.

Candy, I., White, T., Elias, S. (2016) How warm was Britain during the Last Interglacial? A critical review of Ipswichian (MIS 5e) palaeotemperature reconstructions. *Journal of Quaternary Science.* 31(8): 857-868.

Chen, J., Wilson, C., Blankenship, D., Tapley, B. (2009) Accelerated Antarctic ice loss from satellite gravity measurements. *Nature Geoscience.* 2(12): 859-862.

Chen, X., Shearer, P., Walter, F., Fricker, H. (2011) Seventeen Antarctic seismic events detected by global surface waves and a possible link to calving events from satellite images. *Journal of Geophysical Research.* 116(B06311): 1-16.

Choi, Y., Morlighem, M., Rignot, E., Wood, M. (2021) Ice dynamics will remain a primary driver of Greenland ice sheet mass loss over the next century. *Communications Earth and Environment.* 2(26): 1-9.

Christianson, K., Bushuk, M., Dutrieux, P., Parizek, B., Joughin, I., Alley, R., Shean, D., Abrahamsen, E., Anandakrishnan, S., Heywood, K., Kim, T., Lee, S., Nicholls, K., Stanton, T., Truffer, M., Webber, B., Jenkins, A., Jacobs, S., Bindschadler, R., Holland, D. (2016) Sensitivity of Pine Island Glacier to observed ocean forcing. *Geophysical Research Letters.* 43(10): 817-825.

Colville, E., Carlson, A., Beard, B., Hatfield, R., Stoner, J., Reyes, A., Ullman, D. (2011) Sr-Nd-Pb Isotope Evidence for Ice-Sheet Presence on Southern Greenland During the Last Interglacial. *Science.* 333(6042): 620-623.

Commonwealth of Australia (2022) *RSV Nuyina Voyage 2 2021-22 Voyage Data, Southern Ocean, Antarctica, Version 1*. Australian Antarctic Data Centre. Available at: http://dx.doi.org/doi:10.26179/zz6j-e834 [Accessed: 14th October 2022].

Cook, A., Fox, A., Vaughan, D., Ferrigno, J. (2005) Retreating glacier fronts on the Antarctic Peninsula over the past half-century. *Science.* 308(5721): 541-544.

Cook, C. P., van de Flierdt, T., Williams, T., Hemming, S. R., Iwai, M., Kobayashi, M., Jimenez-Espejo, F. J., Escutia, C., González, J. J., Khim, B.-K., McKay, R. M., Passchier, S., Bohaty, S. M., Riesselman, C. R., Tauxe, L., Sugisaki, S., Galindo, A. L., Patterson, M. O., Sangiorgi, F., Pierce, E. L., Brinkhuis, H., Klaus, A., Fehr, A., Bendle, J. A. P., Bijl, P. K., Carr, S. A., Dunbar, R. B., Flores, J. A., Hayden, T. G., Katsuki, K., Kong, G. S., Nakai, M., Olney, M. P., Pekar, S. F., Pross, J., Röhl, U., Sakai, T., Shrivastava, P. K., Stickley, C. E., Tuo, S., Welsh, K., Yamane, M. (2013) Dynamic behaviour of the East Antarctic ice sheet during Pliocene warmth. *Nature Geoscience.* 6(9): 765-769.

Cook, A., Vaughan, D., Luckman, A., Murray, T. (2014a) A new Antarctic Peninsula glacier basin inventory and observed area changes since the 1940s. *Antarctic Science.* 26(6): 614-624.

Cook, C., Hill, D., van de Flierdt, T., Williams, T., Hemming, S., Dolan, A., Pierce, E., Escutia, C., Harwood, D., Cortese, G., Gonzales, J. (2014b) Sea surface temperature control on the distribution of far-traveled Southern Ocean ice-rafted detritus during the Pliocene. *Paleoceanography.* 29: 533-548.

Cook, A., Holland, P., Meredith, M., Murray, T., Luckman, A., Vaughan, D. (2016) Ocean forcing of glacier retreat in the western Antarctic Peninsula. *Science.* 353(6296): 283-286.

Davis, E., Jones, D., Morgan, V., Young, N. (1986) A survey of the Vanderford and Adams Glaciers in East Antarctica (Abstract). *Annals of Glaciology.* 8: 197.

DeConto, R. & Pollard, D. (2016) Contribution of Antarctic to past and future sea-level rise. *Nature.* 531(7596): 591-597.

DeConto, R., Pollard, D., Alley, R., Velicogna, I., Gasson, E., Gomez, N., Sadai, S., Condron, A., Gilford, D., Ashe, E., Kopp, R., Li, D., Dutton, A. (2021) The Paris Climate Agreement and future sea-level rise form Antarctica. *Nature.* 593(7857): 83-89.

Depoorter, M., Bamber, J., Griggs, J., Lenaerts, J., Ligtenberg, S., Van den Broeke, M., Moholdt, G. (2013) Calving fluxes and basal melt rates of Antarctic ice shelves. *Nature*. 502: 89-92.

Diener, T., Sasgen, I., Agosta, C., Fürst, J., Braun, M., Konrad, H., Fettweis, X. (2021) Acceleration of Dynamic Ice Loss in Antarctica From Satellite Gravimetry. *Frontiers in Earth Science.* 9(741789): 1-17.

Dowsett, H. (2007) Faunal re-evaluation of Mid-Pliocene conditions in the western equatorial Pacific. *Micropaleontology.* 53(6): 447-456.

Durand, G., Gagliardini, O., de Fleurian, B., Zwinger, T., Le Meur, E. (2009) Marine ice sheet dynamics: Hysteresis and neutral equilibrium. *Journal of Geophysical Research.* 114(F03009): 1-10.

Dutton, A., Carlson, A., Long, A., Milne, G., Clark, P., DeConto, R., Horton, B., Rahmstorf, S., Raymo, M. (2015) Sea-level rise due to polar ice-sheet mass loss during past warm periods. *Science.* 349(6244): 1-9.

Edwards, T., Brandon, M., Durand, G., Edwards, N., Golledge, N., Holden, P., Nias, I., Payne, A., Ritz, C., Wernecke, A. (2019) Revising Antarctic ice loss due to marine ice-cliff instability. *Nature.* 566(7742): 58-64.

Edwards, T. L., Nowicki, S., Marzeion, B., Hock, R., Goelzer, H., Seroussi, H., Jourdain, N. C., Slater, D. A., Turner, F. E., Smith, C. J., McKenna, C. M., Simon, E., Abe-Ouchi, A., Gregory, J. M., Larour, E., Lipscomb, W. H., Payne, A. J., Shepherd, A., Agosta, C., Alexander, P., Albrecht, T., Anderson, B., Asay-Davis, X., Aschwanden, A., Barthel, A., Bliss, A., Calov, R., Chambers, C., Champollion, N., Choi, Y., Cullather, R., Cuzzone, J., Dumas, C., Felikson, D., Fettweis, X., Fujita, K., Galton-Fenzi, B. K., Gladstone, R., Golledge, N. R., Greve, R., Hattermann, T., Hoffman, M. J., Humbert, A., Huss, M., Huybrechts, P., Immerzeel, W., Kleiner, T., Kraaijenbrink, P., Le clec'h, S., Lee, V., Leguy, G. R., Little, C. M., Lowry, D. P., Malles, J.-H., Martin, D. F., Maussion, F., Morlighem, M., O'Neill, J. F., Nias, I., Pattyn, F., Pelle, T., Price, S. F., Quiquet, A., Radić, V., Reese, R., Rounce, D. R., Rückamp, M., Sakai, A., Shafer, C., Schlegel, N.-J., Shannon, S., Smith, R. S., Straneo, F., Sun, S., Tarasov, L., Trusel, L. D., Van Breedam, J., van de Wal, R., van den Broeke, M., Winkelmann, R., Zekollari, H., Zhao, C., Zhang, T., Zwinger, T. (2021) Projected land ice contributions to twenty-first-century sea level rise. *Nature.* 593(7857): 74-82.

ENVEO. (2021) *ESA Antarctic Ice Sheet Climate Change Initiative (Antarctic_Ice_Sheet_cci): Antarctic Ice Sheet monthly velocity from 2017 to 2020, derived*

from Sentinel-1, v1. NERC EDS Centre for Environmental Data Analysis. doi: http://dx.doi.org/10.5285/00fe090efc58446e8980992a617f632f. [23rd May 2022].

Favier, L., Durand, G., Cornford, S., Gudmundsson, G., Gagliardini, O., Gillet-Chaulet, F., Zwinger, T., Payne, A., Le Brocq, A. (2014) Retreat of Pine Island Glacier controlled by marine ice-sheet instability. *Nature Climate Change.* 4: 117-121.

Feldmann, J. & Levermann, A. (2015) Collapse of the West Antarctic Ice Sheet after local destabilisation of the Amundsen Basin. *PNAS.* 112(46): 14191-14196.

Fettweis, X., Box, J., Agosta, C., Amory, C., Kittel, C., Lang, C., van As, D., Machguth, H., Gallée, H. (2017) Reconstructions of the 1900-2015 Greenland ice sheet surface mass balance using the regional climate MAR model. *The Cryosphere.* 11(2): 1015-1033.

Flament, T. & Rémy, F. (2012) Dynamic thinning of Antarctic glaciers from along-track repeat radar altimetry. *Journal of Glaciology.* 58(211): 830-840.

Fox-Kemper, B., Hewitt, H., Xiao, C., Aðalgeirsdóttir, G., Drijfhout, S., Edwards, T., Golledge, N., Hemer, M., Kopp, R., Krinner, G., Mix, A., Notz, D., Nowicki, S., Nurhati, I., Ruiz, L., Sallée, J., Slangen, A. (2021) 'Chapter 9 - Ocean, Cryosphere and Sea Level Change' in Masson-Delmotte, V., Zhai, P., Pirani, A., Connors, S., Péan, C., Berger, S., Caud, N., Chen, Y., Goldfarb, L., Gomis, M., Huang, M., Leitzell, K., Lonnoy, E., Matthews, J., Maycock, T., Waterfield, T., Yelekci, O., Yu, R., Zhou, B. (Eds) *Climate Change 2021: The Physical Science Basis. Contribution of Working Group I to the Sixth Assessment Report of the Intergovernmental Panel on Climate Change.* Cambridge: Cambridge University Press.

Fricker, H., Coleman, R., Padman, L., Scambos, T., Bohlander, J., Brunt, K. (2009) Mapping the grounding zone of the Amery Ice Shelf, East Antarctic using InSAD, MODIS and ICESat. *Antarctic Science.* 21(5): 515-532.

Friedl, P., Weiser, F., Fluhrer, A., Braun, M. (2020) Remote sensing of glacier and ice sheet grounding lines: A review. *Earth Science Reviews.* 201(102948): 1-29.

Fürst, J., Durand, G., Gillet-Chaulet, F., Tavard, L., Rankl, M., Braun, M., Gagliardini, O. (2016) The safety band of Antarctic ice shelves. *Nature Climate Change.* 6(5): 479-482.

Gao, C., Lu, Y., Zhang, Z., Shi, H. (2019) A Joint Inversion Estimate of Antarctic Ice Sheet Mass Balance Using Multi-Geodetic Data Sets. *Remote Sensing.* 11(653): 1-23.

Gardner, A., Moholdt, G., Scambos, T., Fahnstock, M., Ligtenberg, S., Van den Broeke, M., Nilsson, J. (2018) Increased West Antarctic and unchanged East Antarctic ice discharge over the last 7 years. *The Cryosphere*. 12(2): 521-547.

Gardner, A., Fahnestock, M., Scambos, T. (2022) ITS_LIVE Regional Glacier and Ice Sheet Surface Velocities: Version 1. Data archived at National Snow and Ice Data Center; https://doi:10.5067/6II6VW8LLWJ7. [1st March 2022].

Gasson, E., DeConto, R., Pollard, D., Levy, R. (2016) Dynamic Antarctic ice sheet during the early to mid-Miocene. *PNAS.* 113(13): 3459-3464.

Gasson, E. & Keisling, B. (2020) The Antarctic Ice Sheet: A Paleoclimate Modelling Perspective. *Oceanography.* 33(2): 90-100.

Glasser, N., Scambos, T., Bohlander, J., Truffer, M., Pettit, E., Davies, B. (2011) From ice-shelf tributary to tidewater glacier: continued rapid recession, acceleration and thinning of Röhss Glacier following the 1995 collapse of the Prince Gustav Ice Shelf, Antarctic Peninsula. *Journal of Glaciology.* 57(203): 397-406.

Goldstein, R., Engelhardt, H., Kamb, B., Frolich, R. (1993) Satellite Radar Interferometry for Monitoring Ice Sheet Motion: Application to an Antarctic Ice Stream. *Science.* 262(5139): 1525-1530.

Golledge, N., Kowalewski, D., Naish, T., Levy, R., Fogwill, C., Gasson, E. (2015) The multi-millennial Antarctic commitment to future sea-level rise. *Nature.* 526(7573): 421-425.

Grant, G., Naish, T. , Dunbar, G., Stocchi, P., Kominz, M., Kamp, P., Tapia, C., McKay, R., Levy, R., Patterson, M. (2019) The amplitude and origin of sea-level variability during the Pliocene epoch. *Nature.* 574(7777): 237-241.

Graversen, R. & Wang, M. (2009) Polar amplification in a coupled climate model with locked albedo. *Climate Dynamics.* 33: 629-643.

Greenbaum, J., Blankenship, D., Young, D., Richter, T., Roberts, J., Aitken, A., Legresy, B., Schroeder, D., Warner, R., Ommen, T., Siegert, M. (2015) Ocean access to a cavity beneath Totten Glacier in East Antarctica. *Nature Geoscience*. 8: 294-298.

Greene, C., Blankenship, D., Gwyther, D., Silvano, A., Wijk, E. (2017) Wind causes Totten Ice Shelf melt and acceleration. *Science Advances*. 3(11): 1-7.

Gulick, S., Shevenell, A., Montelli, A., Fernandez, R., Smith, C., Warny, S., Bohaty, S., Sjunneskog, C., Leventer, A., Frederick, B., Blankenship, D. (2017) Initiation and long-term instability of the East Antarctic Ice Sheet. *Nature.* 552(7684): 225-229.

Gwyther, D., Galton-Fenzi, B., Hunter, J., Roberts, J. (2014) Simulated melt rates for the Totten and Dalton ice shelves. *Ocean Science*. 10: 267-279.

Hanna, E., Pattyn, F., Navarro, F., Favier, V., Goelzer, H., van den Broeke, M., Vizcaino, M., Whitehouse, P., Ritz, C., Bulthuis, K., Smith, B. (2020) Mass balance of the ice sheets and glaciers – Progress since AR5 and challenges. *Earth-Science Reviews.* 201(102976): 1-17.

Haran, T., Bohlander, J., Scambos, T., Painter, T., Fahnestock, M. (2005) *MODIS Mosaic of Antarctica 2003 – 2004 (MOA2004) Image Map, Version 1.* Boulder, Colorado USA. National Snow and Ice Data Centre Distributed Active Archive Centre. doi: https://doi.org/10.5067/68TBT0CGJSOJ. [28th February 2022].

Haran, T., Bohlander, J., Scambos, T., Painter, T., Fahnestock, M. (2014) *MODIS Mosaic of Antarctica 2008 – 2009 (MOA2009) Image Map, Version 1.* Boulder, Colorado USA. National Snow and Ice Data Centre Distributed Active Archive Centre. doi: https://doi.org/10.5067/4ZL43A4619AF. [28th February 2022].

Haran, T., Linger, M., Bohlander, J., Fahnestock, M., Painter, T., Scambos, T. (2018) *MEaSUREs MODIS Mosaic of Antarctica 2013-2014 (MOA2014) Image Map, Version 1.* Boulder, Colorado USA. National Snow and Ice Data Centre Distributed Active Archive Centre. doi: https://doi.org/10.5067/RNF17BP824UM. [28th February 2022].

Harig, C. & Simons, F. (2015) Accelerated West Antarctic ice mass loss continues to outpace East Antarctic gains. *Earth and Planetary Science Letters*. 415: 134-141.

Haywood, A., Ridgwell, A., Lunt, D., Hill, D., Pound, M., Dowsett, H., Dolan, A., Francis, J., Williams, M. (2011) Are there pre-Quaternary geological analogues for a future greenhouse warming? *Philosophical Transactions of the Royal Society A.* 369(1938): 933-956.

Herraiz-Borreguero, L. & Garabato, A. (2022) Poleward shift of Circumpolar Deep Water threatens the East Antarctic Ice Sheet. *Nature Climate Change.* 12: 728-734.

Holland, D., Nicholls, K., Basinski, A. (2020) The Southern Ocean and its interaction with the Antarctic Ice Sheet. *Science.* 367: 1326-1330.

Howat, I., Porter, C., Smith, B., Noh, M., Morin, P. (2019) The Reference Elevation Model of Antarctica. *The Cryosphere.* 13: 665-674.

Hughes, T. (1981) The weak underbelly of the West Antarctic Ice Sheet. *Journal of Glaciology.* 27(97): 518-525.

Jenkins, A., Dutrieux, P., Jacobs, S., McPhail, S., Perrett, J., Webb, A., White, D. (2010) Observations beneath Pine Island Glacier in West Antarctica and implications for its retreat. *Nature Geoscience.* 3(7): 468-472.

Jones, M., Bromwich, D., Nicolas, J., Carrasco, J., Plavcová, E., Zou, X., Wang, S. (2019) Sixty Years of Widespread Warming in the Southern Middle and High Latitudes (1957-2016). *Journal of Climate.* 32(20): 6875-6898.

Joughin, I. & Alley, R. (2011) Stability of the West Antarctic ice sheet in a warming world. *Nature Geoscience.* 4: 506-513.

Joughin, I., Smith, B., Medley, B. (2014) Marine Ice Sheet Collapse Potentially Under Way for the Thwaites Glacier Basin, West Antarctica. *Science.* 344: 735-738.

Kellogg, D. & Kellogg, T. (1996) Diatoms in South Pole ice: Implications for eolian contamination of Sirius Group deposits. *Geology.* 24(2): 115-118.

Khazendar, A., Schodlok, M., Fenty, I., Ligtenberg, S., Rignot, E., Van den Broeke, M. (2013) Observed thinning of Totten Glacier is linked to coastal polynya variability. *Nature Communications*. 4(2857): 1-9.

Kim, K., Jezek, K., Liu, H. (2007) Orthorectified image mosaic of Antarctica from 1963 Argon satellite photography: image processing and glaciological applications. *International Journal of Remote Sensing.* 28(23): 5357-5373.

Kitade, Y., Shimada, K., Tamura, T., Williams, G., Aoki, S., Fukamachi, Y., Roquet, F., Hindell, M., Ushio, S., Ohshima, K. (2014) Antarctic Bottom Water production from the

Vincennes Bay Polynya, East Antarctica. *Geophysical Research Letters.* 41(10): 3528-3534.

Konrad, H., Gilbert, L., Cornford, S., Payne, A., Hogg, A., Muir, A., Shepherd, A. (2017) Uneven onset and pace of ice-dynamical imbalance in the Amundsen Sea Embayment, West Antarctica. *Geophysical Research Letters.* 44: 910-918.

Kopp, R., Simons, F., Mitrovica, J., Maloof, A., Oppenheimer, M. (2009) Probabilistic assessment of sea level during the last interglacial stage. *Nature.* 462(7275): 863-868.

Kusahara, K., Hasumi, H., Williams, G. (2011) Impact of the Mertz Glacier Tongue calving on dense water formation and export. *Nature Communications.* 2(159): 1-6.

Lee, J., Marotzke, J., Bala, G., Cao, L., Corti, S., Dunne, J., Engelbrecht, F., Fischer, E., Fyfe, J., Jones, C., Maycock, A., Mutemi, J., Ndiaye, O., Panickal, S., Zhou, T. (2021) 'Chapter 4 - Future Global Climate: Scenario-based Projections and Near-term Information' in Massn-Delmotte, V., Zhai, P., Pirani, A., Connors, S., Péan, C., Berger, S., Caud, N., Chen, Y., Goldfarb, L., Gomis, M., Huang, M., Leitzell, K., Lonnoy, E., Matthews, J., Maycock, T., Waterfield, T., Yelekci, O., Yu, R., Zhou, B. (Eds) *Climate Change 2021: The Physical Science Basis. Contribution of Working Group I to the Sixth Assessment Report of the Intergovernmental Panel on Climate Change.* Cambridge: Cambridge University Press.

Leeson, A., Forster, E., Rice, A., Gourmelen, N., van Wessem, J. (2020) Evolution of Supraglacial Lakes on the Larsen B Ice Shelf in the Decades Before it Collapsed. *Geophysical Research Letters.* 47(e2019GL085591): 1-9.

Lhermitte, S., Sun, S., Shuman, C., Wouters, B., Pattyn, F., Wuite, J., Berthier, E., Nagler, T. (2020) Damage accelerates ice shelf instability and mass loss in Amundsen Sea Embayment. *PNAS.* 117(40): 24735-24741.

Li, X., Rignot, E., Morlighem, M., Mouginot, J., Scheuchl, B. (2015) Grounding line retreat of Totten Glacier, East Antarctica, 1996 to 2013. *Geophysical Research Letters.* 42(19): 8049-8056.

Li, X., Rignot, E., Mouginot, J., Scheuchl, B. (2016) Ice flow dynamics and mass loss of Totten Glacier, East Antarctica, from 1989 to 2015. *Geophysical Research Letters.* 43(12): 6366-6373.

Li, R., Lv, D., Xie, H., Tian, Y., Xu, Y., Lu, S., Tong, X., Weng, H. (2021) A comprehensive assessment and analysis of Antarctic satellite grounding line products from 1992 to 2009. *Science China Earth Sciences.* 64(8): 1332-1345.

Lim, E., Hendon, H., Arblaster, J., Delage, F., Nguyen, H., Min, S., Wheeler, M. (2016) The impact of the Southern Annular Mode on future changes in Southern Hemisphere rainfall. *Geophysical Research Letters.* 43: 7160-7167.

Liu, Y., Moore, J. C., Cheng, X., Gladstone, R. M., Bassis, J. N., Liu, H., Wen, J., Hui, F. (2015) Ocean-driven thinning enhances iceberg calving and retreat of Antarctic ice shelves. *Proceedings of the National Academy of Sciences.* 112(11): 3263-3268.

Martín-Español, A., Zammit-Mangion, A., Clarke, P., Flament, T., Helm, V., King, M., Luthcke, S., Petrie, E., Rémy, F., Schön, N., Wouters, B., Bamber, J. (2016) Spatial and

temporal Antarctic Ice Sheet mass trends, glacio-isostatic adjustment, and surface processes from a joint inversion of satellite altimetry, gravity, and GPS data. *Journal of Geophysical Research: Earth Surface*. 121: 182-200.
Matsuoka, K., Skoglund, A., Roth, G., de Pomereu, J., Griffiths, H., Headland, R., Herried, B., Katsumata, K., Le Brocq, A., Licht, K., Morgan, F., Neff, P. D., Ritz, C., Scheinert, M., Tamura, T., Van de Putte, A., van den Broeke, M., von Deschwanden, A., Deschamps-Berger, C., Van Liefferinge, B., Tronstad, S., Melvær, Y. (2021) Quantarctica, an integrated mapping environment for Antarctica, the Southern Ocean, and sub-Antarctic islands. *Environment Modelling & Software.* 140: 1-14.

Mayer, H. & Herzfeld, U. (2000) Structural glaciology of the fast-moving Jakobshavn Isbræ, Greenland, compared to the surging Bering Glacier, Alaska, U.S.A. *Annals of Glaciology.* 30: 243-249.

McKay, N., Overpeck, J., Otto-Bliesner, B. (2011) The role of ocean thermal expansion in Last Interglacial sea level rise. *Geophysical Research Letters.* 38(L14605): 1-6.

McKay, D., Staal, A., Abrams, J., Winkelmann, R., Sakschewski, B., Loriani, S., Fetzer, I., Cornell, S., Rockström, J., Lenton, T. (2022) Exceeding 1.5°C global warming could trigger multiple climate tipping points. *Science.* 377(6611): 1-10.

McMillan, M., Shepherd, A., Sundal, A., Briggs, K., Muir, A., Ridout, A., Hogg, A., Wingham, D. (2015) Increased ice losses from Antarctica detected by CryoSat-2. *Geophysical Research Letters*. 41(11): 3899-3905.

Medley, B., Joughin, I., Smith, B., Das, S., Steig, E., Conway, H., Gogineni, S., Lewis, C., Criscitiello, A., McConnell, J., Van den Broeke, M., Lenaerts, J., Bromwich, D., Nicolas, J., Leuschen, C. (2014) Constraining the recent mass balance of Pine Island and Thwaites glaciers, West Antarctica, with airborne observations of snow accumulation. *The Cryosphere.* 8(4): 1375-1392.

Meier, W., Stewart, J., Wilcox, H., Hardman, M., Scott, D. (2021) *Near-Real-Time DMSP SSMIS Daily Polar Gridded Sea Ice Concentrations, Version 2. Boulder, Colorado USA. NASA National Snow and Ice Data Center Distributed Active Archive Center. doi: https://doi.org/10.5067/YTTHO2FJQ97K*.

Mengel M. & Levermann, A. (2014) Ice plug prevents irreversible discharge from East Antarctica. *Nature Climate Change.* 4(6): 451-455.

Mercer, J. (1978) West Antarctic ice sheet and CO_2 greenhouse effect: a threat of disaster. *Nature.* 271(5643): 321-325.

Met-READER (2022) Casey temperature. Available at: https://legacy.bas.ac.uk/met/READER/surface/Casey.All.temperature.html [Accessed: 13th July 2022].

Miles, B. (2013) *Synchronous terminus change of East Antarctic outlet glaciers linked to climatic forcing.* Durham theses: Durham University. Available at Durham E-Theses Online: http://etheses.dur.ac.uk/7333/.

Miles, B., Stokes, C., Jamieson, S. (2016) Pan-ice-sheet glacier terminus change in East Antarctic reveals sensitivity of Wilkes Land to sea-ice changes. *Science Advances*. 2(5): 1-7.

Miles, B., Stokes, C., Jamieson, S. (2017) Simultaneous disintegration of outlet glaciers in Porpoise Bay (Wilkes Land), East Antarctica, driven by sea ice break-up. *The Cryosphere.* 11: 427-442.

Miles, B., Stokes, C., Jamieson, S. (2018) Velocity increases at Cook Glacier, East Antarctica, linked to ice shelf loss and a subglacial flood event. *The Cryosphere*. 12: 3123-3136.

Miles, B., Jordan, J., Stokes, C., Jamieson, S., Gudmundsson, H., Jenkins, A. (2021) Recent acceleration of Denman Glacier (1972-2017), East Antarctica, driven by grounding line retreat and changes in ice tongue configuration. *The Cryosphere.* 15: 663-676.

Miles, B., Stokes, C., Jenkins, A., Jordan, J., Jamieson, S., Gudmundsson, G. (2022) Slowdown of Shirase Glacier caused by strengthening alongshore winds. *The Cryosphere Discussions.* [preprint] https://doi.org/10.5194/tc-2022-126.

Milillo, P., Rignot, E., Rizzoli, P., Scheuchl, B., Mouginot, J., Bueso-Bello, J., Prats-Iraola. (2019) Heterogeneous retreat and ice melt of Thwaites Glacier, West Antarctica. *Science Advances.* 5(eaau3433): 1-8.

Millan, R., Mouginot, J., Derkacheva, A., Rignot, E., Milillo, P., Ciraci, E., Dini, L., Bjørk, A. (2022) Ongoing grounding line retreat and fracturing initiated at the Petermann Glacier ice shelf, Greenland, after 2016. *The Cryosphere.* 16: 3021-3031.

Miller, K. G., Wright, J. D., Browning, J. V., Kulpecz, A., Kominz, M., Naish, T. R., Cramer, B. S., Rosenthal, Y., Peltier, W. R., Sosdian, S. (2012) High tide of the warm Pliocene: Implications of global sea level for Antarctic deglaciation. *Geology.* 40(5): 407-410.
Mohajerani, Y., Velicogna, I., Rignot, E. (2018) Mass loss of Totten and Moscow University glaciers, East Antarctica, using regionally optimised GRACE mascons. *Geophysical Research Letters.* 45(14): 7010-7018.

Mohajerani, Y., Jeong, S., Scheuchl, B., Velicogna, I., Rignot, E., Milillo, P. (2021) Automatic delineation of glacier grounding lines in differential interferometric synthetic-aperture radar data using deep learning. *Scientific Reports.* 11(4992): 1-10.

Moon, T. & Joughin, I. (2008) Changes in ice front position of Greenland's outlet glaciers from 1992 to 2007. *Journal of Geophysical Research*. 13(F02022): 1-10.

Moon, T., Joughin, I., Smith, B. (2015) Seasonal to multiyear variability of glacier surface velocity, terminus position, and sea ice/ice mélange in northwest Greenland. *Journal of Geophysical Research: Earth Surface.* 120: 818-833.

Morgan, V., Wookey, C., Li, J., van Ommen, T., Skinner, W., Fitzpatrick, M. (1997) Site information and initial results from deep ice drilling on Law Dome, Antarctica. *Journal of Glaciology.* 43(143): 3-10.

Morlighem, M. (2020) *MEaSUREs BedMachine Antarctica, Version 2.* Boulder, Colorado USA. National Snow and Ice Data Centre Distributed Active Archive Centre. doi: https://doi.org/10.5067/E1QL9HFQ7A8M. [30th May 2022].

Morlighem, M., Rignot, E., Binder, T., Blankenship, D., Drews, R., Eagles, G., Eisen, O., Ferraccioli, F., Forsberg, R., Fretwell, P., Goel, V., Greenbaum, J., Gudmundsson, H., Guo, J., Helm, V., Hofstede, C., Howat, I., Humbert, A., Jokat, W., Karlsson, N., Lee, W., Matsuoka, K., Millan, R., Mouginot, J., Paden, J., Pattyn, F., Roberts, J., Rosier, S., Ruppel, A., Seroussi, H., Smith, E., Steinhage, D., Sun, B., Van den Broeke, M., Ommen, T., Wessem, M., Young, D. (2020) Deep glacial troughs and stabilising ridges unveiled beneath the margins of the Antarctic ice sheet. *Nature Geoscience*. 13(2): 132-137.

Mouginot, J., Rignot, E., Scheuchl, B. (2014) Sustained increase in ice discharge from the Amundsen Sea Embayment, West Antarctica, from 1973 to 2013. *Geophysical Research Letters.* 41(5): 1576-1584.

Nagler, T., Rott, H., Hetzenecker, M., Wuite, J., Potin, P. (2015) The Sentinel-1 Mission: New Opportunities for Ice Sheet Observations. *Remote Sensing.* 7(7): 9371-9389.

Naish, T., Woolfe, K., Barrett, P., Wilson, G., Atkins, C., Bohaty, S., Bücker, C., Claps, M., Davey, F., Dunbar, G., Dunn, A., Fielding, C., Florindo, F., Hannah, M., Harwood, D., Henrys, S., Krissek, L., Lavelle, M., van der Meer, J., McIntosh, W., Niessen, F., Passchier, S., Powell, R., Roberts, A., Sagnotti, L., Scherer, R., Strong, C., Talarico, F., Verosub, K., Villa, G., Watkins, D., Webb, P., Wonik, T. (2001) Orbitally induced oscillations in the East Antarctic ice sheet at the Oligocene/Miocene boundary. *Nature.* 413(6857): 719-723.

Navarro, F. (2021) Sea-Level Rise: Which is the role of glaciers and polar ice sheets? *Mètode.* 11: 173-181.

Nias, I., Cornford, S., Payne, A. (2016) Contrasting the modelled sensitivity of the Amundsen Sea Embayment ice streams. *Journal of Glaciology.* 62(233): 552-562.

Nilsson, J., Gardner, A., Paolo, F. (2022) Elevation Change of the Antarctic Ice Sheet: 1985 to 2020. *Earth System Science Data.* 14: 3573-3598.

Noble, T. L., Rohling, E. J., Aitken, A. R. A., Bostock, H. C., Chase, Z., Gomez, N., Jong, L. M., King, M. A., Mackintosh, A. N., McCormack, F. S., McKay, R. M., Menviel, L., Phipps, S. J., Weber, M. E., Fogwill, C. J., Gayen, B., Golledge, N. R., Gwyther, D. E., Hogg, A. McC., Martos, Y. M., Pena-Molino, B., Roberts, J., van de Flierdt, T., Williams, T. (2020) The Sensitivity of the Antarctic Ice Sheet to a Changing Climate: Past, Present, and Future. *Reviews of Geophysics.* 58(e2019RG000663): 1-89.

Oliva, M., Navarro, F., Hrbáček, F., Hernández, A., Nývlt, D., Pereira, P., Ruiz-Fernández, J., Trigo, R. (2017) Recent regional climate cooling on the Antarctic Peninsula and associated impacts on the cryosphere. *Science of the Total Environment.* 580: 210-223.

Paolo, F., Fricker, H., Padman, L. (2015) Volume loss from Antarctic ice shelves is accelerating. *Science.* 348(6232): 327-331.

Parizek, B., Christianson, K., Anandakrishnan, S., Alley, R., Walker, R., Edwards, R., Wolfe, D., Bertini, G., Rinehart, S., Bindschadler, R., Nowicki, S. (2013) Dynamic (in)stability of

Thwaites Glacier, West Antarctica. *Journal of Geophysical Research: Earth Surface.* 118: 638-655.

Pattyn, F. & Derauw, D. (2002) Ice-dynamic conditions of Shirase Glacier, Antarctica, inferred from ERS SAR interferometry. *Journal of Glaciology.* 48(163): 559-565.

Pattyn, F. & Morlighem, M. (2020) The uncertain future of the Antarctic Ice Sheet. *Science.* 367(6484): 1331-1335.

Paul, F., Bolch, T., Briggs, K., Kääb, A., McMillan, M., McNabb, R., Nagler, T., Nuth, C., Rastner, P., Strozzi, T., Wuite, J. (2017) Error sources and guidelines for quality assessment of glacier area, elevation change, and velocity products derived from satellite data in the Glaciers_cci project. *Remote Sensing of Environment.* 203: 256-275.

Pelle, T., Morlighem, M., Nakayama, Y., Seroussi, H. (2021) Widespread Grounding Line Retreat of Totten Glacier, East Antarctica, Over the 21st Century. *Geophysical Research Letters.* 48(e2021GL093213): 1-11.

Petty, A., Holland, P., Feltham, D. (2014) Sea ice and the ocean mixed layer over the Antarctic shelf seas. *The Cryosphere.* 8: 761-783.

Picton, H., Stokes, C., Jamieson, S., Floricioiu, D., Krieger, L. (2022) Extensive and anomalous grounding line retreat at Vanderford Glacier, Vincennes Bay, Wilkes Land, East Antarctica. *The Cryosphere Discussions.* [preprint] https://doi.org/10.5194/tc-2022-217.

Pollard, D., DeConto, R., Alley, R. (2015) Potential Antarctic Ice Sheet retreat driven by hydrofracturing and ice cliff failure. *Earth and Planetary Science Letters.* 412: 112-121.

Pritchard, H., Arthern, R., Vaughan, D., Edwards, L. (2009) Extensive dynamic thinning on the margins of the Greenland and Antarctic ice sheets. *Nature*. 461: 971-975.

Quiquet, A., Ritz, C., Punge, H., Mélia, D. (2013) Greenland ice sheet contribution to sea level rise during the last interglacial period: a modelling study driven and constrained by ice core data. *Climate of the Past.* 9(1): 353-366.

Reeh, N., Thomsen, H. H., Higgins, A. K., Weidick, A. (2001) Seasonal and interannual variations in ice melange and its impact on terminus stability, Jakobshavn Isbræ, Greenland. *Journal of Glaciology.* 61(225): 76-88.

Reese, R., Gudmundsson, G., Levermann, A., Winkelmann, R. (2018) The far reach of ice-shelf thinning in Antarctica. *Nature Climate Change.* 8: 53-57.

Ribeiro, N., Herraiz-Borreguero, L., Rintoul, S., McMahon, C., Hindell, M., Harcourt, R., Williams, G. (2021) Warm Modified Circumpolar Deep Water Intrusions Drive Ice Shelf Melt and Inhibit Dense Shelf Water Formation in Vincennes Bay, East Antarctica. *Journal of Geophysical Research: Oceans*. 126(8): 1-17.

Rignot, E. (1996) Tidal motion, ice velocity and melt rate of Petermann Gletscher, Greenland, measured from radar interferometry. *Journal of Glaciology.* 42(142): 476-485.

Rignot, E. & Thomas, R. (2002) Mass Balance of Polar Ice Sheets. *Science.* 297(5586): 1502-1506.

Rignot, E., Casassa, G., Gogineni, P., Krabill, W., Rivera, A., Thomas, R. (2004) Accelerated ice discharge from the Antarctic Peninsula following the collapse of Larsen B ice shelf. *Geophysical Research Letters.* 31(L18401): 1-4.

Rignot, E., Mouginot, J., Scheuchl, B. (2011) Antarctic grounding line mapping from differential satellite radar interferometry. *Geophysical Research Letters.* 38(L10504): 1-6.

Rignot, E., Jacobs, S., Mouginot, J., Scheuchl, B. (2013) Ice-Shelf Melting Around Antarctica. *Science.* 341: 266-270.
Rignot, E., Mouginot, J., Morlighem, M., Seroussi, H., Scheuchl, B. (2014) Widespread, rapid grounding line retreat of Pine Island, Thwaites, Smith, and Kohler glaciers, West Antarctica, from 1992 to 2011. *Geophysical Research Letters.* 41: 3502-3509.

Rignot, E., Mouginot, J., Scheuchl, B. (2016) *MEaSUREs Antarctic Grounding Line from Differential Satellite Radar Interferometry, Version 2.* Boulder, Colorado USA. National Snow and Ice Data Centre Distributed Active Archive Centre. doi: https://doi.org/10.5067/IKBWW4RYHF1Q. [28th February 2022].

Rignot, E., Mouginot, J., Scheuchl, B., Van den Broeke, M., Wessem, M., Morlighem, M. (2019) Four decades of Antarctic Ice Sheet Mass Balance from 1979-2017. *PNAS*. 116(4): 1095-1103.

RINGS Action Group (2022) *RINGS: Collaborative international effort to map all Antarctic ice-sheet margins.* Scientific Committee on Antarctic Research (SCAR). Available at: https://doi.org/10.5281/zenodo.6638327

Roberts, J., Galton-Fenzi, B., Paolo, F., Donnelly, C., Gwyther, D., Padman, L., Young, D., Warner, R., Greenbaum, J., Fricker, H., Payne, A., Cornford, S., Le Brocq, A., Ommen, T., Blankenship, D., Siegert, M. (2018) 'Ocean forced variability of Totten Glacier mass loss' in Siegert, M., Jamieson, D., White, D. (Eds) *Exploration of Subsurface Antarctica: Uncovering Past Changes and Modern Processes.* London: The Geological Society of London.

Robinson, A., Calov, R., Ganopolski, A. (2011) Greenland ice sheet model parameters constrained using simulations of the Eemian Interglacial. *Climate of the Past.* 7(2): 381-396.

Sasgen, I., Konrad, H., Ivins, E., Van den Broeke, M., Bamber, J., Martinec, Z., Lemann, V. (2013) Antarctic ice-mass balance 2003 to 2012: regional reanalysis of GRACE satellite gravimetry measurements with improved estimate of glacio-isostatic adjustment based on GPS uplift rates. *The Cryosphere.* 7(5): 1499-1512.

Sato, K., Inoue, J., Simmonds, I., Rudeva, I. (2021) Antarctic Peninsula warm winters influenced by Tasman Sea temperatures. *Nature Communications.* 12(1): 1-9.

Scambos, T., Haran, T., Fahnestock, M., Painter, T., Bohlander, J. (2007) MODIS-based Mosaic of Antarctica (MOA) data sets: Continent-wide surface morphology and snow grain size. *Remote Sensing of Environment*. 111(2-3): 242-257.

Scambos, T., Bell, R., Alley, R., Anandakrishnan, S., Bromwich, D., Brunt, K., Christianson, K., Creyts, T., Das, S., DeConto, R., Dutrieux, P., Fricker, H., Holland, D., MacGregor, J., Medley, B., Nicolas, J., Pollard, D., Siegfried, M., Smith, A., Steig, E., Trusel, L., Vaughan, D., Yager, P. (2017) How much, how fast?: A science review and outlook for research on

the instability of Antarctica's Thwaites Glacier in the 21st century. *Global and Planetary Change.* 153: 16-34.

Scherer, R., Aldahan, A., Tulaczyk, S., Possnert, G., Engelhardt, H., Kamb, B. (1998) Pleistocene Collapse of the West Antarctic Ice Sheet. *Science.* 281: 82-85.

Scherer, R., DeConto, R., Pollard, D., Alley, R. (2016) Windblown Pliocene diatoms and East Antarctic Ice Sheet retreat. *Nature Communications.* 7(12957): 1-9.

Schoof, C. (2007) Ice sheet grounding line dynamics: Steady states, stability, and hysteresis. *Journal of Geophysical Research.* 112(F03S28): 1-19.

Schoof, C. (2010) Beneath a floating ice shelf. *Nature Geoscience.* 3(7): 450-451.

Schröder, L., Horwath, M., Dietrich, R., Helm, V., Van den Broeke, M., Ligtenberg, S. (2019) Four decades of Antarctic surface elevation changes from multi-mission satellite altimetry. *The Cryosphere*. 13(2): 427-449.

Seki, O., Foster, G., Schmidt, D., Mackensen, A., Kawamura, K., Pancost, R. (2010) Alkenone and boron-based Pliocene pCO_2 records. *Earth and Planetary Science Letters.* 292: 201-211.

Seroussi, H., Nowicki, S., Payne, A. J., Goelzer, H., Lipscomb, W. H., Abe-Ouchi, A., Agosta, C., Albrecht, T., Asay-Davis, X., Barthel, A., Calov, R., Cullather, R., Dumas, C., Galton-Fenzi, B. K., Gladstone, R., Golledge, N. R., Gregory, J. M., Greve, R., Hattermann, T., Hoffman, M. J., Humbert, A., Huybrechts, P., Jourdain, N. C., Kleiner, T., Larour, E., Leguy, G. R., Lowry, D. P., Little, C. M., Morlighem, M., Pattyn, F., Pelle, T., Price, S. F., Quiquet, A., Reese, R., Schlegel, N.-J., Shepherd, A., Simon, E., Smith, R. S., Straneo, F., Sun, S., Trusel, L. D., Van Breedam, J., van de Wal, R. S. W., Winkelmann, R., Zhao, C., Zhang, T., Zwinger, T. (2020) ISMIP6 Antarctic: a multi-model ensemble of the Antarctic ice sheet evolution over the 21st century. *The Cryosphere.* 14(9): 3033-3070.

Shen, Q., Wang, H., Shum, C., Jiang, L., Hsu, H., Dong, J. (2018) Recent high-resolution Antarctic ice velocity maps reveal increased mass loss in Wilkes Land, East Antarctica. *Scientific Reports.* 8(4477): 1-8.

Shepherd, A., Wingham, D., Payne, T., Skvarca, P. (2003) Larsen Ice Shelf Has Progressively Thinned. *Science.* 302(5646): 856-859.

Shepherd, A., Gilbert, L., Muir, A., Konrad, H., McMillan, M., Slater, T., Briggs, K., Sundal, A., Hogg, A., Engdahl, M. (2019) Trends in Antarctic Ice Sheet Elevation and Mass. *Geophysical Research Letters*. 46(14): 8174-8183.

Smith, B., Fricker, H., Gardner, A., Medley, B., Nilsson, J., Paolo, F., Holschuh, N., Adusumilli, S., Brunt, K., Csatho, B., Harbeck, K., Markus, T., Neumann, T., Siegfried, M., Zwally, J. (2020) Pervasive ice sheet mass loss reflects competing ocean and atmosphere processes. *Science*. 368(6496): 1239-1242.

Spence, P., Griffies, S., England, M., Hogg, A., Saenko, O., Jourdain, N. (2014) Rapid subsurface warming and circulation changes of Antarctic coastal waters by poleward shifting winds. *Geophysical Research Letters*. 41(13): 4601-4610.

Steig, E., Ding, Q., Battisti, D., Jenkins, A. (2012) Tropical forcing of Circumpolar Deep Water Inflow and outlet glacier thinning in the Amundsen Sea Embayment, West Antarctica. *Annals of Glaciology.* 53(60): 19-28.

Steinthorsdottir, M., Coxall, H., de Boer, A., Huber, M., Barbolini, N., Bradshaw, C., Burls, N., Feakins, S., Gasson, E., Henderiks, J., Holbourn, A., Kiel, S., Kohn, M., Knorr, G., Kürschner, W., Lear, C., Liebrand, D., Lunt, D., Mörs, T., Pearson, P., Pound, M., Stoll, H., Strömberg, C. (2021) The Miocene: The Future of the Past. *Paleoceanography and Paleoclimatology.* 36(e2020PA004037): 1-71.

Stokes, C., Abram, N., Bentley, M., Edwards, T., England, M., Foppert, A., Jamieson, S., Jones, R., King, M., Lenaerts, J., Medley, B., Miles, B., Paxman, G., Ritz, C., van de Flierdt, T., Whitehouse, P. (2022) Response of the East Antarctic Ice Sheet to past and future climate change. *Nature.* 608(7922): 275-286.

Stone, E., Lunt, D., Annan, J., Hargreaves, J. (2013) Quantification of the Greenland ice sheet contribution to Last Interglacial sea level rise. *Climate of the Past.* 9(2): 621-639.

Stroeven, A., Prentice, M., Kleman, J. (1996) On marine microfossil transport and pathways in Antarctica during the late Neogene: Evidence from the Sirius Group at Mount Fleming. *Geology.* 24(8): 727-730.

Stokes, C., Abram, N., Bentley, M., Edwards, T., England, M., Foppert, A., Jamieson, S., Jones, R., King, M., Lenaerts, J., Medley, B., Miles, B., Paxman, G., Ritz, C., van de Flierdt, T., Whitehouse, P. (2022) Response of the East Antarctic Ice Sheet to past and future climate change, *Nature.* 608: 275-286.

Sun, S., Cornford, S., Gwyther, D., Gladstone, R., Galton-Fenzi, B., Zhao, L., Moore, J. (2016) Impact of ocean forcing on the Aurora Basin in the 21st and 22nd centuries. *Annals of Glaciology*. 57(3): 79-86.

Sun, S., Pattyn, F., Simon, E., Albrecht, T., Cornford, S., Calov, R., Dumas, C., Gillet-Chaulet, F., Goelzer, H., Golledge, N., Greve, R., Hoffman, M., Humbert, A., Kazmierczak, E., Kleiner, T., Leguy, G., Lipscomb, W., Martin, D., Morlighem, M., Nowicki, S., Pollard, D., Price, S., Quiquet, A., Seroussi, H., Schlemm, T., Sutter, J., van de Wal, R., Winkelmann, R., Zhang, T. (2020) Antarctic ice sheet response to sudden and sustained ice-shelf collapse (ABUMIP). *Journal of Glaciology.* 66(260): 891-904.

Sutter, J., Gierz, P., Grosfeld, K., Thoma, M., Lohmann, G. (2016) Ocean temperature thresholds for Last Interglacial West Antarctic Ice Sheet collapse. *Geophysical Research Letters.* 43(6): 2675-2682.

Sutter, J., Eisen, O., Werner, M., Grosfeld, K., Kleiner, T., Fischer, H. (2020) Limited retreat of the Wilkes Basin Ice Sheet during the Last Interglacial. *Geophysical Research Letters*. 47(e2020GL088131): 1-7.

Sutterley, T., Velicogna, I., Rignot, E., Mouginot, J., Flament, T., Van den Broeke, M., van Wessem, J., Reijmer, C. (2014) Mass loss of the Amundsen Sea Embayment of West Antarctica from four independent techniques. *Geophysical Research Letters.* 41: 8421-8428.

The IMBIE Team (2018) Mass balance of the Antarctic Ice Sheet from 1992 to 2017. *Nature*. 558(7709): 219-222.

Thoma, M., Jenkins, A., Holland, D., Jacobs, S. (2008) Modelling Circumpolar Deep Water intrusions on the Amundsen Sea continental shelf, Antarctica. *Geophysical Research Letters.* 35(L18602): 1-6.

Thomas, Z., Jones, R., Turney, C., Golledge, N., Fogwill, C., Bradshaw, C., Menviel, L., McKay, N., Bird, M., Palmer, J., Kershaw, P., Wilmshurst, J., Muscheler, R. (2020) Tipping elements and amplified polar warming during the Last Interglacial. *Quaternary Science Reviews.* 233: 1-17.

Thompson, A., Stewart, A., Spence, P., Heywood, K. (2018) The Antarctic Slope Current in a Changing Climate. *Reviews of Geophysics.* 56: 741-770.

Trusel, L., Das, S., Osman, M., Evans, M., Smith, B., Fettweis, X., McConnell, J., Noël, B., van den Broeke, M. (2018) Nonlinear rise in Greenland runoff in response to post-industrial Arctic warming. *Nature.* 564(7734): 104-108.

Turner, J., Lu, H., White, I., King, J., Phillips, T., Hosking, J., Bracegirdle, T., Marshall, G., Mulvaney, R., Deb, P. (2016) Absence of 21st century warming on Antarctic Peninsula consistent with natural variability. *Nature.* 535(7612): 411-415.

Turner, J., Orr, A., Gudmundsson, H., Jenkins, A., Bingham, R., Hillenbrand, C., Bracegirdle, T. (2017a) Atmosphere-ocean-ice interactions in the Amundsen Sea Embayment, West Antarctica. *Reviews of Geophysics.* 55: 235-276.

Turner, J., Phillips, R., Marshall, G., Hosking, J., Pope, J., Bracegirdle, T., Deb, P. (2017b) Unprecedented springtime of Antarctic sea ice in 2016. *Geophysical Research Letters.* 44: 6868-6875.

Turner, J., Holmes, C., Harrison, T., Phillips, T., Jena, B., Reeves-Francois, T., Fogt, R., Thomas, E., Bajish, C. (2022) Record Low Antarctic Sea Ice Cover in February 2022. *Geophysical Research Letters.* 49(e2022GL098904): 1-11.

Turney, C., Jones, R., McKay, N., van Sebille, E., Thomas, Z., Hillenbrand, C., Fogwill, C. (2020) A global mean sea surface temperature dataset for the Last Interglacial (129-116 ka) and contribution of thermal expansion to sea level change. *Earth System Science Data.* 12(4): 3341-3356.

van den Broeke (2005) Strong surface melting preceded collapse of Antarctic Peninsula ice shelf. *Geophysical Research Letters.* 32(L12815): 1-4.

van der Veen, C. (2007) Fracture propagation as means of rapidly transferring surface meltwater to the base of glaciers. *Geophysical Research Letters.* 34(L01501): 1-5.

van Wessem, J., Ligtenberg, S., Reijmer, C., van de Berg, W., van den Broeke, M., Barrand, N., Thomas, E., Turner, J., Scambos, T., van Meijgaard, E. (2016) The modelled surface mass balance of the Antarctic Peninsula at 5.5 km horizontal resolution. *The Cryosphere.* 10: 271-285.

Velicogna, I., Sutterley, T., Van den Broeke, M. (2014) Regional acceleration in ice mass loss from Greenland and Antarctica using GRACE time-variable gravity data. *Geophysical Research Letters*. 41: 8130-8137.

Wang, L., Davis, J., Howat, I. (2021) Complex patterns of Antarctic ice sheet mass change resolved by time-dependent rate modelling of GRACE and GRACE follow-on observations. *Geophysical Research Letters.* 48(e2020GL090961): 1-10.

Webb, P., Harwood, D., McKelvey, B., Mercer, J., Stott, L. (1984) Cenozoic marine sedimentation and ice-volume variation on the East Antarctic craton. *Geology.* 12(5): 287-291.

Weertman, J. (1974) Stability of the junction of an ice sheet and an ice shelf. *Journal of Glaciology.* 13(67): 3-11.

Williams, T., van de Flierdt, T., Hemming, S. R., Chung, E., Roy, M., Goldstein, S. (2010) Evidence for iceberg armadas from East Antarctica in the Southern Ocean during the late Miocene and early Pliocene. *Earth and Planetary Science Letters*. 290: 351–361.

Wilson, D., Bertram, R., Needham, E., van de Flierdt, T., Welsh, K., McKay, R., Mazumder, A., Riesselman, C., Jimenez-Espejo, F., Escutia, C. (2018) Ice loss from the East Antarctic Ice Sheet during late Pleistocene interglacials. *Nature.* 561(7723): 383-386.

Winsborrow, M., Clark, C., Stokes, C. (2010) What controls the location of ice streams? *Earth Science Reviews.* 103: 45-49.

Yamazaki, K., Aoki, S., Katsumata, K., Hirano, D., Nakayama, Y. (2021) Multidecadal poleward shift of the southern boundary of the Antarctic Circumpolar Current off East Antarctica. *Science Advances.* 7(eabf8755): 1-10.

Young, D., Wright, A., Roberts, J., Warner, R., Young, N., Greenbaum, J., Schroeder, D., Holt, J., Sugden, D., Blankenship, D., Ommen, T., Siegert, M. (2011) A dynamic early East Antarctic Ice Sheet suggested by ice-covered fjord landscapes. *Nature*. 474: 72-75.

Yu, H., Rignot, E., Seroussi, H., Morlighem, M. (2018) Retreat of Thwaites Glacier, West Antarctica, over the next 100 years using various ice flow models, ice shelf melt scenarios and basal friction laws. *The Cryosphere.* 12: 3861-3876.

Zhao, C., King, M., Watson, C., Barletta, V., Bordoni, A., Dell, M., Whitehouse, P. (2017) Rapid ice unloading in the Fleming Glacier region, southern Antarctic Peninsula, and its effect on bedrock uplift rates. *Earth and Planetary Science Letters.* 473: 164-176.

Zheng, F., Li, J., Clark, R., Nnamchi, H. (2013) Simulation and Projection of the Southern Hemisphere Annular Mode in CMIP5 Models. *Journal of Climate.* 26: 9860 – 9879.

Zwally, H., Giovinetto, M., Beckley, M., Saba, J. (2012). *Antarctic and Greenland Drainage Drainage Systems.* GSFC Cryospheric Sciences Laboratory. Accessed using Quantarctica.

8. Appendices

Appendix 1. Details of satellite imagery used within this study. Note that multiple scenes were required for each year in order to provide full coverage across Vincennes Bay.

Date	Satellite	Scene ID	Bands	Resolution (m)	Error (m)
10/02/2022	Sentinel 2B	L1C_T49DDG_A025754_20220210T014534	4, 3, 2	10	15
10/02/2022	Sentinel 2B	L1C_T49DDF_A025754_20220210T014534	4, 3, 2	10	15
10/02/2022	Sentinel 2B	L1C_T48DXM_A025754_20220210T014534	4, 3, 2	10	15
08/02/2021	Sentinel 2B	L1C_T49DDF_A020506_20210208T015541	4, 3, 2	10	15
26/01/2021	Sentinel 2B	L1C_T49DDG_A020320_20210126T014540	4, 3, 2	10	15
16/01/2021	Sentinel 2B	L1C_T48DXM_A020177_20210116T014540	4, 3, 2	10	15
27/02/2020	Landsat 8	LC08_L2SR_105107_20200227_20201016_02_T2	4, 3, 2	30	45
01/02/2020	Sentinel 2B	L1C_T49DDF_A015172_20200201T014533	4, 3, 2	10	15
01/02/2020	Sentinel 2B	L1C_T48DXM_A015172_20200201T014533	4, 3, 2	10	15
16/02/2019	Sentinel 2B	L1C_T49DDG_A010167_20190216T014609	4, 3, 2	10	15
16/02/2019	Sentinel 2B	L1C_T48DXL_A010167_20190216T014609	4, 3, 2	10	15
16/02/2019	Sentinel 2B	L1C_T48DXM_A010167_20190216T014609	4, 3, 2	10	15
16/02/2018	Sentinel 2A	L1C_T49DDG_A013856_20180216T014537	4, 3, 2	10	15
16/02/2018	Sentinel 2A	L1C_T49DDF_A013856_20180216T014537	4, 3, 2	10	15
16/02/2018	Sentinel 2B	L1C_T48DXM_A013856_20180216T014537	4, 3, 2	10	15
25/01/2017	Sentinel 2A	L1C_T49DDF_A008322_20170125T015534	4, 3, 2	10	15
12/01/2017	Sentinel 2A	L1C_T49DDG_A008136_20170112T014531	4, 3, 2	10	15
12/01/2017	Sentinel 2A	L1C_T48DXM_A008136_20170112T014531	4, 3, 2	10	15
14/02/2016	Landsat 8	LC08_L2SR_107107_20160214_20201016_02_T2	4, 3, 2	30	45
22/01/2016	Landsat 8	LC08_L2SR_106107_20160122_20201016_02_T2	4, 3, 2	30	45
19/12/2015	Landsat 8	LC08_L2SR_108107_20151219_20201016_02_T2	4, 3, 2	30	45
05/12/2015	Landsat 8	LC08_L2SR_106107_20151205_20201016_02_T2	4, 3, 2	30	45
10/01/2015	Landsat 8	LC08_L2SR_107107_20150110_20201016_02_T2	4, 3, 2	30	45
01/02/2014	Landsat 8	LC08_L2SR_106107_20140201_20201016_02_T2	4, 3, 2	30	45
25/01/2014	Landsat 8	LC08_L2SR_105107_20140125_20201016_02_T2	4, 3, 2	30	45
22/02/2013	Landsat 7	LE07_L1GT_106107_20130222_20200908_02_T2	3, 2, 1	30	45
07/01/2013	Landsat 7	LE07_L1GT_104107_20130107_20200908_02_T2	3, 2, 1	30	45
20/12/2012	Landsat 7	LE07_L1GT_106107_20121220_20200908_02_T2	3, 2, 1	30	45
28/01/2012	Landsat 7	LE07_L1GT_105107_20120128_20200909_02_T2	3, 2, 1	30	45
26/01/2012	Landsat 7	LE07_L1GT_107107_20120126_20200909_02_T2	3, 2, 1	30	45
01/02/2011	Landsat 7	LE07_L1GT_106107_20110201_20200910_02_T2	3, 2, 1	30	45
25/01/2011	Landsat 7	LE07_L1GT_105107_20110125_20200910_02_T2	3, 2, 1	30	45
21/02/2010	Landsat 7	LE07_L1GT_107107_20100221_20200911_02_T2	3, 2, 1	30	45
14/02/2010	Landsat 7	LE07_L1GT_106107_20100214_20200911_02_T2	3, 2, 1	30	45
02/02/2009	Landsat 7	LE07_L1GT_107107_20090202_20200912_02_T2	3, 2, 1	30	45
19/01/2009	Landsat 7	LE07_L1GT_105107_20090119_20200912_02_T2	3, 2, 1	30	45
10/01/2009	Landsat 7	LE07_L1GT_106107_20090110_20200912_02_T2	3, 2, 1	30	45
03/01/2009	Landsat 7	LE07_L1GT_105107_20090103_20200912_02_T2	3, 2, 1	30	45
11/02/2008	Landsat 7	LE07_L1GT_104107_20080211_20200913_02_T2	3, 2, 1	30	45
09/02/2008	Landsat 7	LE07_L1GT_106107_20080209_20200912_02_T2	3, 2, 1	30	45
21/01/2007	Landsat 7	LE07_L1GT_106107_20070121_20200913_02_T2	3, 2, 1	30	45
14/01/2007	Landsat 7	LE07_L1GT_105107_20070114_20200913_02_T2	3, 2, 1	30	45
12/01/2003	Landsat 7	LE07_L1GT_104107_20030112_20200916_02_T2	3, 2, 1	30	45
16/12/2002	Landsat 7	LE07_L1GT_107107_20021216_20200916_02_T2	3, 2, 1	30	45
06/12/2001	Landsat 7	LE07_L1GT_106107_20011206_20200917_02_T2	3, 2, 1	30	45
22/01/2001	Landsat 7	LE07_L1GT_104107_20010122_20200917_02_T2	3, 2, 1	30	45
02/01/2000	Landsat 7	LE07_L1GT_106107_20000102_20200918_02_T2	3, 2, 1	30	45

11/02/1991 02/02/1991	Landsat 5 Landsat 5	LT05_L1GS_105107_19910211_20200915_02_T2 LT05_L1GS_106107_19910202_20200915_02_T2	3, 2, 1 3, 2, 1	30 30	45 45
08/01/1990	Landsat 4	LT04_L1GS_104107_19900108_20200916_02_T2	3, 2, 1	30	45
30/12/1989 18/02/1989	Landsat 4 Landsat 4	LT04_L1GS_105107_19891230_20200916_02_T2 LT04_L1GS_108107_19890218_20200916_02_T2	3, 2, 1 3, 2, 1	30 30	45 45
06/12/1973 17/11/1973 12/03/1973	Landsat 1 Landsat 1 Landsat 1	LM01_L1GS_112107_19731206_20200908_02_T2 LM01_L1GS_111107_19731117_20200909_02_T2 LM01_L1GS_113107_19730312_20200909_02_T2	7 7 7	60 60 60	90 90 90
1963	KH-5 ARGON	ARGON mosaic (Kim *et al*., 2007)	-	140	210

Appendix 2. Percentage velocity data coverage within defined boxes **a)** Inland (IN), **b)** Up-glacier of the grounding line (GL), **c)** Floating tongue (FT). Missing values reflect velocity data omitted from our analysis due to either < 25% data coverage or associated errors being > 50% of the calculated velocity magnitude (Section 3.3).

a) IN

Year	Vanderford	Adams	Anzac	Bond East	Bond West	Underwood
2000	39	61	-	-	-	49
2002	-	-	-	100	-	97
2006	41	65	-	100	-	-
2007	-	-	100	100	-	75
2008	58	98	100	100	34	97
2009	35	68	68	100	-	85
2010	-	84	100	100	-	59
2011	99	100	100	100	-	98
2012	47	82	-	100	44	-
2013	100	100	100	100	100	100
2014	100	100	100	100	100	100
2015	100	100	100	100	100	100
2016	100	100	100	100	100	100
2017	100	100	100	100	100	100
2018	100	100	100	100	100	100
2019	100	100	100	100	43	100
2020	100	100	100	100	43	100
2021	100	100	100	100	32	100

b) GL

Year	Vanderford	Adams	Anzac	Bond East	Bond West	Underwood
2000	100	94	70	-	-	27
2002	100	-	67	100	99	91
2006	99	98	89	92	100	-
2007	100	98	91	100	100	80
2008	100	99	100	100	100	100
2009	100	97	99	100	100	94
2010	100	99	88	100	100	77
2011	100	100	100	100	100	99
2012	100	90	-	100	100	79
2013	100	100	100	100	100	100
2014	100	100	100	100	100	100
2015	100	100	100	100	100	100
2016	100	100	100	100	100	100
2017	100	100	100	100	100	100
2018	100	100	100	100	100	100
2019	100	100	100	100	100	100
2020	100	100	100	100	100	84
2021	100	100	100	100	100	92

c) FT

Year	Vanderford	Adams	Anzac	Bond East	Bond West	Underwood
2000	39	61	-	-	-	49
2002	-	-	-	100	-	97
2006	41	65	-	100	-	-
2007	-	-	100	100	-	75
2008	58	98	100	100	34	97
2009	35	68	68	100	-	85
2010	-	84	100	100	-	59
2011	99	100	100	100	-	98
2012	47	82	-	100	44	-
2013	100	100	100	100	100	100
2014	100	100	100	100	100	100
2015	100	100	100	100	100	100
2016	100	100	100	100	100	100
2017	100	100	100	100	100	100
2018	100	100	100	100	100	100
2019	100	100	100	100	43	100
2020	100	100	100	100	43	100
2021	100	100	100	100	32	100